Energy Saving Through An Innovative Aircraft Turbine Thermal Control

Maria Pia Monterossi
* * * * * *

I hereby declare that, the contents and organization of this dissertation constitute my own original work and does not compromise in any way the rights of third parties, including those relating to the security of personal data.

…………………………….....

Maria Pia Monterossi

Turin, April 28, 2018

Summary

One of the most important challenges for the next generation of aircraft propulsion systems is an engine more efficient, with less pollutants emission and so definitely more sustainable.

To reach this goal a lot of new technical solutions must be exhibit in order to optimize the main engine parts, but the attention should also be focused on how the different engine components work, due to the thermal loads they undergo during the different phases of the flight. Typical examples of the effects that the thermal loads produce are the gaps among the different components, producing unavoidable leakages, due to their differential thermal expansion.

Actually in the Low Pressure Turbines (LPT) one of the countermeasures applied to control and to minimize these gaps consists in blowing into the stator cavities some relatively cold air bled from one of the compressor stages. This technique, even if effective for the turbine thermal control, results in supplementary fuel consumption.

In this research a first attempt to reduce the required cooling air, by introducing insulating materials in the proper LPT cavities, is shown. The preliminary numerical analyses performed to point out and compare suitable configurations are here presented. The configuration, identified as the most performing, has been used to forecast the insulation technology effectiveness.

The obtained numerical results evaluated both in terms of temperature decreasing of the Casing plate and of Cooling air reduction, are reported.

The technological solution, numerically pointed out, has been experimentally validated by means of the available testing facility, whose Test Article reproduces, properly scaled, one stage of a modern LPT.

After the experimental campaign, the experimental data and the ones obtained by running the numerical model have been compared in order to evaluate the final model accuracy.

Finally, a thermal insulating selection has been performed to overcome the limits that the tested technology has exhibited. The studied alternative solutions and the obtained results are here reported and compared with the ones obtained with the technology previously implemented.

Contents

List of Tables

List of Figures

Chapter 1

Introduction

1.1 Research context

Starting from the early nineties, the global warming has become one of the major reasons of interest for the international community. In 1992, during the UNFCCC (United Nations Framework Convention on Climate Change), known as the Rio negotiate, a first agreement has been signed about the need to reduce the greenhouse gases emissions to contrast the Earth global warming. This first negotiate, not legally binding for the signatory states, was the base for the following agreements and, in particular, for the Kyoto protocol, stipulated in 1997. In this last agreement the signatories committed themselves to reduce all the greenhouse gases emissions (carbon dioxide, methane, nitrogen oxides, sulfur oxides and particulates) and in particular the CO_2 emissions, being these last responsible for more than 55% of the total emissions (Figure 1.1).

Considering the total amount of US greenhouse gas emissions in 2003, the part due to transportation amounted to 27% of the total emissions, with a 9% ascribable to aviation [2], a sector that is still growing.

In this scenario, during the UNFCCC, held in Bali in 2007, the participating states proposed a global emissions regulation, which provided for a general reduction of around 20%-40% with respect to what has been measured in 1990. Moreover, during the convention, the importance of the aircrafts emissions regulation to reduce the total greenhouse gases emissions was evident.

Following the guidelines proposed during the UNFCCC, the International Civil Aviation Organization (ICAO) set some worldwide norms in order to reduce significantly the pollution produced by the aircrafts [3].
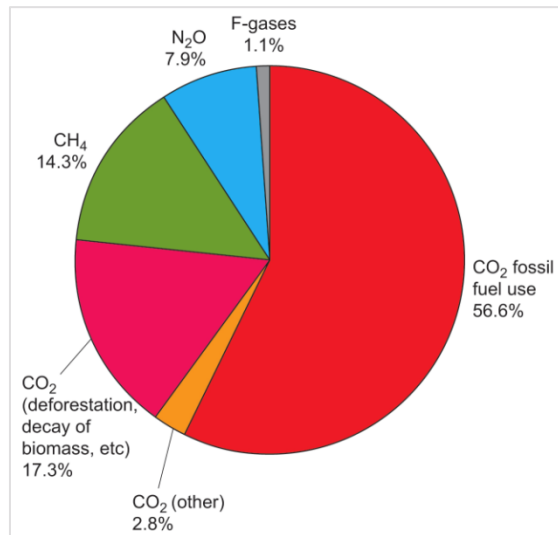
Figure 1.1: Greenhouse emissions [1]

In this frame the European Commission in accordance with the ACARE (Advisory Council for Aeronautics Research in Europe) vision, has set some strategic goals, for the environmental sustainability of the next aircrafts generation, to be achieved within 2020: a 50% reduction in CO_2, an 80% reduction in nitrogen oxides and a decrease in the perceived noise by 10 dB.

Moreover, the ACARE experts have also stated the engine had to contribute in getting the overall targets with a 15%-20% reduction in CO_2 emissions. Therefore, in addressing the challenges for a green aircraft, a special attention must be paid to the engine in order to improve its performance and to decrease its weight, reducing, at the same time, the fuel consumption and consequently the gas emissions.

To get the CO_2 emissions reduction targets, a lot of initiatives, involving both private and public research centers, have been launched in order to develop technological improvements capable of reducing the aircrafts environmental impact.

Adaptive technologies [2], aimed at improving the engine components efficiency or at reducing the engine weigh, have been developed with benefits in terms of CO_2 reductions. For instance: combustion control technologies have been developed to reduce emissions, allowing to provide both lean-burning combustors and more uniform and efficient burning by way of a local combustion process control. Flow control technologies have been adopted to manipulate the engine components air, injecting or extracting it by means of mechanical protuberances or plasma actuators, through or around the engine components. High-temperature and high loading magnetic bearings have been introduced to control both the structural vibrations and the compressor stall. Variable area fan nozzles and high bypass-ratios have been considered to increase the fan pressure ratio.

Significant engine improvements have been reached, during the last years, by increasing the turbine pressure ratios and the inlet temperatures, providing engines with better performances, lower pollutant emissions and reduced weight and costs.

In particular, many efforts have been spent to achieve turbine inlet pressure ratios and inlet temperatures up to 50 and to 1800-2000 K respectively [4].

Some researchers, as for instance Guha [5], argue that an optimum pressure ratio exists and it is a function of an optimum temperature ratio, T_{in_T}/T_{in_C} (ratio between the inlet turbine temperature and the inlet compressor temperature), and it is strictly related with the turbine and compressor efficiencies. Moreover, Guha states that there is an optimum inlet turbine temperature which depends on the thermodynamic of the real gases and which is not simply the maximum allowed temperature that the resistance of the material dictates. This optimum temperature increases as the pressure ratio rises, but, despite this, the best performances not necessarily coincide with the highest inlet turbine temperature.

In the past 30 years, the turbine materials and coatings have been improved significantly, but it is well known that a turbine, even if made by using the best existing materials and coatings, allows for a rotor inlet temperature lower than 1480 K if not equipped with a proper cooling system. An increase in turbine inlet temperature, therefore, requires an upgrade in the cooling system. Today the amount of air, bled from the compressor, used to cool down the hot components of the high and low pressure turbines, ranges from 20% to 30% of the total amount of the compressed air [6]. This air, by- passing the combustor, negatively impacts on the engine performance because the amount of air, available for the combustion, is decreased and, at the same time, the power used to compress this air is not balanced out with the power development in turbine. Therefore, an improvement in the cooling efficiency cannot be pursued simply by increasing the amount of cooling air because this solution would imply a further reduction in the performances of the engine. Thus, the cooling system upgrade has to consist in designing new solutions able to satisfy the following requirements: minimum possible amount of cooling air, low weight and reduced impact on the engine performance.

The cooling system design, therefore, due to the complexity of the issue, represents a very tough challenge requiring the designers to be aware of the problems related with safety, performance, environmental impact, weight, affordability and cost. The traditional "step-by-step" engine design process, according to Glezer's dissertation [7], cannot be adopted because of these very complex problems, but it has to be dealt with a multi-disciplinary approach, being each involved discipline fundamental to the final design success.

For the reasons described above, despite many improvements have been performed in protective coatings (TBC) and manufacturing materials (single crystal materials), the turbine cooling technology is still considered the breakthrough technology to enhance the engine efficiency, with a forecasted fuel burn reduction of about 25% within 2025 [6].

In literature different solutions, aimed at improving the cooling system efficiency, are shown, but to a large extent they are related to the rotor disks cooling as the cooling potential of this specific area is considered not yet completely exploited. In addition, special efforts are aimed to the active clearance

control system (ACC) improvement [8-10] and to the sealing technologies [11-14]. In fact, the cooling air bled from the compressor is used not only to cool down the rotor blades, allowing a higher inlet rotor temperature. This air is also used to control the gaps due to the thermal expansions and contractions that the turbine undergoes, because of the power changes occurring during the different phases of the flight (take off, cruise, landing), which produce unavoidable leakages. Among these gaps the one considered more critical for the engine efficiency is the clearance, i.e. the gap between the rotating blade tips and the external Casing, surrounding them circumferentially in the outward direction. The hot gas leakages passing through this gap produce no effect on the turbine blades and consequently increase the fuel consumption and decrease the engine performance. Therefore, the reduction of the clearance height allows the decrease of the specific fuel consumption and of the gas emissions of the engine on the whole.

Nowadays, to control the clearance height, a secondary cooling air system, the ACC system, is used to cool down the external Casing surface. In addition, cooling air is blown into the stator cavities in order to cool down the Casing plate acting on its inner surface.

Another method used to control the clearance dimension is the use of sealing technologies to reduce the hot gas leakages between the blades and the shroud, meanwhile increasing the engine lifetime [10, 15].

The clearance control, performed by means of the secondary cooling system, even if effective for the hot gas leakages reduction, represents a power loss for the engine. Therefore an optimized clearance control, able to minimize the amount of air required to cool down the turbine stator cavities, can significantly improve the engine performances, reducing, at the same time, the pollutant emissions.

While, as previously said, special efforts have been devoted to the ACC system improvement, only few efforts have been dedicated to the reduction of the Cooling air blown into the stator cavities.

Although it is not completely clear whether, in the next years, the improvement of the technologies described above will be the most effective answer to the need of an increased engine efficiency [16], or whether new design concepts should be introduced [17-19], in this PhD thesis the attention is focused on the development of a new methodology that allows the minimizing of the cooling air used to control the Casing temperature.

To pursue this goal, a lot of numerical and experimental studies about the thermal and fluid-dynamic fields, occurring within the turbine, are surely required with particular attention to those phenomena, such as heat transfer mechanisms and fluid phenomena, taking place in the zones neighboring the clearance.

From the numerical point of view, numerical models representing the main turbine features have to be developed with the aim to reproduce, with a high accuracy level, not only the major phenomena, taking place within the turbine, but also the small air leakages between components or sealing systems, significantly affecting the thermal behavior of the whole turbine. In this way the models can be also used to forecast the fluid and thermal responses due to the introduction of

new technologies. To reach this target a deep knowledge about the turbine inner components thermal behavior is necessary, because their temperatures are the result of the hot and cold airflows interactions. Therefore a multidisciplinary approach has to be adopted to evaluate correctly the mutual influence of the fluid and thermal phenomena affecting the resulting turbine temperature distribution.

Furthermore, in order to tune the models with the required accuracy, it is essential to have an appropriate set of experimental data that can be obtained only through test campaigns. As, for a number of reasons, the experimental data cannot be obtained by performing experiments directly on the engine, a test rig facility has been designed at the Energy Department of the Politecnico di Torino [20], with the double aim to provide experimental data, compulsory to tune the numerical models, and to test the new technologies, numerically pointed out.

1.2 Research outline

As just said, the purpose of the research activity, here reported, is the study of an optimized turbine thermal control, able to minimize the cooling air injected into the stator cavities to control the Casing temperature.

The strategy, here proposed, is the reduction of the Casing thermal load, using insulating materials (called thermal blankets or simply blankets in what follows) to minimize the demand of cooling air bled from the compressor.

The performed research activity, reported in the following chapters, can be summarized in three macro steps concerning an early numerical activity, an experimental phase, and a second numerical activity.

First of all, a short description of the available testing facility, including the explanation of the main assumptions used in performing its design, is reported in Chapter 2. In addition, summaries of the rig and test article instrumentation, together with the results obtained during a first test campaign, are provided.

In Chapter 3 the implemented numerical model, as well as the method used for the tuning and the obtained results, are presented.

In Chapters 4 and 5 the activity steps, which have led to bring out the insulating technologies, are described. In particular, the numerical studies carried out to find a suitable insulation methodology and the obtained results are presented in Chapter 4, critically comparing different insulation configurations, realized by varying the blankets number, position and size. Moreover, numerical simulations have been performed with the aim of forecasting the proposed solution effectiveness in terms of reduction of both the Casing plate temperature and the Cooling air.

The configuration, numerically identified as the most performing, has been experimentally tested using the available facility. The obtained results are critically assessed in order to quantify the benefits of the insulating material application. Furthermore, these results are compared with the ones numerically evaluated, to rate the numerical model accuracy and its capability in forecasting

the changes in the fluid and thermal behavior due to the application of the blankets.

In Chapter 5, alternative insulation methodologies are investigated with the aim of overcoming the defects that the previously proposed and tested insulation configuration has shown.

The results obtained through this selection process are reported and compared to the ones obtained with the previously tested solution, highlighting the observable advantages.

Finally, in Chapter 6, the summary of the performed research activities is reported together with some conclusions about the performed research.

Chapter 2

Testing Facility

2.1 Introduction

As previously said, a deepened study of the LPT fluid and thermal behavior must be faced by means of a multidisciplinary approach, which allows a systemic vision of the turbine behavior. The need of a systemic vision is clearly explained by considering that in a turbine the amount of heat transferred among its different components depends on how the turbine behaves as a whole.

The temperatures of the components, during the operations, are the result of the heat transfer mechanisms (radiative heat transfer, conduction and convection) taking place in the different cavities and, more in particular, of the heat transfer by convection. But the amount of heat exchanged by convection strongly depends on both the flow velocity fields and the amount of air. At the same time, the amounts of air and the way the different flow rates are split within the turbine cavities are directly associated with the whole turbine behavior because the gaps among the different components and the effectiveness of the sealing systems, in turn, depend on the element deformations and so on their temperatures.

A detailed analysis of the turbine thermal behavior, paying particular attention to the clearance and to the smaller gaps among the different components, is, therefore, to be considered fundamental to any related study and design improvement.

The testing facility employed, in this work, to support this systemic vision in studying the different heat and mass transfer phenomena occurring inside a LPT, is a static rig, named Thermalcase, available at the Energy Department of the Politecnico di Torino. Its Test Article (TA) has been designed, paying particular attention to the external airtight cylinder (Casing), containing the turbine elements, and to the zone above the rotating blades, where the clearance seals are placed. Furthermore the design of the TA has been carried out through a scaling procedure (reference values typical of a standard LPT available in literature), in order to reproduce the minimum circular sector of the whole turbine, which can be

considered still representative of its thermal and fluid behavior, which corresponds to less than one tenth of a full angle.

In fact, as explained in more detail in [21], taking as a reference a typical standard LPT geometry (Figure 2.1), to properly study the LPT fluid and thermal phenomena, it is not compulsory to reproduce the whole turbine. It is sufficient that the TA contains at least three liners to obtain a proper replication of the 3D phenomena, simulating the air leakages between these sectors and avoiding boundary effects. Moreover, again to avoid the boundary effects, the TA has to replicate also two vanes, one placed downstream and the other upstream of the blade element. For these reasons, therefore, the TA has been designed in order to reproduce one and a half low-pressure engine turbine stage, including the blade tip labyrinth seal.
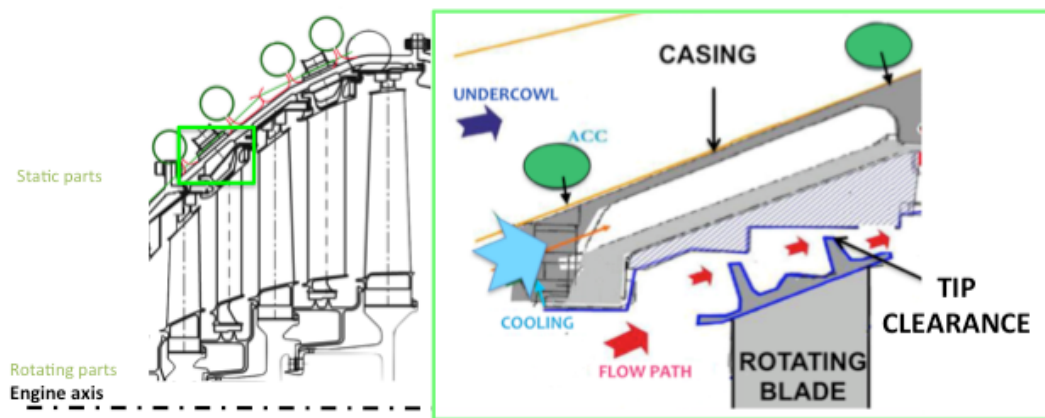
Figure 2.1: Schematic of the LPT reference geometry

From the fluid-dynamic point of view, the turbine stages are crossed by hot and cold airflows, which have to be reproduced within the TA, because they significantly affect the thermal distribution. Referring to the schematic of the LPT reference (Figure 2.1) it is possible to observe the turbine may be subdivided in two separate regions. The lower region is the one where the main hot stream, called Flow Path (FP), flows producing work, and where is also present a second flow, at lower temperature, called Cooling (Coo). This last flow, whose reduction is one of the goals of this dissertation, is bled from the compressor and injected into the stator cavities where it can mix with the main flow. In the upper cavities, physically separated from the previous ones by the external cylinder (Casing), the ACC (Active Clearance Control) and the Undercowl flows interact and mix with the aim of cooling down the Casing surface. In the TA project all the listed mass flow rates have been reproduced except for the Undercowl, because the study of the effects of its interaction with the ACC air and its impact on the cooling efficiency of the Casing is not one of the aims of the rig.

Moreover, in order to work in fluid and thermal similitude with a typical standard LPT, reproducing the different operating conditions, the FP and Coo mass flow rates have to be regulated from a null value to a maximum one. Furthermore, both these flows must be heated up to a temperature of about 1100-

1300 K and compressed up to 8-10 bar. In addition, the Reynolds numbers must be replicated, providing Reynolds numbers up to 10^5, for the FP, and up to 10^4, for the ACC [21].

The angular reduction by itself, although it allows catching the desired phenomena, leads, on one side, to a TA with geometrical dimensions too small and not easy to manufacture and tool and, on the other side, requires a very high power to compress and heat up the different mass flow rates as well as materials, for both the TA and the pipes, that have to be capable of withstanding the high temperatures and pressures.

For these reasons, in the TA design, the geometrical features and quantities, typical of a standard LPT available in literature, have been properly scaled, in order to obtain a final design in which the geometrical dimensions are increased and the maximum pressures and temperatures are reduced.

In what follows, a general description about the scaling procedure is provided together with a brief summary about the main features and instrumentation of the facility.

2.1 Scaling methodology

Starting from the reduced angle, the scaling procedure [21] has been carried out with the aim of enlarging the TA size and of reducing the inlet temperature and pressure values. These inlet values are the ones typical of a LPT intermediate stage and are reported in Table 2.1

Table 2.1: Initial temperature and pressure values

Flow	Temperature (K)	Pressure (bar)
Flow Path	1300	8
Cooling	1300	8
ACC	500	2

Starting from the reference geometry, the scaling factors, employed for the test section design, have been chosen taking into account the non-dimensional numbers characterizing the fluid dynamics and heat transfer phenomena.

The scaling has been performed referring to the Buckingham π-theorem that states the dimensionless groups, regardless of whether the calculations are performed by using the original or the scaled quantities, will assume the same values. Therefore, all the variables have to be scaled according to their dimensional analysis.

The quantities considered in the scaling procedure are: the geometric dimensions, the temperatures and pressures, the densities, the velocities, the reduced turbine angle and time.

The examined dimensionless numbers, relevant from the thermal and fluid dynamic point of view, are the Nusselt (Nu) number, the Reynolds (Re) number,

and the Prandtl (Pr) number. Being the heat transfer dependent on the Nu number, this last one has to be maintained during the scaling. In order to maintain the Nu, it is necessary that both the Pr and the Re numbers are maintained, because the Nu depends on these two dimensionless numbers. In particular, the attention has been focused on the values assumed by the Re number because, being the used fluid only air, which behaves as an ideal gas, the Pr number can be considered constant.

However, from the thermal point of view, during the scaling, it is important, not only to maintain the Nu number, but also the Biot (Bi) number and the Fourier (Fo) number. In fact, the Bi number conservation allows reproducing, in the TA, the ratio between the conduction thermal resistances, (through the solid components) and the convective ones (between the fluid and the solid components) typical of a LPT. The Fo number conservation, instead, is fundamental for the correct evaluation of the transient conditions.

Finally, the Mach (Ma) number must be reproduced because it is relevant from the fluid dynamic point of view.

Following these guidelines, suitable scaling coefficients have been pointed out both for the TA geometrical dimensions and for the temperature, pressure and mass flow rate values.

The resulting TA presents geometrical dimensions, which have been increased as much as necessary in order to displace the desired number of measurement sensors, and operating temperature and pressure values that have been reduced (Table 2.2).

Table 2.2: TA maximum operating conditions

Flow	Temperature (K)	Pressure (bar)
Flow Path	873	2,2
Cooling	573	2,2
ACC	293	2

2.2 ThermalCase Rig

The Thermalcase rig facility (Figure 2.2) has been designed, as previously said, with the double aim of providing experimental data compulsory to create high accuracy numerical models, useable during the design phase of an improved performance turbine module, and of evaluating the efficiency of the new technologies numerically pointed out. Thanks to the scaling procedure, the facility TA is able, not only to be representative of the main turbine geometrical features, but also to work in thermal similitude with the engine, reproducing the typical dimensionless number of an actual LPT.

In what follows, a short description of the rig, of its instrumentation and of the available experiments control and management system, is provided.
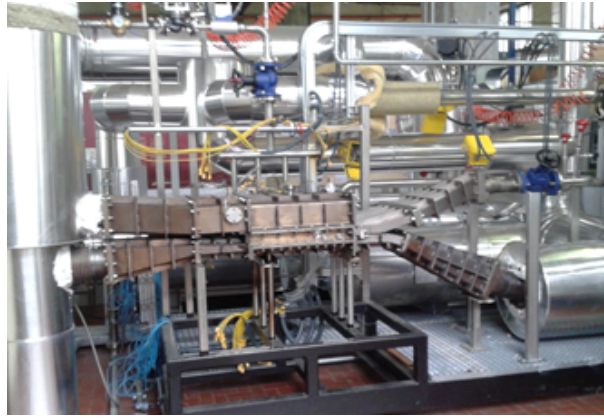
Figure 2.2: Thermalcase rig [20]

In Figure 2.3, the Rig layout and its main components are sketched. As it is possible to see, the three mass flow rates are provided by two supply lines, one for the FP and Coo air, and the other one for the ACC system.

The FP and Coo air are supplied by a screw compressor, suitable for providing a fixed amount of compressed air equal to 0.56 kg/s, while the ACC mass flow rate is delivered to the ACC system by another compressor.

A manual valve V1 placed on the chimney, at the TA exit, allows increasing the pressure of the compressed air, supplied by the screw compressor, up to 2.5 barA, providing a TA inlet pressure, considering the unavoidable supply line pressure losses, up to 2.2 barA. The valve PR1, instead, allows reducing the ACC air pressure from 7 barA, which is the compressor working pressure, to the desired values.

The compressed air, provided by the screw compressor, is then subdivided into two dedicated pipes, one for the FP and the other for the Coo. Two valves, CV6 and CV7, placed along the FP and Coo lines respectively, are used, in combined action with two supplementary electro-pneumatic control valves (CV1 and CV3), to regulate the amount of the two flow rates incoming the TA, which are measured by using the mass flow controllers FT1 and FT2.

The air flowing in the ACC supply line is adjusted, by means of the electro-pneumatic control valve CV5, to the desired mass flow rate value, which is measured by using the mass flow meter FT4. Then, in order to simulate different pipes, the ACC mass flow rate is subdivided, before entering the TA, into four pipes. The ACC mass flow rate, exiting from the pipes, is injected in a chamber physically separated from the lower one by the Casing plate and directly connected to the external environment through the chimney. Since this chamber is at ambient pressure (p_{out}), in order to obtain the β (p_{in}/p_{out}) values required to guarantee the Re numbers typical of an actual LPT, the pressure that must be regulated is only p_{in}.

The FP and Coo mass flow rates temperatures are set and controlled by using two separated electrical heaters: HE1 (320 kW) and HE2 (10kW), warming up the FP and Coo air up to 923K and 573K, respectively. A security system guarantees

the protection of the electrical heaters, switching off the electrical resistances in case of over temperature.

The ACC temperature is not regulated and is approximately at room temperature because the ACC supply line is not equipped with an electrical heater.
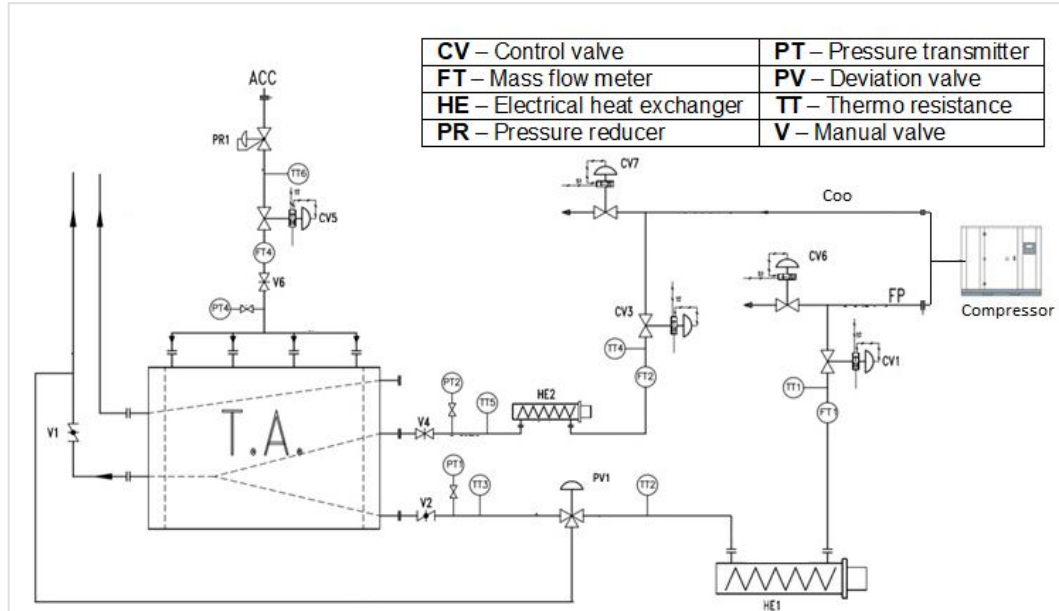
Figure 2.3: Thermalcase rig layout

The Flow Path line is characterized by a by-pass circuit, implemented by means of a deviation valve (PV1) placed after the electrical heater, with the aim of redirecting the air directly to the chimney, performing tests under transient conditions.

A system, which provides nebulized water, reduces the air temperature of the Coo and FP flows, vented to chimney, before rejecting it to the surroundings.

Each described line, in order to check the air temperatures and to measure the absolute pressures of the air entering the TA, is characterized by dedicated pressure and temperature sensors displaced along the paths. In particular: thermo-resistances TT1-TT2- TT3 on the FP line, TT4-TT5 on the Coo line and TT6 on the ACC line; pressure transmitters PT1, PT2 and PT4 on the FP, Coo and ACC line respectively. In addition, in order to allow a further pressure control, each supply line is equipped with three manual valves (V2, V4, V6).

2.3 Test Article

The Test Article, placed in the Thermalcase rig, as previously said, reproduces an angular sector of a modern LPT stage and in particular one and a half stage of a turbine rotor tip region with a rows scheme of Vane-Blade-Vane, where the first and second row create a turbine stage, and the second Vane is part of the following stage. It has been designed in such a way to be representative of

12

the casing and shroud regions of an aeronautical turbine, and in particular of the blade tips (because the cold and hot air mass flow rates crossing these regions can significantly contribute to determine the clearance height).

Moreover, the ACC impingement manifolds are reproduced on the region external to the Casing. The Vane platform and the Shroud are made of three sectors, sealing the resulting tangential gaps by means of spline seals (Figure 2.4).

In Figure 2.5 a TA cross section, with its main components, is sketched. In the same Figure it is also possible to identify the typical mass flow rates passing through the TA.
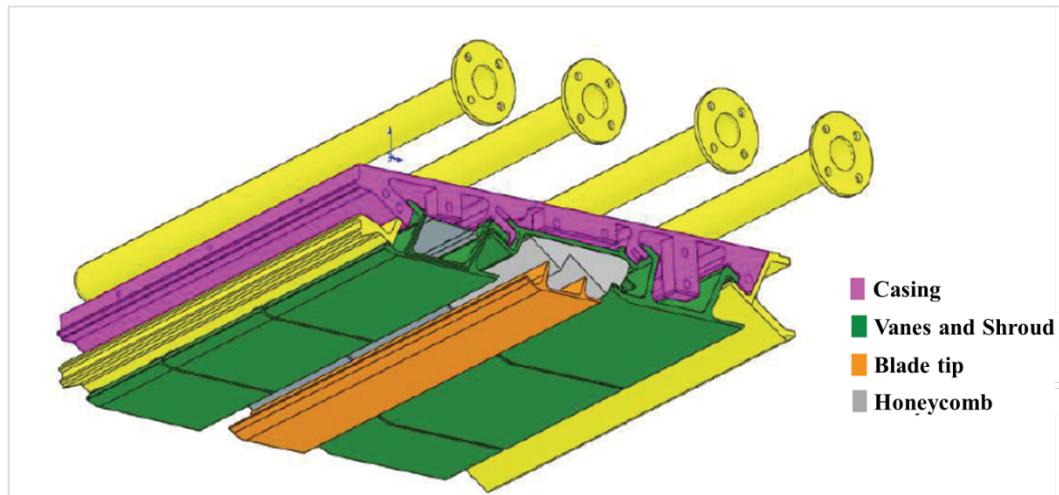
Figure 2.4: Test Article

By considering both the temperatures that the TA has to withstand during the experiments and the thermal behavior that the used material has to present, in order to replicate the same thermal behavior shown by the LPT material, the material chosen to build the TA is AISI 316 super alloy. In order to reduce the heat losses and to accomplish safety policies, the TA external surface is thermally insulated from the ambient by using an insulating material made of ceramic wool which guarantees a temperature between 303K and 323° C on its upper surface.

The resulting TA presents analogies and differences in respect to an actual LPT. By considering the analogies it is possible to state the geometries, even if with some simplifications, are almost respected, the Coo path is faithfully reproduced, the liners are physically separated and a radiative screen made of a metal sheet is placed in the first vane cavity.
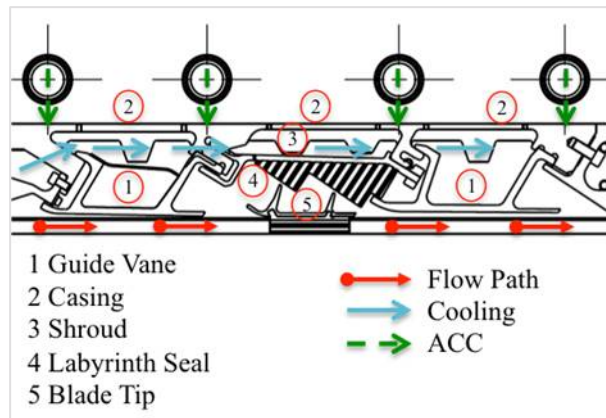
Figure 2.5: Test article cross section

Regarding the differences, instead, the TA doesn't reproduce the rotating parts of a real turbine but it is static and only the blade tips are represented. However, the insertion of a flow restricting device below the blade tip (Figure 2.6), which provides the desired pressure drop condition, between the upstream and the downstream mass flow rates, the rotating part of the engine dictates to the flow, allows maintaining the similarity with the real LPT. Another difference concerns the TA shape that is straightened instead cylindrical as in an actual turbine. Finally, the different TA components are assembled directly in operating conditions, in other words with backlash- free coupling. Therefore to simulate the air passages among the different components, calibrated plates are used to be aware of the proper air passages, and bolted sheets are used for the fastening to the Shroud.

Furthermore, the working fluid isn't a hot gas, resulting from a combustion process, but is simply compressed air heated up to the desired temperature by using the electrical heat exchangers. This way the materials thermo-physical properties and a long instrumentation life are preserved. Despite these differences, concerning the shape and the operational mode, the TA allows to reproduce the main phenomena usually taking place in an actual turbine.
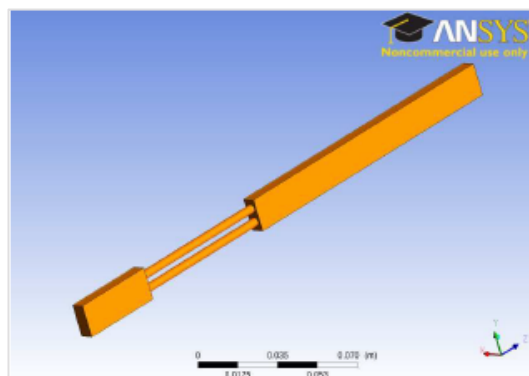
Figure 2.6: Flow restrictor

With the aim to collect a large amount of experimental data, the TA has been equipped with a large number of sensors (Figure 2.7): air thermocouples (25), metal thermocouples (40) and pressure gauges (17). To obtain a better thermal mapping at some locations, along the TA length, a redundancy of the metal thermocouples is performed in the direction of the TA depth. This is particularly useful due to the fact that the TA numerical model is a 2D model, as described in the following chapter, and so this choice allows comparing the calculated numerical temperature with the corresponding experimental values averaged along the TA depth.
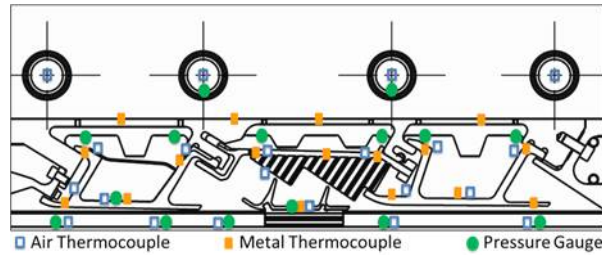
Figure 2.7: Ta instrumentation

In particular, considering the pressure gauges (Figure 2.8): 5 sensors have been placed in the FP regions (P1, P2, P7, P10, P15); 6 pressure gauges have been located in the regions where the Coo flows (P2, P4, P8, P11, P13, P14); 2 pressure transducers have been installed in order to record the pressures on the backward Vane (P3) and on the blade tip plate (P9) while 2 supplementary sensors (P6, P12) have been placed inside two ACC pipes.
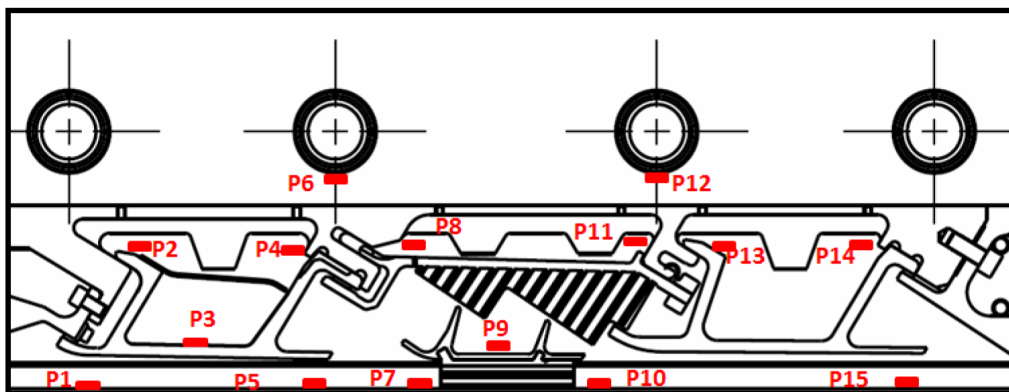
Figure 2.8: Pressure gauges position and nomenclature

The thermocouples used to record the air and metal temperatures are K-type, encapsulated in an Inconel 600 probe, 1 mm in diameter. They are accurate to ± 1.5 °C.

The air thermocouples positions, shown in Figure 2.9, are: 7 thermocouples in the FP region (T1, T7, T8, T11, T17); 7 sensors in the zones where the Coo flows (T4, T6, T9, T12, T14, T16); 5 thermocouples in the chambers in the middle

region (T2, T5, T10, T13, T18). To be noted the sensor T1 presents a redundancy in the tangential direction (T1A, T1B, T1C).

While, for the metal thermocouples, they are located on the relevant TA elements, as sketched in Figure 2.10: 10 sensors on the Vanes platforms, with a redundancy in the depth direction (M3 and M14); 2 redundant sensors placed on the blade tip plate (M8); 7 thermocouples on the Shroud back plate (M7, M9, M11), with a redundancy performed for the sensor M9; 12 sensors placed on the Casing external surface (M4, M6, M10 and M17) with 3 sensors replicated along the TA depth; 4 sensors located in the zones near the Rails (M2, M5, M12, M15).
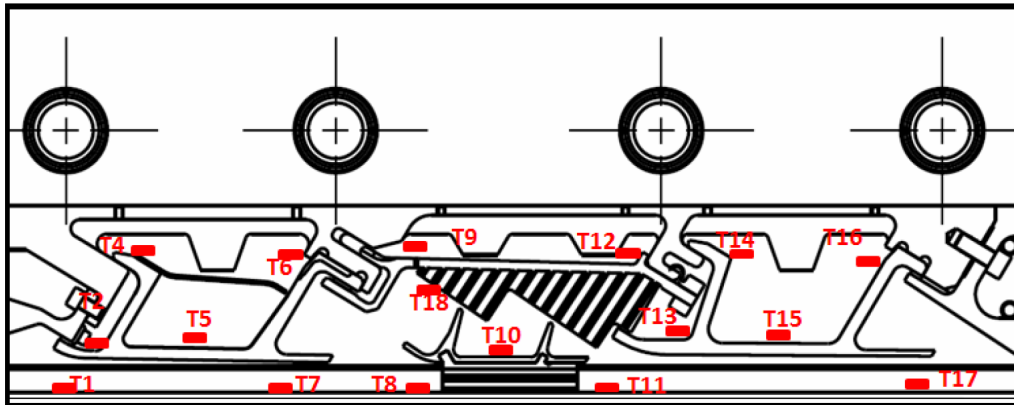
Figure 2.9: Air thermocouples position and nomenclature
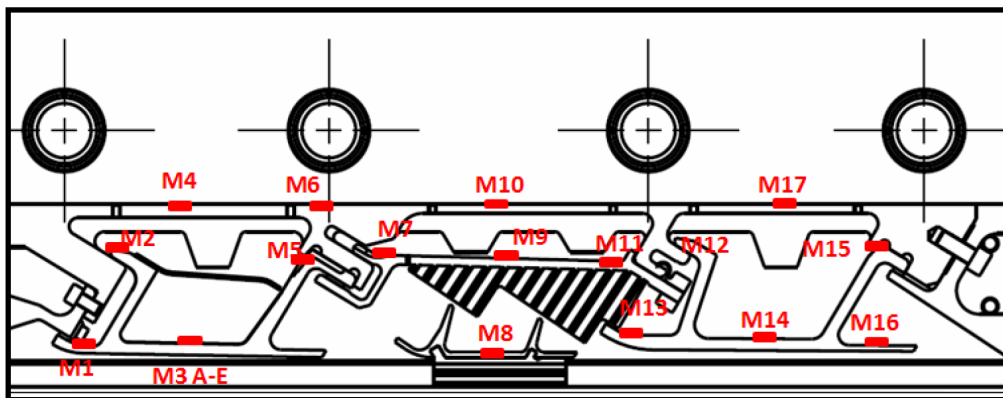
Figure 2.10: Metal thermocouples position and nomenclature

2.4 Data acquisition system

A specific computer program, specifically implemented, by using the Labview software, for the Thermalcase rig, allows the remote management of the rig instrumentation signals.

The remote control system is capable of performing data storage, rig operability control and rig and test parameters monitoring by means of PID closed

loops. All the measurements are live monitored, during the testing operations, by using the control panel reported in Figure 2.11.

In addition, all the pressures and temperatures acquired, within the TA during the rig operation, are recorded by using the SignalExpress software.
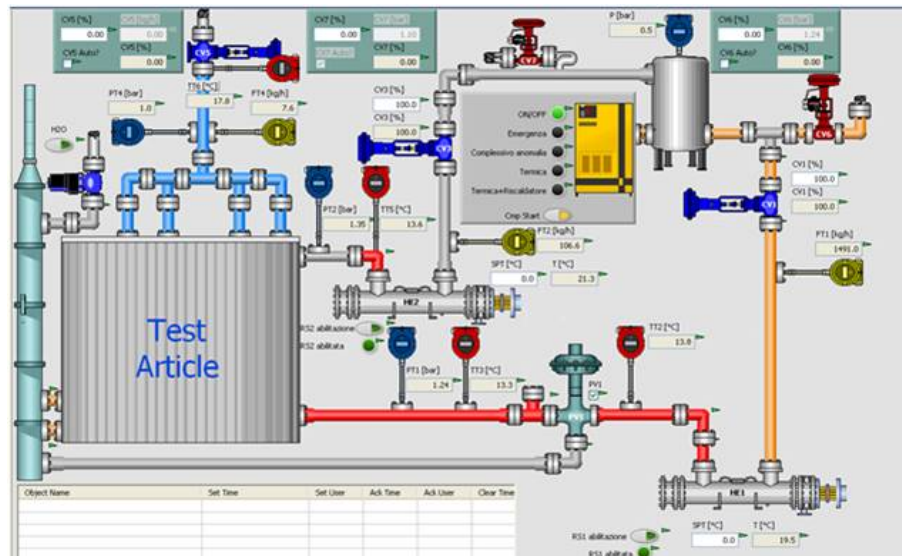
Figure 2.11: Thermalcase control panel

2.5 Test campaign

A series of test campaigns have been performed using the Thermalcase rig, in order to investigate the turbine fluid and thermal behavior, by varying the main control parameters.

The test campaign (test matrix shown in Figure 2.12) of interest for this thesis can be subdivided in two main phases. During the first phase, tests have been performed with the full amount of Coo air and without thermal blankets. The tests have been carried out at two different FP temperatures equal to 723 K and 873 K and at two Coo temperatures equal to 473 K and 573 K, respectively. The results of these tests have been used as a *reference* for the study and comparison of the different insulating technologies introduced in the following chapters.

In general, all the experiments have been performed with:

- Cooling pressure ≈ 110% Flow Path pressure;
- Cooling base mass flow rate ≈ 10% Flow Path mass flow rate;
- Cooling mass flow rate variable: 100%, 75%, 50%, 25%;
- ACC mass flow rate ≈ constant values (0.013 kg/s);
- β ACC ≈1.05 ÷ 1.1
- ACC temperature ≈ room temperature.

In the second phase, the tests have been carried out by reducing the amount of Cooling air injected in the Casing cavities. In order to allow a correct comparison between the results obtained in the two phases, the tests in the second phase have been performed with the same inlet boundary conditions except for the Coo mass flow rate, which has been progressively reduced. Therefore particular attention has been focused on the regulation system with the aim to reproduce as faithful as possible the inlet conditions before set.

The pressure and temperature values, recorded during the phase 1 of the experimental campaign, have been used to tune the numerical model, as described in the following Chapter.

Test		FP pressure [bar]		Coo pressure [°C]		Flow Pat temperature [°C]				FP mass flow rate [kg/s]	Coo temperature [°C]		Coo mass flow rate [kg/s]			ACC mass flow rate [kg/s]
		1,4	1,8	1,4	1,8	400	450	500	600	base	200	327	base	base - 25%	base - 50%	base
1		x		x		x				x	x		x			x
2		x		x		x				x		x	x			x
3		x		x			x			x	x		x			x
4		x		x			x			x		x	x			x
5		x		x				x		x	x		x			x
6	Phase 1	x		x				x		x		x	x			x
7			x		x	x				x	x		x			x
8			x		x	x				x		x	x			x
9			x		x		x			x	x		x			x
10			x		x		x			x		x	x			x
11			x		x			x		x	x		x			x
12			x		x			x		x		x	x			x
13			x		x					x		x		x		x
14			x		x					x		x			x	x
15	Phase 2		x		x		x			x		x		x		x
16			x		x		x			x		x			x	x
17			x		x			x		x		x		x		x
18			x		x			x		x		x			x	x

Figure 2.12: Experimental test matrix

Chapter 3

Numerical Approach

3.1 Numerical models

The first important requirement for a numerical model, in order to correctly simulate what happens inside the turbine, is to be able to reproduce all the thermal and fluid phenomena. In other words, it has to reproduce both the fluid and thermal fields resulting from the main flows, and also the impact on the turbine thermal behavior due to the leakages among the different components influencing the final temperature distribution. Therefore, due to the close correlation between fluid and thermal fields, the final numerical model has to be multidisciplinary.

For this reason, the numerical model developed for the TA [22] has been implemented by using two software packages, working in an integrated way by running alternatively the fluid-dynamic and the thermal calculation. The first one, Flowmaster, is used for the fluid field simulation and the second, MSC Patran Thermal, to evaluate the thermal field.

The TA numerical model, here considered, doesn't include the structural analysis, required in an actual engine model, because the deformations taking place in the clearance zone, due to the main loads, can be considered negligible.

In fact, in an actual engine the turbine clearances are subjected to great deformations due to centrifugal forces, aerodynamic forces, high pressures and temperatures. In the TA these deformations are certainly more contained considering that: the TA is static, and so it does not undergo centrifugal forces; the TA is not equipped with the entire blade and its disk, but only the blade tip is reproduced, therefore, the aerodynamic forces are null (Flow Path stream does not run over rotating parts) and the thermal field can produce only very small tip deformations; finally, the operating pressures, arising during the experiments, are lower than in an actual engine.

Moreover, even if the software, used for the thermal calculation, allows both 3D and 2D studies, for this application a 2D study has been chosen, introducing another simplification at the model level, considering that, during the design

phase, the problem can be simplified as an axisymmetric problem [23], simulating only an averaged behavior in the direction transverse to the flow, i.e. the TA depth. The use of a 3D modeling, instead, would require high calculation powers and times. For this reason, the availability of a numerical model, easy to handle and fast to run, has been considered more important.

In the following paragraphs, a short description about the models (fluid and thermal) and about how they are involved in the integrated simulation is provided.

3.1.1 Fluid network

Typically, the LPTs are characterized by the presence of two main streams (FP and Coo), at different temperatures (hot and cold), which flow and interact with each other. For a more in depth thermal analysis, therefore, the fluid dynamic calculations and the knowledge of both the mass transfer (e.g. hot flow leakages from the FP to the Casing cavities, even if small, could significantly warm up the Casing surface) and the fluid flows properties (e.g. mass flow rate and pressure) are of primary interest.

The method applied to simulate the fluid flows in the Test Article is the fluid network approach, commonly utilized in the aircraft engine secondary ducts as an alternative to the CFD techniques. The fluid network approach is particularly helpful during the design phase, when a high number of variables are involved, because this method allows to reduce considerably the calculation time.

As previously said, the fluid field modeling is implemented, by means of the software Flowmaster, drawing a 1D fluid network, shown in Figure 3.1, which sketches the TA flows. The main 1D elements employed to build the fluid network are: *"Orifice"* type, which are the ones more commonly used, representing the passage areas from a cavity to another; *"Discrete Loss"* type, placed especially in the FP area, simulating the distributed pressure drops inside a pipe; *"Hot Clearance"* type, placed in the clearance region, to simulate the sealing effect; *"Source"* type, located at the inlets and at the outlet of the TA, reproducing the boundary conditions (pressures and mass flow rates). In particular, the *"Hot Clearance"* elements are customized elements (working as a black box for the user), able to reproduce the air leakages between the blade tip and the honeycomb seal. These customized elements require as input all the geometrical information describing the clearance region as, for instance, the distances between the blade tip and the honeycomb cells, the length and the inclination angle of the blade teeth, etc..

Moreover, as it is possible to observe in Figure 3.1, the fluid network represents only the TA cavities placed below the Casing, where the FP and Coo streams flow. In fact, in the upper part, where only the ACC flows, the pressure, the mass flow rate and the temperature are input data, directly set up in the thermal analysis, and therefore calculations performed by using a fluid network are not required.
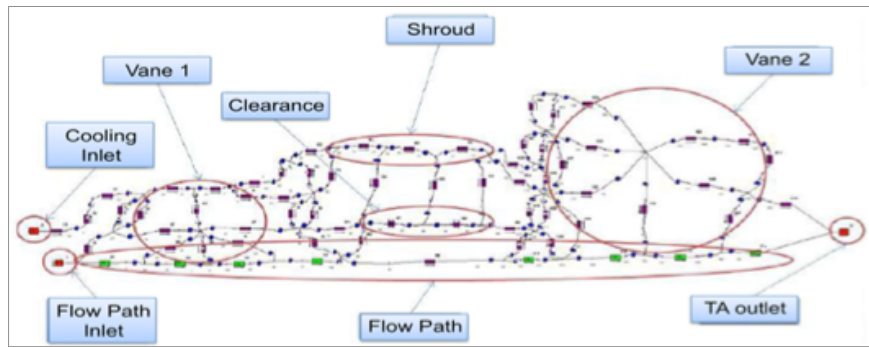
Figure 3.1: Test Article fluid network [22]

3.1.2 Thermal model

The thermal model, shown in Figure 3.2, as already said, is not a 3D but simply a 2D model. The 2D model has been created, by using MSC Patran Thermal, with finite elements 2D, solid, 4 knots QUAD4 (fluid and metal nodes) and reproduces one representative section of the test bench. In order to take into account the third dimension, the material properties (density and thermal conductivity) have been properly scaled, considering the material void-solid ratio in the TA depth direction, and suitable boundary conditions have been set.

With the aim of reproducing in the thermal model exactly the same 1D fluid network, described above, "advection bars" (i.e. 1D elements with 2 nodes and a mass flow rate flowing in an assigned direction) have been used, simulating both the airflow and the heat transport. In fact, except for the bars used to simulate the ACC flow, each fluid bar in the P-Thermal model has a corresponding element in Flowmaster.
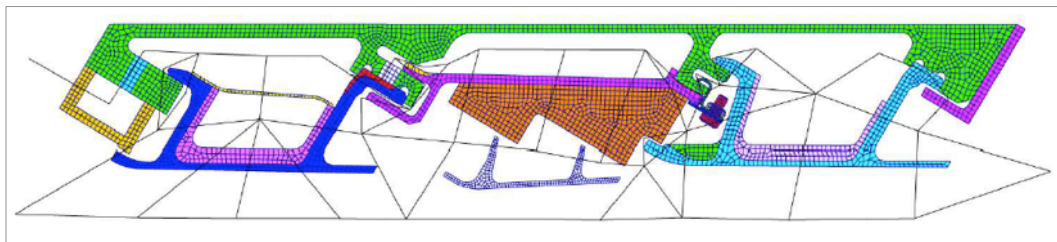
Figure 3.2: 2D TA model (mesh and fluid network)[22]

In the TA all the three heat transfer mechanisms are present: radiation among the cavity surfaces and conduction through metal components, convection heat transfer between the fluid and solid surfaces. In particular, the heat transfer by radiation is managed connecting the FEM elements of the involved surfaces, while the software directly evaluates the contributions due to the heat transfer by conduction, simply requiring the material properties as inputs. The heat transfer by convection between a fluid node (having a specific air temperature and pressure, read in Flowmaster) and a solid surface is obtained connecting the node

with the proper solid element surfaces and by setting the heat transfer coefficients (HTC). The information about the fluid node air temperature and pressure are read in Flowmaster as well as the mass flow rate associated with the fluid bar. Moreover, suitable coefficients, which consider the material void-solid ratio in the TA depth direction, have been set in order to take into account the third dimension. In this way it is possible to correctly evaluate the heat transfer in some TA zones as, for instance, the clearance one, where the honeycomb structure, over the blade shroud, is modeled as a solid.

3.1.3 Integrated simulation

The turbine thermal behavior is the result of the mutual influence of fluid dynamic phenomena, heat transfer and heat balance within each component, and of structural deformations due to mechanical and thermal loads.

The study of these complex phenomena separately may lead to the introduction of a certain number of approximations. Hence, the phenomena occurring inside a turbine have to be faced, as previously said, with a multidisciplinary approach.

The two software packages, taken into consideration, work in a coupled way allowing managing a fully associated numerical model (Figure 3.3). P-Thermal gets inputs from Flowmaster about the mass flow rates, the pressures and the temperatures. By using the first two inputs, P-Thermal recalculates new values for the temperatures that are then compared with the ones provided by Flowmaster. If the convergence is not reached, Flowmaster is run again with an iterative process during which the last calculated temperatures are reintroduced in Flowmaster, until an integrated compatible solution between the numerical solvers is obtained.

For more details about the integrated procedure of a multidisciplinary thermal and fluid analysis, applied to turbine engines, refer to [23].
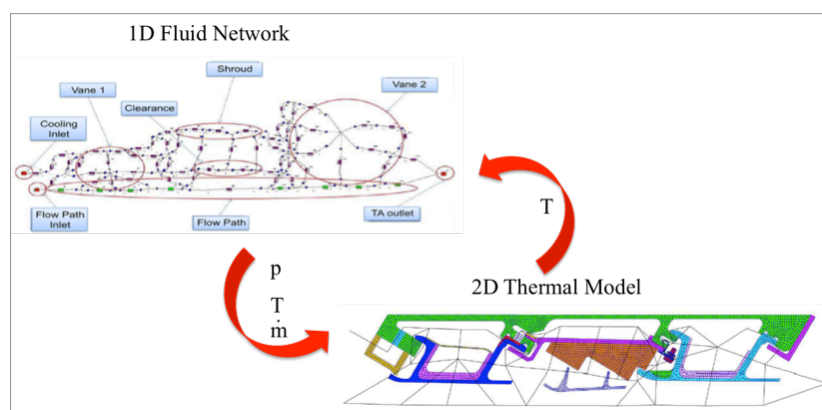
Figure 3.3: Integrated simulation sketch

As well known, even if the convergence is reached, this is not sufficient to state that the model is able to accurately describe the physics of the involved phenomena. To have a well-tuned numerical model, a calibration process, performed by using data provided by experiments, is required.

3.2 Numerical models tuning

To start the tuning procedure, an initial check of the discrepancies between the numerical and the experimental data must be carried out simply by running the model with the same experimental boundary conditions (i.e. the inlet pressures and temperatures for the three flow lines, the outlet pressure and temperature for the FP and the mass flow rate for the ACC line), as shown in Figure 3.4.
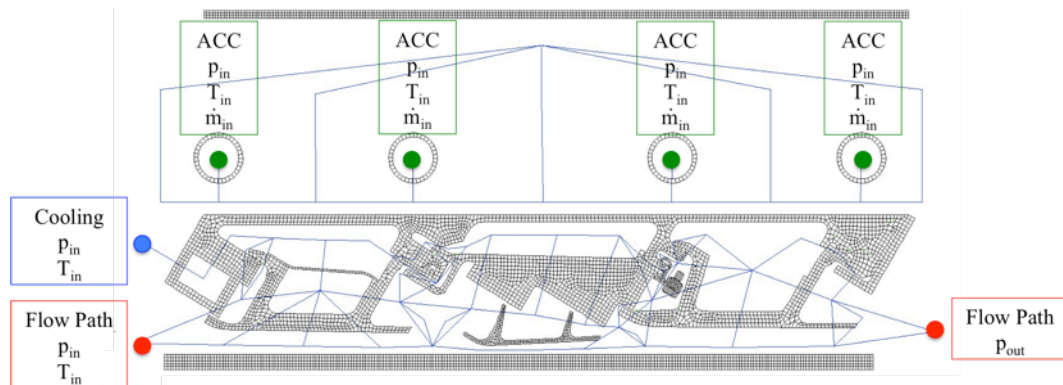
Figure 3.4: Numerical model boundary conditions

The pressure (Figure 3.5) and temperature (Figure 3.6) values, obtained by running the numerical model, are then compared with the ones recorded by the corresponding TA sensors, by calculating the differences.
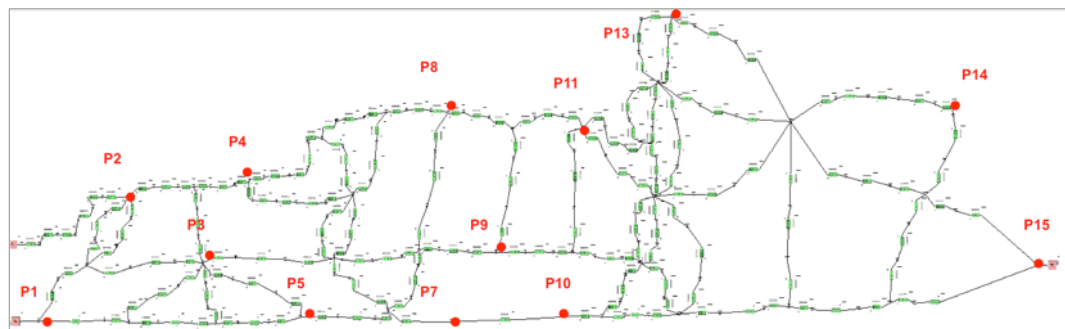
Figure 3.5: Pressure gauges position in the fluid network [22]

On the basis of this first check, it is possible to start the tuning procedure (Figure 3.7), for the fluid and thermal models, called in what follows Thermal Match (TM).

The TM is an investigation technique that allows defining the thermal optimum. In other words, this technique allows assigning specific values to some significant parameters, in order to get a numerical thermal mapping equal to the one experimentally obtained.
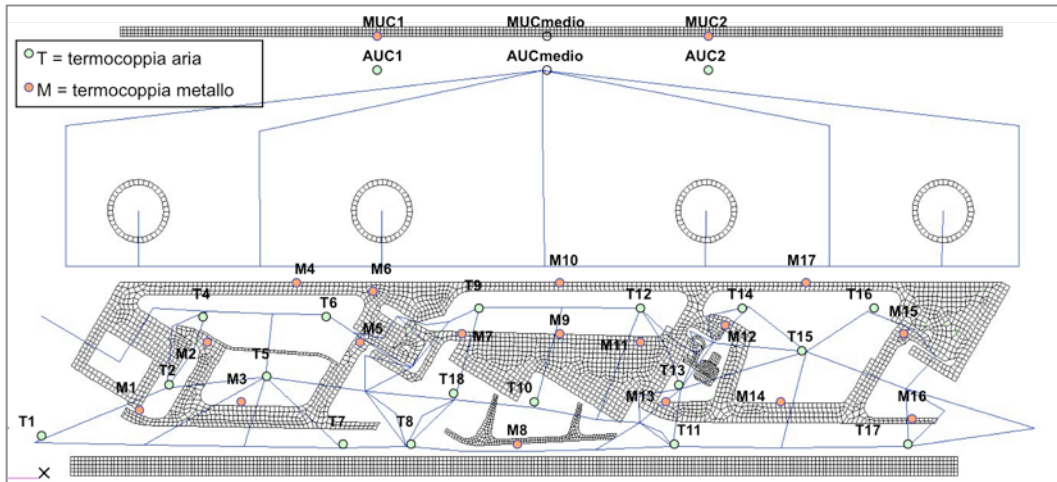
Figure 3.6: Thermocouples position in the thermal model [22]
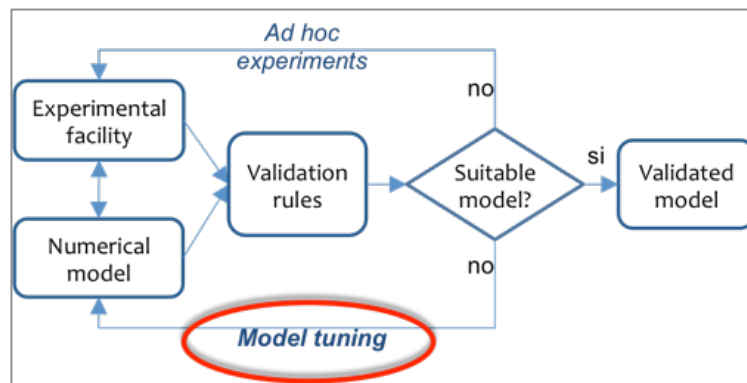
Figure 3.7: Tuning model procedure

The adopted strategy for the TM is based on the optimum problem formulation, associated with the reduced problem shown in Figure 3.8 (red box).

In fact, the procedure reference area, used to minimize the discrepancies between the numerical and experimental values, has been reduced, assuming the numerical models free of mistakes. Thus, in what follows, the analysis of possible errors, due to a wrong modeling, is neglected, since it has been considered to be beyond the TM purposes here described.

The analysis and simulation problem for the TA application involves:

- A physical/experimental device of the studied system. This device provides the reference data, recorded under specific operating conditions, in terms of pressure (p_{exp}) values, air temperature (T_{exp}) and metal temperature (M_{exp}) values;

24

- Two integrated numerical models for the simulation of the fluid and thermal behavior of the studied system. In this case, the fluid and thermal models, described above, and in particular their optimization variables, are involved. The optimization variables are:

  - The dimensionless coefficients Cd presented in the constitutive relations of the isentropic loss elements inside the fluid network;

  - The dimensionless coefficients Hmult, i.e. the HTC (Heat Transfer Coefficient) multipliers, presented in the constitutive equations of the convective heat transfer correlations in its free and forced components.
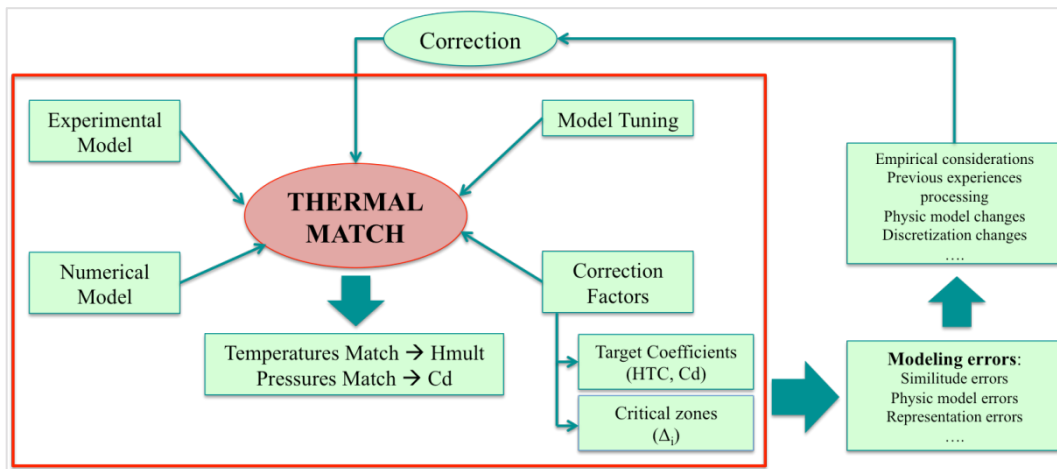
Figure 3.8: Thermal Match problem schematization

The two models work in an iterative way until the convergence is reached with the aim of calculating pressure, mass flow rate and temperature values along the ducts of the studied system, under specific operating conditions (the same conditions considered for the experimental tests).

Taking into account this TM structure and the data to be managed, the TM is described as an optimization problem so defined:

$$min_{(Cd,Hmult,Amult)} J(Cd, Hmult, Amult) = \sum_{i=1}^{N_a} \Delta T_{i,air} + \sum_{i=N_a+1}^{N_{a}+N_m} \Delta T_{i,metal} + \sum_{j=1}^{N_p} \Delta P_i$$

$$
\begin{cases}
\Delta T_{i,air}^{MIN} \leq \Delta T_{i,air} \leq \Delta T_{i,air}^{MAX} & i = 1:N_a \\[4pt]
\Delta T_{i,metal}^{MIN} \leq \Delta T_{i,metal} \leq \Delta T_{i,metal}^{MAX} & i = N_a + 1 : N_a + N_m \\[4pt]
\Delta p_j^{MIN} \leq \Delta p_j \leq \Delta p_j^{MAX} & j = 1:N_p
\end{cases}
$$

$$
\begin{cases}
H_{mult,conv1}^{MIN} \leq H_{mult,conv1} \leq H_{mult,conv1}^{MAX} & conv1 = 1:2N_1 \\[4pt]
H_{mult,conv2}^{MIN} \leq H_{mult,conv2} \leq H_{mult,conv2}^{MAX} & conv2 = 1:2N_2 \\[4pt]
A_{mult,conv3}^{MIN} \leq A_{mult,conv3} \leq A_{mult,conv3}^{MAX} & conv3 = 1:N_3 \\[4pt]
Cd_l^{MIN} \leq Cd_l \leq Cd_l^{MAX} & l = 1:N_{isent} \\[4pt]
f_{conv1}(H_{mult,conv1}) = 0 \quad H_{mult,conv1} = [H_{mult,conv1}^{free}, H_{mult,conv1}^{forced}] & conv1 = 1:N_{conv1} \\[4pt]
f_{conv2}(H_{mult,conv2}) = 0 \quad H_{mult,conv2} = [H_{mult,conv2}^{free}, H_{mult,conv2}^{forced}] & conv2 = 1:N_{conv2} \\[4pt]
f_{conv3}(A_{mult,conv3}) = 0 \quad conv3 = 1:N_{conv3} \\[4pt]
f_{isent,l}(Cd_l) = 0 \quad l = 1:N_{isent}
\end{cases}
$$

Before accomplishing the effective tuning procedure, some preliminary activities, described in what follows and sketched in Figure 3.9, must be performed.
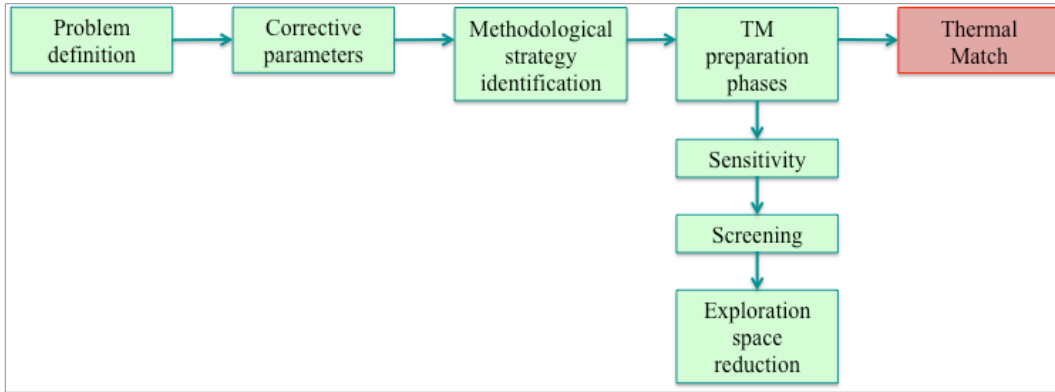
Figure 3.9: TM preliminary activities sketch

3.2.1 Problem definition

The aim of the TM is to perform the numerical models calibration so that the temperature and pressure values, evaluated by running the numerical model, exhibit the minimum discrepancy (D_i) with the corresponding values experimentally recorded.

Suitable maximum values have been fixed for the allowed discrepancies ΔT_i and Δp_i.

$$\Delta T_i = \left| T_{experimental\_i} - T_{numerical\_i} \right| \tag{1}$$

$$\Delta p_j = \left| p_{experimental\_j} - p_{numerical\_j} \right| \tag{2}$$

Where ΔT_i (Eq.1) is the difference between the temperature experimentally recorded and the one numerically calculated in correspondence with the i-th reading point, while Δp_j (Eq.2) is the difference between the pressure experimentally recorded and the one numerically calculated in correspondence with the j-th reading point.

A cross-check on the values of the discrepancies, evaluated in neighboring and consecutive locations, allows identifying as a "suspicious case" the one for which the difference $|D_{i+1} - D_i|$ between adjacent discrepancies is too high and/or the two values (D_{i+1} and D_i) have opposite signs.

3.2.2 Corrective parameters

The corrective parameters are coefficients that directly affect and calibrate the physic relations used for the numerical simulation. Their identification is based on the following considerations:

- *Thermal analysis contribution*: regarding the thermal analysis the involved correlations are those related to conduction, radiation and convection.
  - *Conduction*: it depends on materials, geometry and discretization. If the numerical model is congruent with the physical device, this type of heat exchange is not to be considered the more critical from the numerical - experimental match point of view. Being the numerical model congruent with the TA, because the model material sheet is compiled with the TA materials proprieties, this correlation will not be corrected.
  - *Radiation*: it is important when high temperature gradients between the facing surfaces are present and this is not the case. So also radiation will not be considered for the thermal match.
  - *Convection*: it is considered the main reason of discrepancy between the numerical model and the physic/experimental device. In fact, the convective heat transfer coefficients are evaluated by using data, e.g. the temperature, which, being directly calculated by the model may be different from the experimental ones. If these differences are small, it is possible to act on the involved coefficients, calibrating them; if the differences are relevant it is compulsory to understand the reasons of this great discrepancy. For small differences, it is possible to modify the heat transfer

27

coefficient (HTC) by means of the multiplier Hmult. Due to the presence of free and forced convective phenomena, the same correlation usually contains a couple of multiplier factors (Hmult free and Hmult forced).

- *Fluid network contribution*: Regarding the fluid network, the more relevant elements for the thermal match problem are those modeling the isentropic losses. The "isentropic loss" model takes into account the dimensionless factor, Cd, defined as the ratio between the effective passage area, used by the solver to simulate the phenomenon, and the real geometrical one. This coefficient, therefore, is applied for the correction of the area utilized in the isentropic mass flow rate calculation.

By taking into account the technical, procedural and empiric considerations, previously reported, it is possible to state that the Thermal Match procedure has to:

1. Perform a numerical calibration of the models through the comparison with the experimental data, identifying the corrective values of the factors (Hmult and Cd) for which it is possible to obtain a minimization of the discrepancies between the temperature and pressure values experimentally recorded and numerically calculated.
2. Highlight the target values of the coefficients (HTC, Cd), in order to indicate if, in the examined region, the numerical model correctly reproduces the physics of the problem. A check of the absolute values and of the signs of the discrepancies, between the experimental and calculated values, suggests if the used corrective factors must be increased or decreased.
3. Highlight the zones in which the numerical model doesn't work correctly. In other words, the TM procedure has to highlight where high corrective coefficients should be used in order to match the experimental results, detecting possible errors in the numerical model.

3.2.3 Methodological strategy identification

In order to identify the operative strategy for the methodology development, the main features of the problem and the available methodological strategies have been considered.
The Thermalcase problem is:

- **Multidisciplinary.** The simulation problem is considered as characterized by a single discipline, the integrated fluid-thermal analysis. The integrated simulation is considered as a black-box and

therefore what happens inside the box is negligible. In this way, the problem belongs to the MDO (Multi Disciplinary Optimization) family [24-26].

- **Multivariable.** The optimization problem depends on a large number of significant variables and therefore it is a multidimensional problem. In this contest, a deepened analysis of the input variables, showing a high impact on the outputs, is important. For this reason, a methodology based on the screening of the variables is useful to reduce the dimensions of the optimization problem, with a consequent decrease in computational time. Among the different available methodologies, for the TM problem, a strategy, based on the evaluation of the elementary effects, has been implemented. In particular, by using the Morris algorithm [27], a sampling of the space of the variables has been performed. The implemented sampling is a radial type strategy, which starts from the quasi random DOE (Design of Experiment), and is stratified and space-filling. The number of sampling tracks has been evaluated by considering the dimensions and the extension of the exploration space by means of heuristic considerations developed on an empirical base. The elementary effects, of the input variables on the outputs, have been evaluated starting from this exploration.

- **Multi-objective.** The optimization problem can be considered a multi-objective problem because it aims to achieve two specific targets: the minimum evaluation in the ΔT and Δp values. Being the space of the solutions characterized by many different dimensions, discontinuity and no linearity, the useful algorithm for the exploration of the space, in researching the optimal solution, has to be chosen between the *Scalarization approach* and the *Pareto approach* [24,28,29]. As, for this specific application, it is not possible to identify targets that can be considered more significant than others, the Scalarization method must be excluded. The used algorithm is, therefore, based on the Pareto approach [31].

3.2.4 Thermal Match preparation phases

The main preparation phases, performed before accomplishing the Thermal Match, are: the sensitivity phase and the screening phase together with the analysis of the elementary effects. In what follows, a short description of these phases is reported.

Sensitivity

During the sensitivity phase the total design space, defined by all the design variables, is explored. In this application case, the design space is made of 201 thermal variables, related to the Hmult coefficients, and of 135 fluid variables, associated to the Cd coefficients. Therefore, the design space is defined by 336 dimensions. Moreover, for each kind of variable (fluid and thermal), two values are set as the minimum and the maximum bound, identifying the variation range for the coefficients.

As previously explained, the algorithm chosen for the space sampling is the Morris one, which allows evaluating the variables in terms of elementary effects.

With the aim to obtain a radial Morris sampling, two sampling of points r "*latin hypercube*[1]", in the design space with k dimensions (k=336), are used, obtaining the A and B matrices. The radial design technique (Figure 3.10) consists in starting from a point (located in the i-th row of the A matrix), considered as a reference, and in moving in the radial direction along the k dimensions, the element (j) in the i-th row of the A matrix (a_{ij}) is substituted with the corresponding one in the B matrix (b_{ij}). The same procedure is applied for all the r points, in order to provide, at the end of the sampling, the Morris algorithm with a number of points equal to $N = r (k+1)$. In order to perform a good sampling, the r parameters have to assume values between 10 and 20. This is the reason why, in this application, r has been set at 10.

$$
\begin{matrix}
a_{i1} & a_{i2} & \cdots & a_{ij} & \cdots & a_{ik} \\
b_{i1} & a_{i2} & \cdots & a_{ij} & \cdots & a_{ik} \\
a_{i1} & b_{i2} & \cdots & a_{ij} & \cdots & a_{ik} \\
\vdots & \vdots & \vdots & \vdots & \vdots & \vdots \\
a_{i1} & a_{i2} & \cdots & b_{ij} & \cdots & a_{ik} \\
\vdots & \vdots & \vdots & \vdots & \vdots & \vdots \\
a_{i1} & a_{i2} & \cdots & a_{ij} & \cdots & b_{ik} \\
\end{matrix}
$$

Figure 3.10: Radial design technique schematization

The sensitivity phase has been carried out by means of the software Matlab.

At the end of the process the Matlab output will be an R matrix containing in each row the data obtained during one simulation.

Screening and Elementary Effects evaluation

During the screening phase, all the design input variables are analyzed, evaluating their effects on the outputs. At the end of this phase, the design space dimensions are reduced.

---

[1] *Latin hypercube:* statistic technique utilized in the multidisciplinary approach

Among the available screening techniques, as just said, the one used for a complete space exploration, named DOE Morris 1991, is based on the evaluation of the elementary effects. The elementary effect of the j-th element, calculated referring to the output y (x), in a x= (x$_1$,…, x$_k$) point, is defined as EE$_j$ (x):

$$EE_j(x_1, \ldots, x_k) = \frac{y(x_1,x_2,\ldots,x_{j-1},x_j+\Delta_j,\ldots,x_k)-y(x_1,\ldots,x_k)}{\Delta_j} \qquad (3)$$

where k is the number of the input variables and Δ_j is the distance between the reference point x and the considered point along the j direction, related to the j-th input.

Since EE$_j$ represents a local measure, the average of the EE$_j$ absolute values, referred to the r sampling points, is defined as:

$$\mu_j^* = \frac{\sum_{i=1}^{r}|EE_j|}{r} = \mu_j^*(x_j) \qquad (4)$$

The results obtained during the screening and EE analyses are graphs, one for each analyzed temperature, showing the effects (μ_j^*) of each variable on the outputs in comparison with the experimental data.

Thanks to the screening analysis, it is possible to identify a certain number of variables to be used for the real Thermal Match, reducing the exploration space. The variables to be examined are the ones with a greater effect (high μ_j^*) in almost all the graphs. Moreover, since for all the temperatures the variables showing a higher impact are those related to the convective correlations applied in the near zones, it is possible to state that the problem is correctly defined. In fact, even if the sampling is quasi random, the stream direction is respected and so what is downstream is affected by what is upstream.

3.2.5 Tolerance criteria

Tolerance criteria have been set for the pressures and temperatures match on the basis of the common engine practices:

- Tolerance on Δp (experimental-numerical) has been set equal to the maximum value observed between the accuracy of the pressure transducer (± 0,009 bar) and 5% of the difference between the TA inlet and outlet pressures, experimentally measured.

    Pressure tolerance = max [5% (p$_{in}$-p$_{out}$), instrument precision]   (5)

- Tolerance on ΔT (experimental-numerical) has been set equal to 5% of the difference between the inlet and outlet temperatures of a common LPT (Figure 3.11).

$$\text{Temperature tolerance} = T_{in} - T_{out} \approx 26 \text{ K} \qquad (6)$$
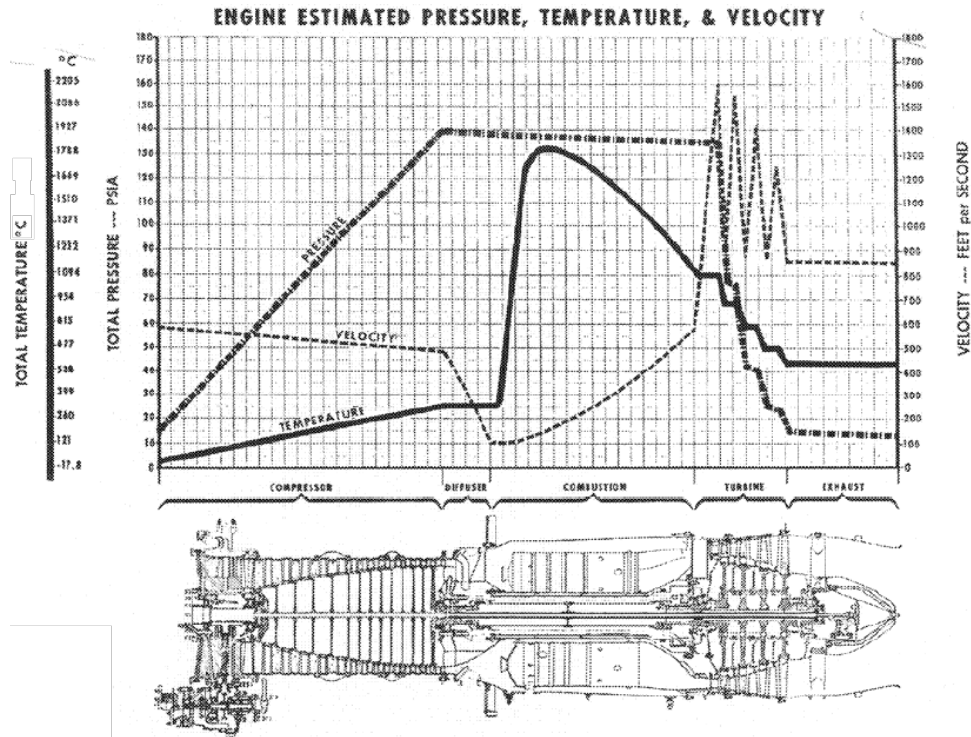
Figure 3.11: Common turbine temperatures [32]

3.2.6 Tuning methodology

The screening phase and the EE analysis, previously introduced, have allowed identifying the relevant variables, reducing the number of coefficients to be managed during the Thermal Match procedure. On the basis of these first results, the calibration procedure for the fluid and thermal models has been started.

The procedure, unlike what has been done during the preparatory phases, has been carried out manually because it requires not only a deep knowledge of the model, but also of the involved physical phenomena, in order to critically evaluate the obtained results. Moreover, performing the tuning procedure manually allows not only to calibrate the presented model but also to identify a standard method applicable whenever a similar case study must be developed.

In what follows, a brief description of the applied tuning procedure is reported (Figure 3.12), while further details are reported in [22].

Because of the difficulty to simultaneously manage a very large number of parameters, the Thermal Match has been performed in two steps, carried out in series, due to the mutual influence of the fluid and thermal fields (by changing the pressure, the air flow distribution changes and, consequently, also the temperature distribution, and so on). First of all, the calibration process of pressures has been

32

carried out by changing the discharge coefficients (Cd) and by obtaining a suitable set of values. Subsequently, using the results, obtained with the matched fluid network, the temperatures tuning has been performed by changing the heat transfer coefficients (HTC) through the introduction of corrective factors. In addition, the resulting HTCs have been critically evaluated in order to avoid altering the physical phenomena occurring within the TA.

The match procedure for the fluid network has been performed in the opposite direction to the airflow, analyzing the components near the TA outlet, first, and, then, going back to the TA inlet. After each Cd change, the resulting effects, not only on the examined area, but also on the global network, have been evaluated.

On the contrary, the tuning of the temperature values have been carried out, in the airflow direction, by performing "global" changes, which have an immediate impact on all the TA areas, and, then, by carrying out "local" focused changes, in order to reduce the differences between the calculated and measured temperatures.

With the aim of confirming the final model accuracy, over a wide range of TA inlet temperatures and pressures, the Thermal Match has been carried out referring to only a specific experiment. Then the accuracy of the tuned model has been verified by running it with the boundary conditions used for the other experiments.
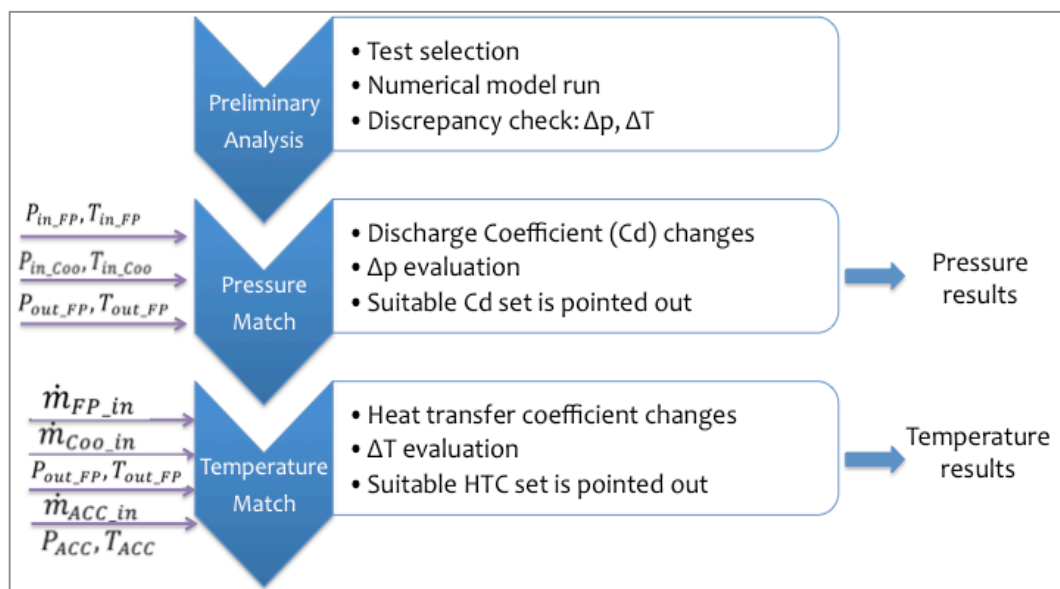
Figure 3.12: Thermal Match procedure details

3.2.7 Tuning results

In this section, in order to show the results of the tuning procedure, the differences between the experimental and numerical values, for both the temperatures and the pressures, obtained after the Thermal Match procedure application, are provided. Moreover, with the aim of bringing out the tuning

quality, the same differences, between the experimental and numerical values, calculated, this time, before the Thermal Match, are also shown.

Here, for briefness, only the results obtained by using one set of experimental data, the one used to carry out the Thermal match, are shown. This test is the one exhibiting the maximum ΔT ($T_{FP} - T_{Coo}$) between the temperatures at the inlets; in fact, during this test, the temperature is set at 873 K for the Flow Path mass flow rate and at 473K for the Cooling mass flow rate.

In Table 3.1, the differences pre-Thermal Match between the experimental and numerical values, both for the pressures (Δp) and the temperatures (ΔT), are reported.

As it is possible to observe, all the calculated Δp are outside the tolerance range except the ones concerning the sensor P1 and P15, because, initially, these values have been chosen as boundary conditions during the Flowmaster simulations. A similar situation can be noted by examining the ΔT columns where only four sensors satisfy the tolerance criteria, and one of them, T1, is a boundary condition for the P-Thermal run. In Table 3.2 results obtained after the application of the tuning procedure are shown. In the considered case, the total number of sensors exhibits Δp and/or ΔT values in the tolerance ranges. It is to be noted that, in this case, the Δp evaluated for the sensor P1 is different from zero because its value, during the tuning procedure, has been numerically calculated and not set as a boundary condition, as in the initial comparison. For the tuning of the fluid model, the inlet pressures, both for the FP and for the Coo line, have been substituted with the corresponding two values of the inlet mass flow rates, while, the inlet temperatures and the FP outlet pressure and temperature have remained set as boundary conditions (Figure 3.13).
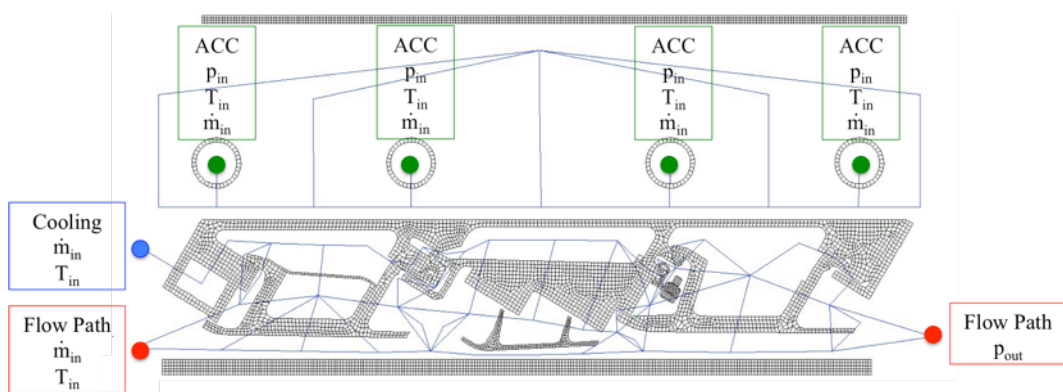
Figure 3.13: New numerical model boundary conditions

The reason of this boundary change depends on a problem concerning the calculation of the FP and Coo inlet mass flow rates.

In fact, in performing the match of the fluid network, given that the pressures are boundary conditions, the mass flow rates values, calculated by Flowmaster, independently from the Cd used to tune the fluid model, have turned out to be different from the ones read by the mass flow meters, placed in the rig, by an

amount larger than the device accuracy. This behavior is explained by the fact that the input pressure (p_1), recorded for the FP, is measured within the TA, while the Coo inlet pressure is measured by the PT2 transducer, located, outside the TA, along the Cooling inlet pipe.

Moreover, the manual valve V4, providing a further pressure regulation, is displaced beyond the PT2 transducer, along the pipe. This valve causes an additional pressure loss, before the Coo enters into the TA.

Therefore, the setting of the FP and Coo mass flow rates as inputs of the fluid model allows a more correct calculation of the pressure values within the network.

Table 3.1: Δp and ΔT pre Thermal Match process

Pre Thermal Match								
	Δp			**ΔT**				**ΔT**
P1	0	✅	T1	0	✅	M1	44,7	❌
P2	-0,056	❌	T2	224,6	❌	M2	66,4	❌
P3	-0,070	❌	T4	21,2	✅	M3	4,7	✅
P4	-0,064	❌	T5	127,4	❌	M4	37,0	❌
P5	-0,038	❌	T6	27,6	❌	M5	39,5	❌
P7	-0,024	❌	T7	10,4	✅	M6	55,4	❌
P8	-0,072	❌	T8	29,3	❌	M7	28,4	❌
P9	-0,051	❌	T9	17,1	✅	M8	42,9	❌
P10	-0,037	❌	T10	45,6	❌	M9	65,7	❌
P11	-0,057	❌	T11	51,9	❌	M10	37,1	❌
P13	-0,034	❌	T12	55,7	❌	M11	62,1	❌
P14	-0,037	❌	T13	62,0	❌	M12	61,7	❌
P15	0	✅	T14	105,8	❌	M13	47,6	❌
			T15	74,9	❌	M14	56,8	❌
			T16	87,1	❌	M15	99,6	❌
			T17	49,9	❌	M16	56,7	❌
			T18	28,1	❌	M17	87,1	❌

✅ Tolerance respected
❌ Outside tolerance

Table 3.2: Δp and ΔT post Thermal Match process

Post Thermal Match								
	Δp			**ΔT**				**ΔT**
P1	-0,003	✅	T1	0	✅	M1	24,8	✅
P2	0,008	✅	T2	6,8	✅	M2	-2,1	✅
P3	-0,006	✅	T4	6,6	✅	M3	-0,9	✅
P4	0,000	✅	T5	12,9	✅	M4	0,1	✅
P5	-0,007	✅	T6	2,9	✅	M5	17,7	✅
P7	0,007	✅	T7	5,4	✅	M6	-8,8	✅
P8	-0,006	✅	T8	11,3	✅	M7	11,3	✅
P9	-0,007	✅	T9	20,0	✅	M8	10,0	✅
P10	-0,003	✅	T10	-7,5	✅	M9	25,8	✅
P11	0,009	✅	T11	26,0	✅	M10	-24,5	✅
P13	-0,004	✅	T12	25,6	✅	M11	19,6	✅
P14	-0,003	✅	T13	20,6	✅	M12	-9,8	✅
P15	0	✅	T14	23,7	✅	M13	9,8	✅
			T15	15,6	✅	M14	13,8	✅
			T16	-4,9	✅	M15	24,9	✅
			T17	24,4	✅	M16	19,1	✅
			T18	-24,6	✅	M17	-9,5	✅

✅ Tolerance respected
❌ Outside tolerance

In general, the results of the Thermal Match have shown a good agreement between the experimental and the numerical data. After the model tuning, the number of pressure sensors outside the tolerance range has decreased from 62% to 15%, with a maximum error, located in the second Vane region, lower than 1%. From the temperatures point of view, the total number of sensors is within the tolerance range, despite 75% of the starting values were outside the range. In this case, the maximum observed error is lower than 4,5% and is located in the Casing region.

On the basis of the obtained results, it is possible to state that the numerical model is able to describe, with a good accuracy level, the fluid and thermal phenomena taking place inside the TA. For this reason, this model can be used to study and forecast numerically the effects of the application of new technical solutions intended to achieve a new turbine concept with a lower environmental impact.

Chapter 4

Insulation technology

4.1 Introduction

As underlined in the introduction, the design of aircraft propulsion systems requires, for the new engine generation, combining very high efficiency with very low pollutant emissions.

The strategy identified to achieve these goals is the development of new technologies capable of optimizing the main parts of the engines.

In particular, in this thesis the attention has been focused on the LPT, because, in this frame, the turbine thermal control can play a particular role. In fact, the FP leakages crossing the clearance, because of the differential thermal expansions between the rotating blade tip and the external Casing, are responsible for the lower turbine efficiency.

Nowadays, the method applied to control and to minimize these gaps, in the LPT, consists in using a Secondary Cooling Air System. This system bleeds relatively cold air from one of the compressor stages and blows it onto the Casing (ACC air) or into the stator cavities (Cooling air), cooling down the Casing actively and controlling the thermal expansions and contractions of the components.

This countermeasure, though effective for the clearance control, has the disadvantage of representing a power loss for the engine and, consequently, of being responsible for the supplementary fuel consumption and for the reduction of the engine performance.

For this reason, the thermal control of the turbine, obtained by pointing out innovative solutions, capable of strongly minimizing these power losses, is considered one of the major areas of interest to be investigated in order to increase the engine efficiency.

In particular, a special focus will be laid on the reduction of the Cooling air, blown into the Casing cavities, as shown in Figure 4.1.
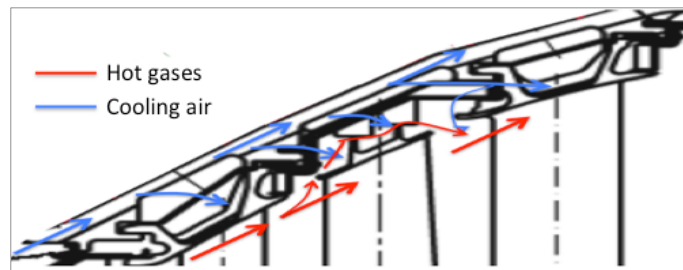
Figure 4.1: Cooling air blown into the Casing cavities

Furthermore, it is important to take into account that if an unsuitable Cooling method is used to cool down the Casing, local thermal cracks and structural failures, due to thermal stresses and reduced material strength at high temperature, could take place [33]. This extreme situation must be avoided considering the important roles played by the Casing of a gas turbine. In fact, the Casing main aims, from a structural point of view, are: to guarantee the turbine rotor axial symmetry, to keep elements, such as nozzles and shroud segments, in their fixed position; to tolerate the moment arising due to the loads related to components such as the exhaust chamber, the combustion chamber and the compressor; to tolerate failure of its moving parts such as the turbine blades.

The Casing, due to the relatively large thickness of its different parts, results particularly vulnerable to high temperatures and high temperature gradients between internal and external surfaces, producing phenomena of material deterioration and of mechanical and thermal fatigue.

Hence, in studying new technologies, capable of reducing the Cooling air, a particular attention will be focus on the Casing temperatures, since the feasibility of the air reduction is strictly bound by the need of keeping the Casing temperature below a certain level.

4.2 Available technologies overview

In this paragraph, an overview of the available technologies, exploitable for the minimizing of the Cooling air, is provided.

In the open literature, different kinds of methodologies are suggested to reduce the amount of air used to cool down the stator vane and the disk cavities:

- Morris et al. [34], to inhibit the ingestion of hot flow path gases into the circumferential locations of the turbine disk cavities, proposed an inhibitor of the disk cavity ingestion, realized by using supplementary cooling air, provided thanks to a set of cooling air holes, located on each side of the turbine nozzle airfoil trailing edge. This way, the cavity purge air, which enters into the disk cavity through the holes, produces dynamic pressure cooling air jets. These air jets force the incoming (ingestion) hot air to turn circumferentially and to go back in

the Flow Path before entering the turbine disk cavity. The consequence is a reduction in the hot gas ingestion and a decrease in the metal temperatures of the rotor and static structures.

Moreover, the amount of cooling air, required to purge the turbine disk cavities from the ingested hot Flow Path gasses, is reduced because the point of ingestion thereby needs less cooling air to maintain temperatures tolerable.

- Elovic [35] proposed an air-to-air heat exchanger to reduce the quantity of cooling air, bled from the compressor, required to cool down the hot parts of the turbine. The heat exchanger, located within the compressor bypass duct, uses the heat sink capability of the engine fuel to cool down the relatively cold air, heating up, at the same time, the fuel. The fuel is successively burned, reintroducing the extracted energy into the propulsive cycle.

- Lee at al. [36], instead, introduced a flow control insert device into the trailing edge cooling passages for the turbine vanes. This insert device is made of a thin strip of metal, formed with a wavy or a twisted shape, and of a top and a bottom support tab, perpendicular to the plane of the metal strip, which keep the insert in the center of the cooling passage. The insert causes an air flow acceleration and directs the cooling air against the vane walls, increasing the convective heat transfer between the walls and the cooling air, and reducing, consequently, the amount of the cooling air required.

These technologies, although effective for the reduction of the cooling air of the stator and of the rotor disks, need to be modified and adapted, in order to be applied to the Casing cooling air.

For this reason, these kinds of technologies have been considered difficult to be implemented.

A more promising strategy, to minimize the Cooling air, is the use of insulating technologies. These solutions have been already applied, for several purposes, to other parts of the engine. Some examples of insulating technologies are provided in what follows.

- *Insulating blankets* (Figure 4.2)*.* They are commonly used in exhaust systems, in turbochargers and in other heat generating elements of boats, ships, trucks and power generators. Generally, the blankets are made of an inner layer of fibrous insulating material encapsulated in an outer coat of thin stainless steel [37], [38]. Moreover, the blankets may contain a layer of fire-blocking material to be attached to adjacent structural frame members of the fuselage [39]. The operating temperatures of the materials, used to produce the blankets, allow the application inside the Casing cavities.
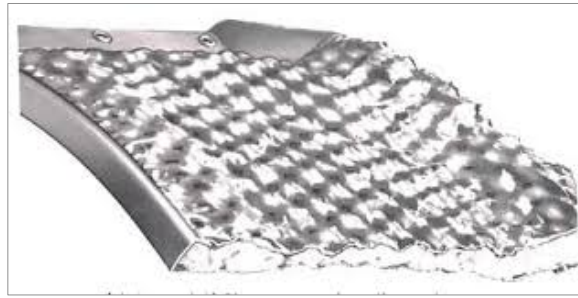
Figure 4.2: Insulating blanket [40]

- *Aerogel blankets* (Figure 4.3) [41]. They are typically installed as thermal barriers in combustors and/or turbine sections of a gas turbine engine. The insulating material is an Aerogel (preferred composition SiO_2 / Al_2O_3), with an operating temperature up to 923K, encapsulated between a composite layer and a backing layer. The composite layer is made of a resin matrix material with reinforcement fibers (glass). Its operating temperature can reach about 1073K without burning or charring. The backing layer has an operating temperature of about 473K and is used as a support for the blanket.
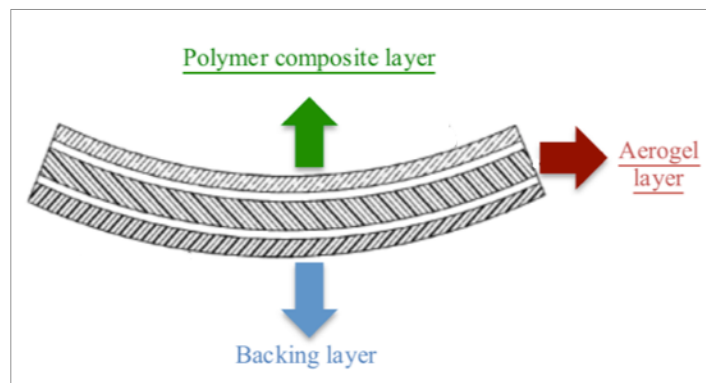
Figure 4.3: Aerogel blanket

Comparing the first kind of blankets, typically adopted to surround a core engine of a high by-pass gas turbine engine, denominated in what follows "Conventional", and the Aerogel ones (Table 4.1), with the same insulating materials and with the same thicknesses of the external layers, it may be noted that the two blankets have the same behavior when they undergo the fire test. Furthermore, the measured thermal conductivities are almost the same, while the Aerogel

blanket has a lower density compared to the conventional one (about 35% less than the other). Therefore, both weights being equal, a greater Aerogel thickness can be used in order to obtain better thermal insulation efficiency. The disadvantage of this kind of blankets is the low operating temperature of the backing layer material, which is not suitable for the application in the Casing cavities.

Table 4.1: Conventional vs aerogel blanket [41]

	Conventional blanket	Aerogel blanket
Composition	Silica particles, Metal oxides, reinforcement fibers	Aerogel, composite material (resin matrix with reinforcement fibers),backing composite material
Conductivities tests (@323K)	$\lambda \approx 0,054$ W/mK	$\lambda \approx 0,048 \div 0,052$ W/mK
Fire Test (direct flam for 1000s)	T range 973 ÷ 1173 K	T range 1073 ÷ 1273 K

- *Insulating Paints Cerablak$^\circledR$ HTP(High Temperature Paint)* Figure 4.4. Usually, they find application in furnace linings, heat exchangers, power generation, jet engine nozzles and exhaust structures.

  This solution differs entirely from the ones proposed above because the thermal insulation should be provided through the application of paints directly on the Casing inner surface.

  In particular, Cerablak is a high-emissivity spray-on coating, applicable to metal and ceramic surfaces that are exposed to high temperatures, in order to control the radiative heat transfer through a change in the surface emissivity. The emissivity values of Cerablak remain larger than 85% as long as the temperatures of the surface are lower than 1473 K. Moreover, the paints provide protection from oxidation, corrosion and fire for the components on which they are sprayed.
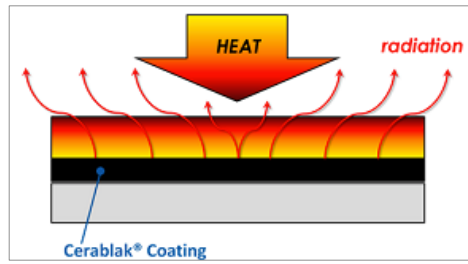
Figure 4.4: Cerablak$^{®}$ HTP [42]

4.3 Thermal Blanket

On the basis of the considerations introduced above, the strategy identified to perform a first attempt to control the thermal behavior of the LPT is the application, inside the proper turbine Casing cavities, of Thermal Blankets. The main advantage of this technique should be a lower amount of air bled from the compressor and used to cool down the Casing cavities, thanks to a reduced thermal load in the Casing region.

The Thermal blankets, experimentally tested in this work, are filled with a thermal insulating material (glass wool), with a low thermal conductivity and a good resistance to high operating temperatures (Table 4.2), enveloped by a very thin external metal layer, characterized by a high surface roughness. The external layer, indispensable to give a suitable stiffness to the inner downy structure, avoids the dispersion of the insulating material fibers and it facilitates, at the same time, the insertion of the blankets into the cavities.

Table 4.2: Insulating material proprieties

	Stone wool	Glass wool
Thermal conductivity [W/mK]	0,035-0,040	0,032-0,053
Density [Kg/m^3]	30-130	10-70
Specific heat capability [J/kgK]	1030	840-1030
Melting temperature [K]	1400-1600	1600-1800

In Figure 4.5 the flow chart of the performed activities is sketched. As it is possible to note, the main activities can be summarized in three macro steps: the numerical analyses, carried out comparing critically different insulation configurations, in order to find a suitable insulation methodology; the experimental validation step, during which the technology is experimentally tested; and the post processing analysis that is performed comparing the experimental and numerical data with the aim of evaluating the numerical model accuracy and of analyzing the possible upgrades of the proposed insulation solution.
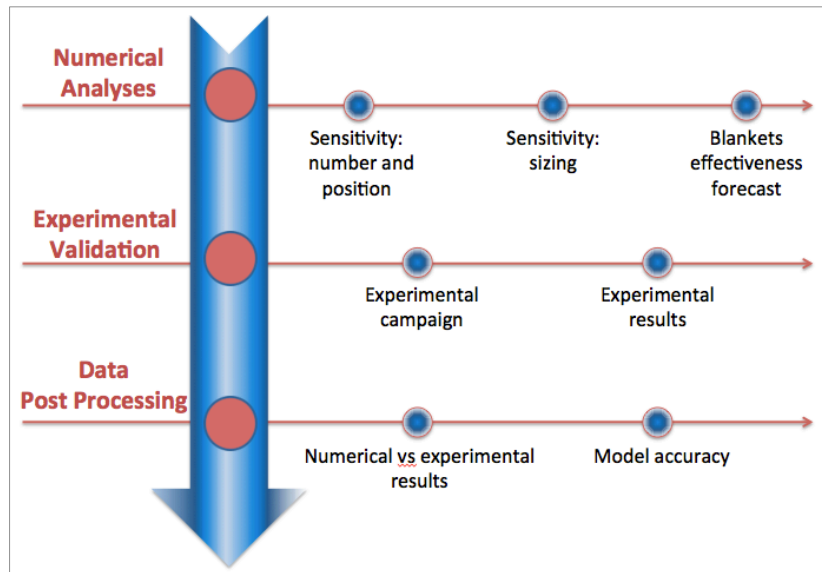
Figure 4.5: Thermal Blanket activities flow chart

4.3 Numerical analyses

The first step, carried out to study the new insulation technology, consists in a numerical analysis (Figure 4.6). This step was, initially, devoted to preliminary numerical analyses, performed with the purpose of identifying the suitable number of blankets, their position and dimensions and, subsequently, of studying the fluid and thermal effects resulting from the application of the insulating blankets. According to this thesis only the two most promising configurations, implemented to decrease the thermal load that the Casing undergoes during the operations, are reported.

Moreover, once the more suitable design of the blankets had been identified, supplementary analyses were carried out to forecast the effectiveness of the identified insulation methodology.

The main analyses and their results are reported in the following paragraphs.
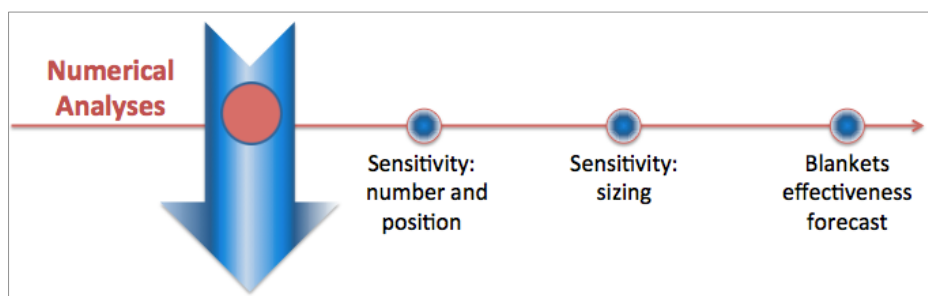
Figure 4.6: Numerical analysis steps – flow chart

4.3.1 Sensitivity about number and position of the blankets

A preliminary analysis about the new proposed technology has been performed, by using the available numerical model, in order to evaluate the suitable number and position of the blankets. Among the studied configurations, the attention has been focused on the two most promising configurations (Figure 4.7), obtained by using either 3 or 5 blankets. The two configurations, taken into account, will be examined and compared in this paragraph. The first configuration has been implemented by introducing 3 blankets in the cavities below the rails, while the second, has been implemented maintaining the 3 previous blankets in the same positions, and adding 2 supplementary blankets, placed both below the Casing plate, one in the cavity over the first Vane and the other one over the Shroud.

The application of the thermal blankets inside the turbine cavities has the double advantage of reducing both the radiative heat transfer among the cavities surfaces and the Casing plate temperature, with the same amount of injected Cooling air mass flow rate.
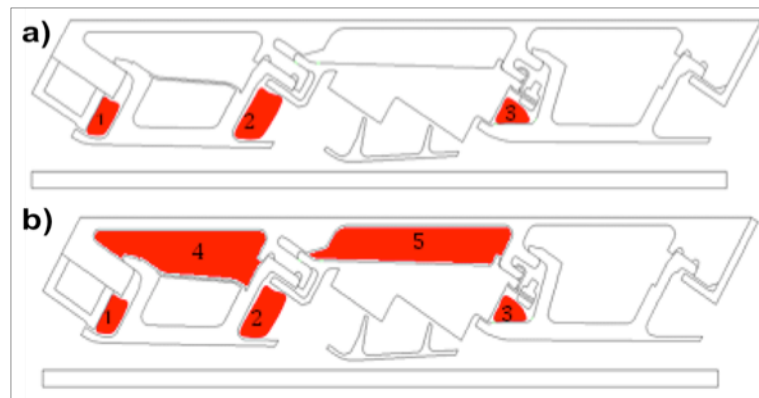
Figure 4.7: Configurations a) 3 blankets, b) 5 blankets

Initially, in order to perform the preliminary simulations, for both the configurations, the blankets have been considered completely filling the cavities. Consequently, in the numerical model, the size of each blanket has been set almost equal to the dimensions of the cavity, where it is placed, except for the small gap (about 1 mm) due to the roughness of the blanket metal layer surfaces. Moreover, to analyze the TA thermal and fluid behavior, resulting from the application of the blankets, the model, previously introduced (Chapter 3), has been properly modified in order to take into account the presence of the insulating material. The implemented changes refer both to the fluid network and to the thermal model. In the fluid network, *rectangular pipe* elements (red circle in Figure 4.8) have been introduced to simulate the air passages between the cavities and the surfaces of the blankets. These elements are characterized by suitable

lengths and by hydraulic diameters, in order to permit the evaluation of both the components pressure losses and the mass and volumetric flow rates passing through each element. In the thermal model the blankets have been implemented by using 2D finite element (QUAD 4), like every other solid part of the TA (Figure 4.9). The material properties have been set considering the technical datasheet of the materials (Table 4.2). Each element introduced in the fluid network to reproduce the air passages around the blankets, has one, or more than one, corresponding *advection bar* element in the FEM model, like all of the elements already present in the model. The number of *advection bar* elements depends on the application mode of the convective correlations.

The correlations for the convective heat exchange (*conv*) have been implemented by considering the general rules already adopted in the whole model. In all the cavities, where the blankets are placed, the radiative heat exchange correlations, if any, have been deleted because the radiation can be considered negligible due to the small temperature differences between the blankets and the facing cavity surfaces.
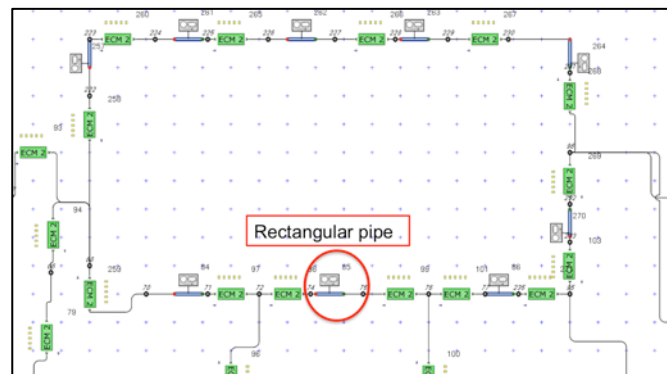
Figure 4.8: Example of blanket schematization in the fluid network
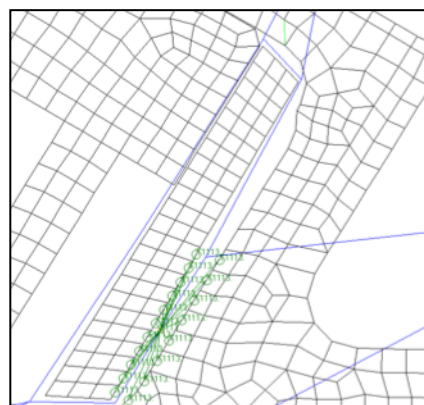
Figure 4.9: Example of a blanket schematization and *conv* application in the FEM model

In Figure 4.10 and Figure 4.11 the fluid and thermal models, obtained after the modeling of the blankets, are shown.
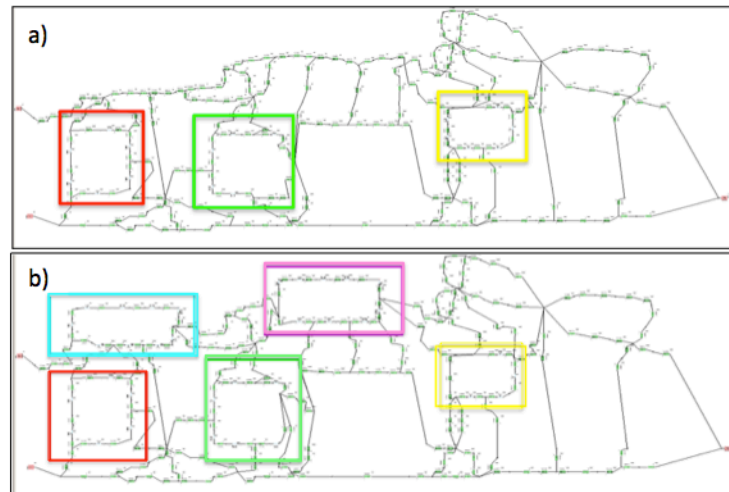
Figure 4.10: Fluid network a) 3 blankets, b) 5 blankets
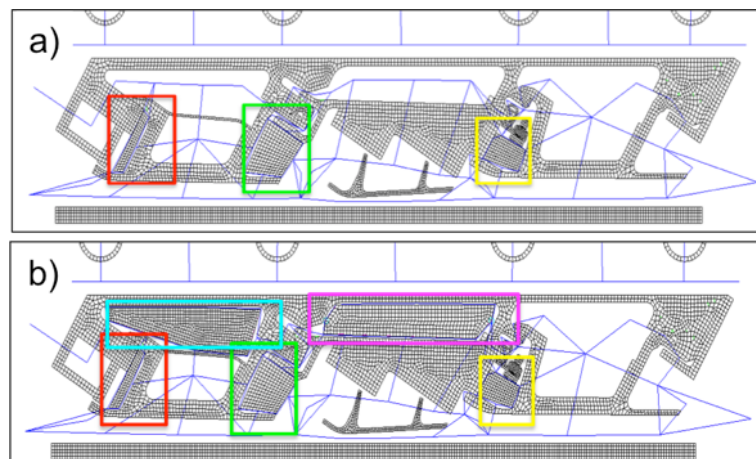
Figure 4.11: Thermal model a) 3 blankets, b) 5 blankets

The numerical simulations have been performed by setting for the FP the boundary conditions at the inlet (mass flow rate, pressure, temperature), whilst, for the Coo the inlet temperature and pressure are fixed but the mass flow rate, in the different simulations, has been reduced from 100% (full amount) to 5%.

Moreover, the ACC is at about room temperature.

For each examined case, the resulting distributions of temperature have been compared with the ones obtained by running the so called *reference* model, i.e. the previous tuned model without blankets (described in Chapter 3 and shown in Figure 3.13) run with the same FP and Coo inlet conditions, except for the Coo mass flow rate (equal to 100% in the *reference* model).
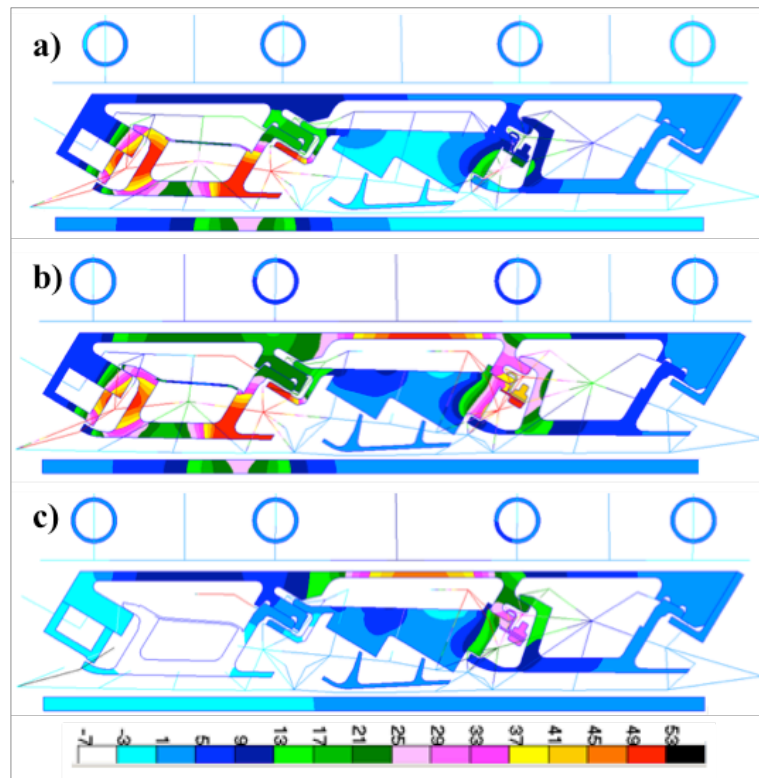
Figure 4.12: Temperature difference between: a) reference
model and 3 blankets configuration model; b) reference model and
5 blankets configuration model; c) 3 and 5 blankets configuration
models

In Figure 4.12 the thermal map obtained calculating, at each location inside the TA model, the difference between the *reference* distribution of temperature, carried out by running the *reference* model, and the one obtained with 3 blankets, is shown. Checking the temperature scale in the previous Figure, which reports the range of temperature differences, it is possible to note that temperatures always decrease, in the Casing region, after the application of the blankets.

As expected, examining the Figure, it is possible to observe a general decrease in the TA temperatures due to the insertion of the 3 blankets.

The higher temperature reductions are detected in the first Vane region and along the Casing plate, while the advantage, following the insertion of the blankets, becomes almost negligible in the second Vane region.

The same comparison has been performed for the configuration carrying 5 blankets and is shown in Figure 4.12b. According to the thermal map reporting the temperature differences ($T_{reference} - T_{5blankets}$), there is a general decrease in temperatures, such as in the previous case, but also a couple of other interesting differences, ascribable, for sure, to the two additional blankets, can be noted. Firstly, the difference of temperatures between the *reference* case and the 5

blankets configuration is intensified in the first Vane region and along the Casing plate; secondly, the presence of insulating materials results in a reduction of temperatures also in the second Vane region.

Figure 4.12c reports the difference between the numerical temperatures obtained with the 3 blankets configuration and the 5 blankets configurations, respectively. This comparison allows a better understanding of the different insulating capabilities. As it is possible to see, the 5 blankets configuration results in a slight increase of temperatures in the bottom part of the first Vane cavity, while, in the upper parts of the TA, especially in the zone of the Casing over the Shroud, an interesting decrease in temperature can be observed. The thermal distributions, just shown, can be justified by a further analysis of the way the Coo mass flow rate splits up inside the TA.

For this reason, some simple sketches, reporting the Coo mass flow rate splitting, both for the *reference* case (Figure 4.13), and, around the blankets, for the two configurations here analyzed (Figure 4.14,Figure 4.15), are provided. For a quick comparison, the mass flow rate values are displayed as a percentage fraction of those in input to the Coo branch.

Starting with the *reference* case (Figure 4.13), it is interesting to note the strong decrease in mass flow rate the Coo undergoes passing through the first Vane.

In this zone a relevant fraction of Coo, due to the slight overpressure it exhibits at the inlet in respect to the FP, flows in the bottom direction mainly through the spline seals, but also through the small leakages among the different components. For this reason, the amount of Coo reaching the cavity over the Shroud is less than one half of the incoming quantity. In the Shroud region a further loss in Coo mass flow rate can be noted, in fact, the Cooling flow, entering the second Vane, is reduced to 2% of the incoming amount.
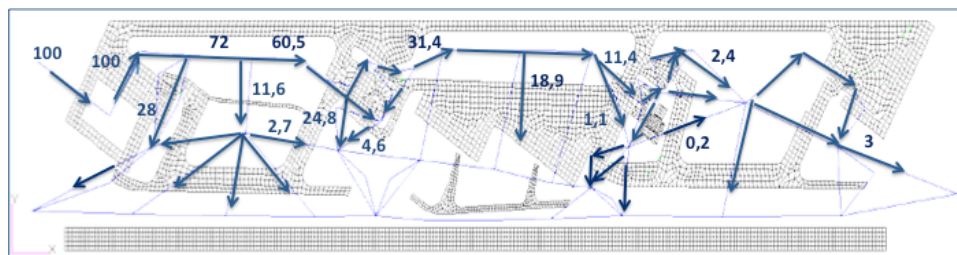
Figure 4.13: Reference case - Coo flows splitting

The introduction of 3 blankets in the lower cavities (Figure 4.14), represents an obstacle for the Coo mass flow rate, reducing its descent towards the FP and promoting its passage under the Casing, with the effect of cooling it further down.

Furthermore, the blankets, as any insulating material, reduce the heat flux transferred to the upper cavities so that the first Vane area is colder than in the reference case.
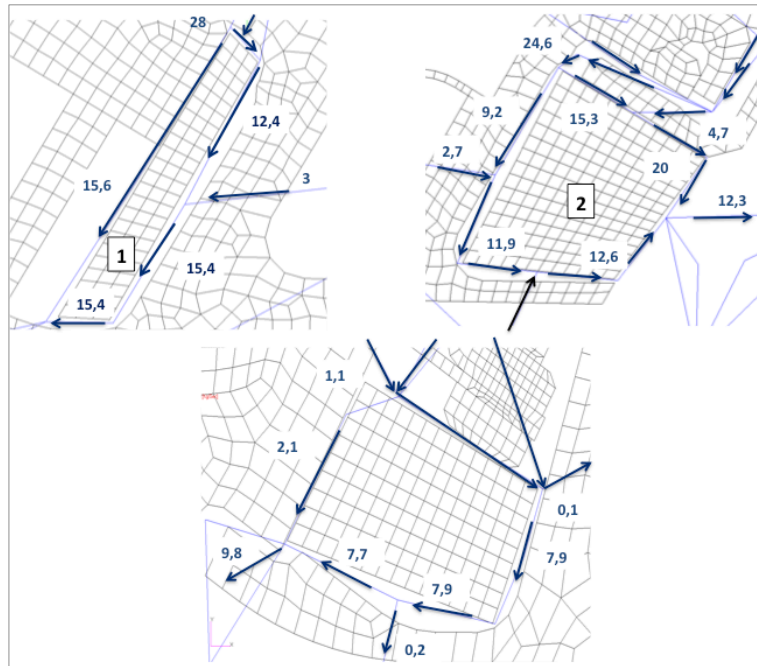
Figure 4.14: 3 blankets configuration - flows splitting around the blankets

The introduction of two additional blankets in the 5 blankets configuration (Figure 4.15), changes further the flow distribution.

In fact, the blankets number 4 and 5, placed in the cavities under the Casing, divide the Coo flow, forcing it to pass around them, and minimize the heat transferred to the Casing plate.

So, with the same inlet Coo flow, the 5 blankets configuration results to be the more effective one and, for this reason, the following numerical studies will refer only to this configuration.

In Figure 4.16 an example of the allowed reductions of the Cooling mass flow rate, (i.e. the Coo mass flow rate reduction practicable without any average temperature, calculated on the Casing plate, overcoming the *reference* one) for both the configurations with 3 and 5 blankets, is shown. The numerical temperatures have been fitted with the help of interpolating lines (Poly.) in order to simplify the identification of the allowed Coo air reductions. As it is possible to see, for the 3 blankets configuration, the average Casing temperature, obtained at different Coo mass flow rate reductions, overcomes the *reference* temperature when the Coo is reduced by 50%, while for the 5 blankets configuration the overcoming is obtained with a higher Coo mass flow rate reduction of around 85%.
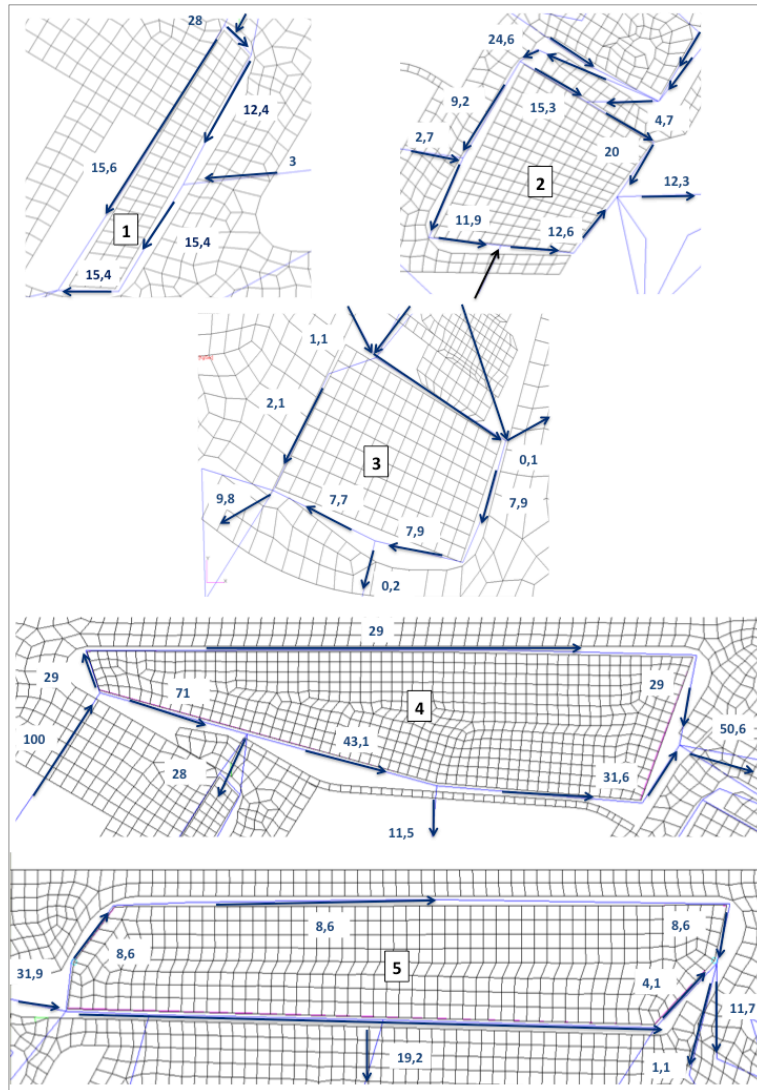
Figure 4.15: 5 blankets configuration - flows splitting around
the blankets
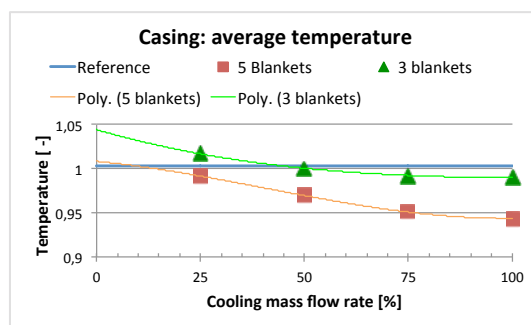
Figure 4.16: Allowed Coo mass flow rate reductions

4.3.2 Sensitivity about sizing of the blankets

As explained in the paragraph concerning the testing facility, a large number of temperature sensors have been used in order to obtain a thermal mapping as accurate as possible. These sensors, especially the air thermocouples, require for their positioning a certain amount of space (more than 10 mm).

This requirement obviously inhibits the use of a blanket completely filling the cavity.

For this reason, forecasting an experimental campaign to validate the results obtained by running the numerical models, a supplementary analysis has been carried out in order to point out the effects related to the size of the blankets.

Limited to the 5 blankets configuration, three different sets of dimensions have been analyzed:

- Sizing1: it is the case examined in the previous paragraph (3.3.1) in order to compare the 3 and the 5 blankets configurations. It exhibits the minimum gap among the blankets and the surfaces facing them, which is the one due to the roughness of the external metallic layer ($\cong$ 0.75 mm). This sizing is obviously not feasible because it requires the instrumentation is completely removed.

- Sizing2: it has the aim of preserving the total amount of the instrumentation and so it requires gaps, among the blankets and the surrounding surfaces, where the thermocouples are placed, of almost one order of magnitude larger than the ones used in the previous case (Sizing1).

- Sizing3: it represents an intermediate stage between the previous two sizing. Its aim is to preserve the metal thermocouples, removing only the air thermocouples that require a larger gap.

A typical example of space occupied by the air (T2) and metal thermocouples (M1 and M2) is shown in Figure 4.17.
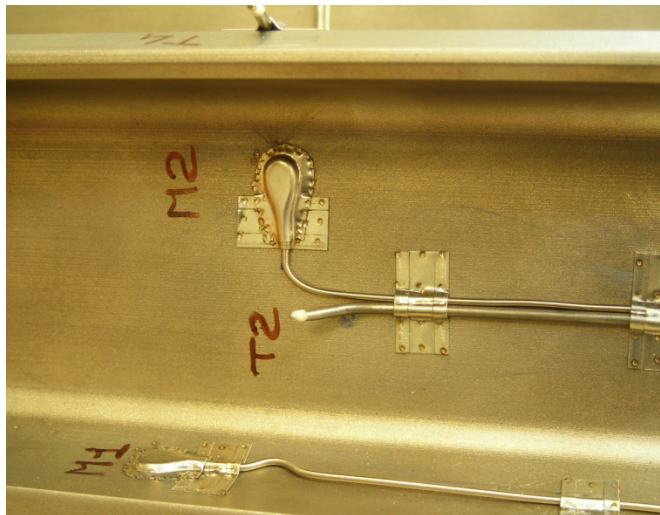
Figure 4.17: Thermocouples example

Figure 4.19 and the tables from Table 4.3 to Table 4.7 show, for all the five blankets, the dimensionless gaps introduced in each of the cases studied. All the gaps have been reported as a percentage fraction of the maximum gap required considering all the three sizing. To be noted that the gap between the left side of the blanket 3 and the honeycomb surface has been calculated by considering the area of the honeycomb cells exposed to the cavities. The area of the cells has been calculated considering half hexagon (Figure 4.18).
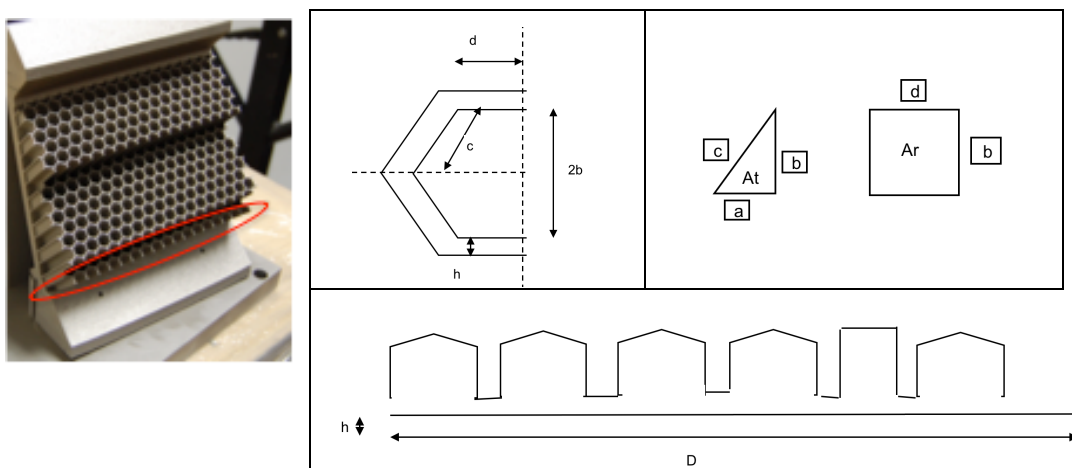
Figure 4.18: Honeycomb cells – area calculation parameters

Figure 4.20, instead, pointing out the differences between the thermal maps obtained in the three examined cases, allows highlighting the effects of the different blankets sizing.

The temperature distributions, here reported, are the ones obtained applying for the tests the same boundary conditions used before to carry out the sensitivity about the number and position of the blankets.

As shown in Figure 4.20, the changes in the blankets size, at least in the range of our interest, do not significantly affect the resulting thermal field.
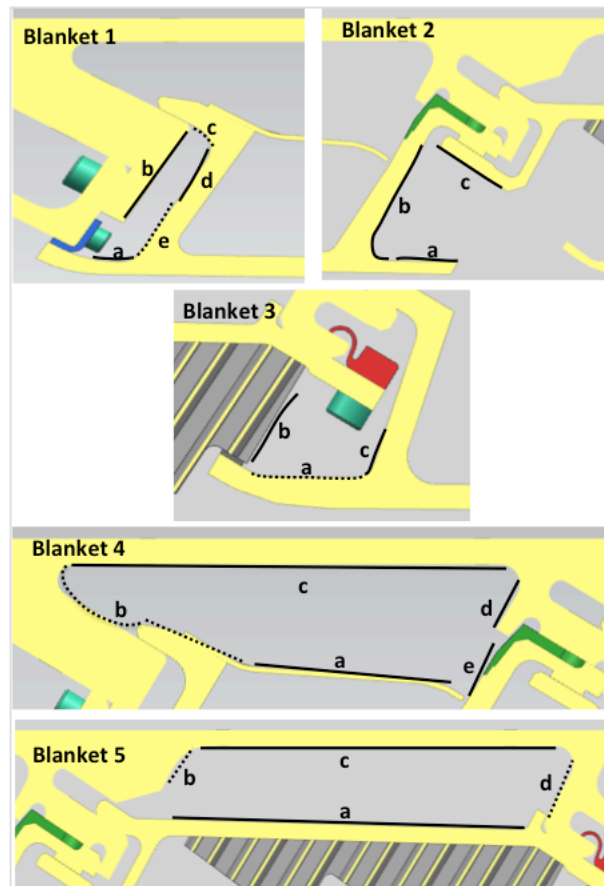
Figure 4.19: Blankets gaps position

Table 4.3: Blanket 1 gaps

Gap [%]

Sizing	a	b	c	d	e
1	13	13	13	13	13
2	46	38	38	46	46
3	46	38	38	13	46

Table 4.4: Blanket 3 gaps

Gap [%]

Sizing	a	b	c
1	13	75	13
2	46	100	46
3	13	75	13

Table 4.5: Blanket 2 gaps

Gap [%]

Sizing	a	b	c
1	13	13	13
2	13	13	13
3	13	13	13

Table 4.6: Blanket 4 gaps

Gap [%]

Sizing	a	b	c	d	e
1	13	13	13	13	13
2	13	46	46	13	46
3	13	46	46	46	38

Table 4.7: Blanket 5 gaps

Gap [%]

Sizing	a	b	c	d
1	13	13	13	13
2	46	30	30	30
3	13	46	46	46
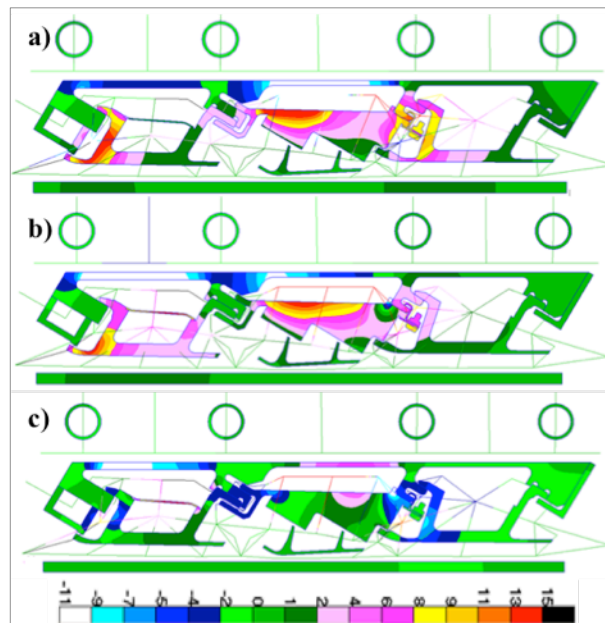
Figure 4.20: Differences between the temperature distributions: a) Sizing2-Sizing1, b) Sizing3-Sizing1, c) Sizing3-Sizing2

In order to verify the validity of this result also under different Cooling conditions, a further sensitivity has been performed reducing the Coo mass flow rate. The study has been carried out paying attention to the Rails and Casing regions (shown in Figure 4.21), and evaluating, at different percentages of the Coo mass flow rate (100%, 75%, 50%), the average and maximum temperatures of the Rails and of the Casing.
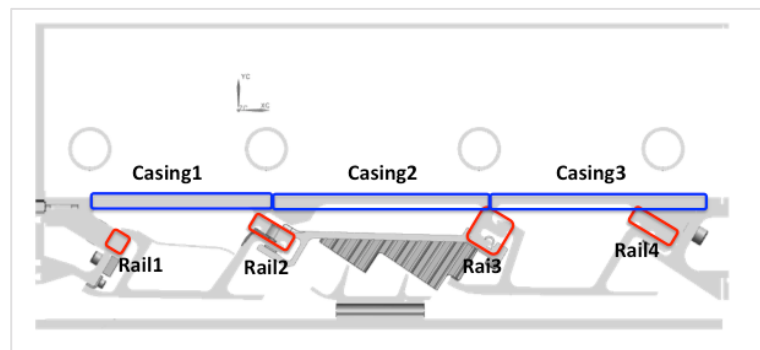
Figure 4.21: Test Article analysis regions

In Figure 4.22 and Figure 4.23 the dimensionless average and maximum temperatures, obtained performing the sensitivity analysis, are shown.

Starting from the sensitivity outputs, it is possible to state that the differences in the distributions of the average temperature, resulting from the changes of the gaps, are almost negligible. For this reasons, the configuration called Sizing2, which allows avoiding changes in the TA instrumentation, has been chosen as the starting point for the design and the production of the blankets.
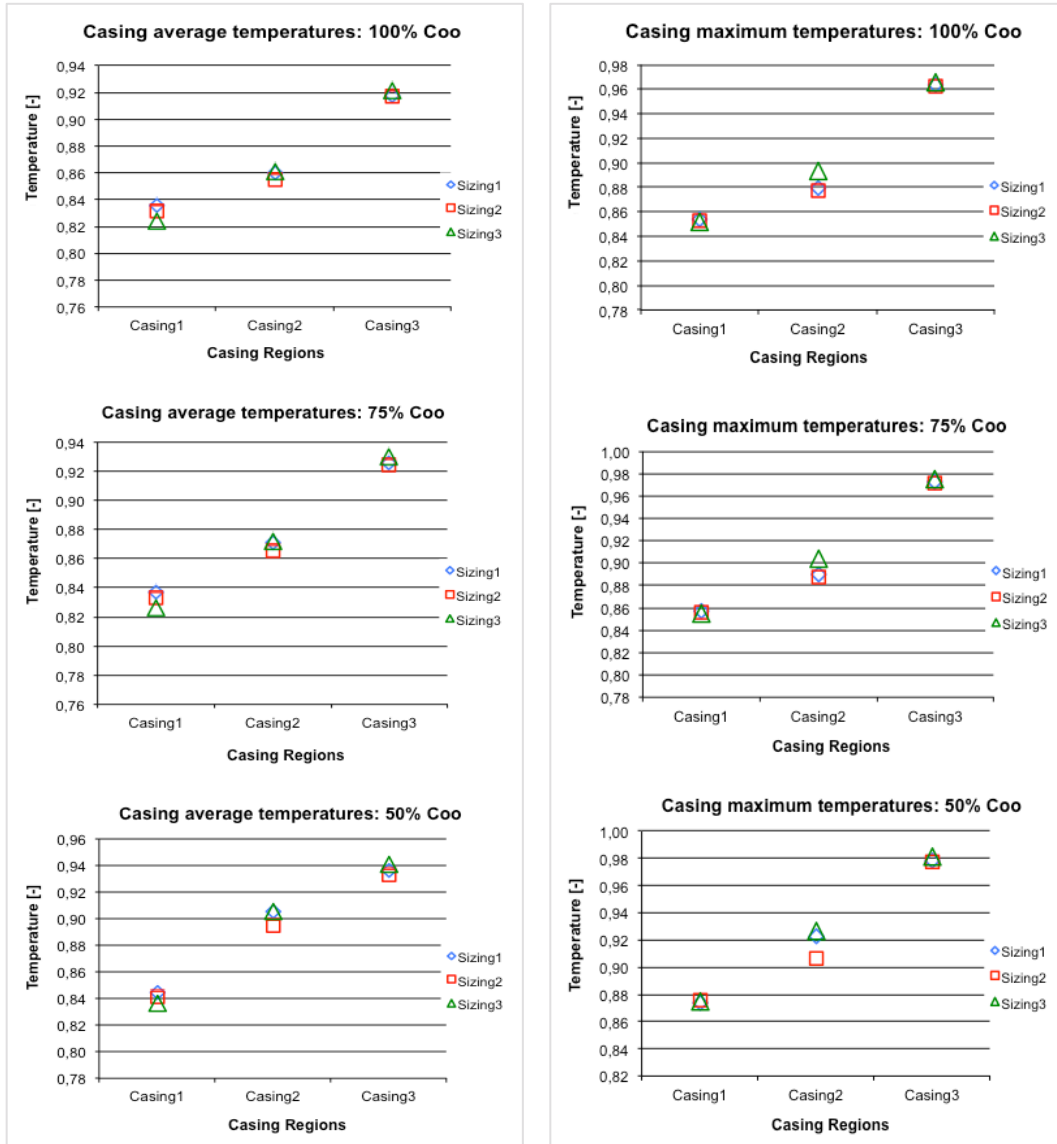
Figure 4.22: Casing average and maximum temperature for the 3 Sizing
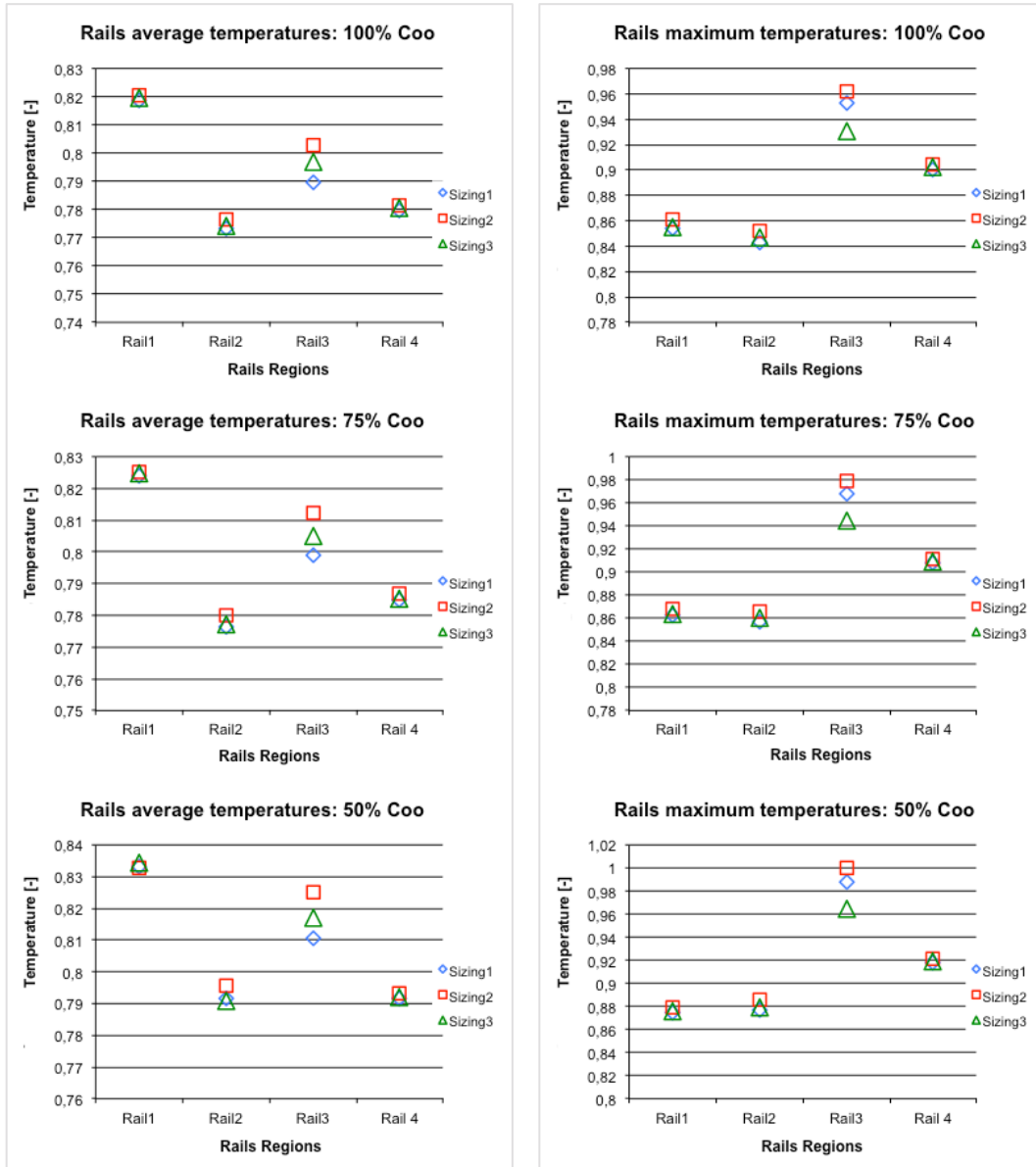
Figure 4.23:Rails average and maximum temperature for the 3 Sizing

4.3.3 Numerical forecasting

The final design solution, shown in Figure 4.24, has been used to numerically forecast, under different operating conditions, the effectiveness of the insulation methodology. In addition, in the same Figure, the position of the metal thermocouples of the Casing, used to compare the TA thermal behavior with and without the insulation blankets, is also indicated.
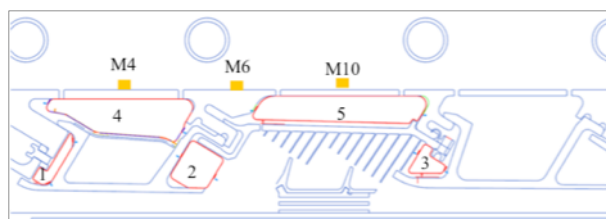
Figure 4.24: Blankets design and Casing thermocouples position

The numerical simulations have been performed fixing for the FP the inlet temperature, pressure and mass flow rate, while, for the Coo only the inlet temperature and pressure are fixed and the mass flow rate changes from 100% to 5%. The temperature and mass flow rate of the ACC have been set at a constant value for all the examined cases.

In particular, the results, reported in what follows, refer to three sets of experiments performed at the fixed FP and Coo temperatures and pressures, listed in Table 4.8, and changing the Coo mass flow rate.

Table 4.8: FP and Coo inlet conditions

| | Flow Path | | Cooling |
	p (bar)	T (K)	T (K)
Set 1	1,8	873	573
Set 2	1,8	873	473
Set 3	1,8	723	473

In order to quantify the benefits due to the application of the blankets, the temperatures, resulting from the numerical simulation, are compared one by one with the experimental reference (*exp. reference*), i.e. the temperature measured by the same sensor in a previous test campaign, performed without the blankets (Chapter 2.5), with the full amount of Coo and under the same inlet (temperature and pressure) conditions. The effectiveness of the blankets has been assessed evaluating how much the Coo mass flow rate can be reduced without any Casing metal thermocouple (M#, sketched in Figure 4.24) overcoming the corresponding *exp. reference* temperature.The obtained results, here reported, refer to the inlet boundary conditions of Set 1, which have been reported in Table 4.8. In Figure 4.25, for the selected Casing sensors (M4, M6 and M10), the numeric dimensionless temperatures, obtained with the blankets at different Coo mass flow rates, are shown. In each graph, the temperature recorded by the same sensor, without the blankets and with the full amount of Coo mass flow rate (*exp. reference*), is also displayed. While, in Table 4.9, the ΔT between the *exp. reference* temperatures and the ones obtained with the blankets, are reported.
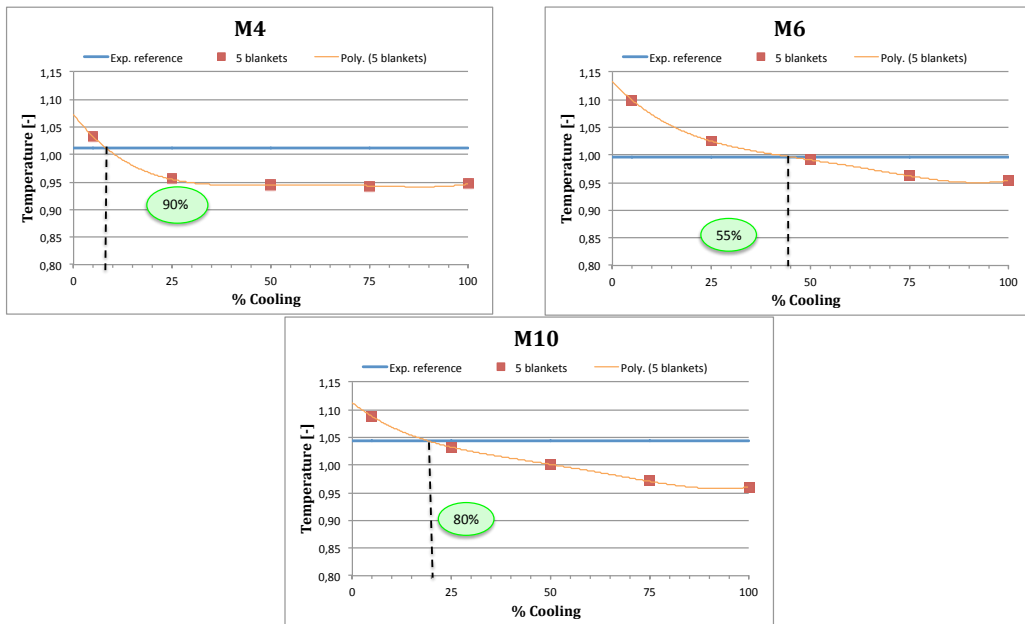
Figure 4.25: Numerical results for the Casing thermocouples –
Set 1

Table 4.9: Casing thermocouples ΔT – Set 1

	Casing thermocouples ΔT		
% Coo	**M4**	**M6**	**M10**
100%	36,8	24,0	47,6
75%	38,8	19,4	41,8
50%	38,0	2,8	24,2
25%	32,1	-16,5	6,4
5%	-12,3	-59,0	-25,3

By examining the graphs, with the help of the line interpolating the obtained numerical temperatures (Poly 5 blankets), it is possible to detect that the percentage of Coo reduction at which the calculated temperature overcomes the *exp. reference* is not the same for all the three sensors. For example, the sensors M4 and M10 placed in the Casing regions, directly above the blankets number 4 and 5, benefit more from the presence of the blankets allowing a Coo reduction up to 90% and 80%, respectively. Instead, the sensor M6, located in an intermediate position between the previous two thermocouples, being over the Rail and farther away from the application regions of the blankets, benefits in a reduced way of their insulating action and allows only a 55% Coo reduction.

Therefore, considering the whole Casing length, the 5 blankets configuration, under these specific boundary conditions, allows a decrease in Coo mass flow rate to 55%. This percentage is evaluated taking into account the minimum reduction of allowed Coo air that is practicable, along the whole Casing plate, without any thermocouple overcoming the *exp. reference*.

The same numerical analyses have been performed under other operating conditions, Set 2 and Set 3 in (Table 4.8), changing the inlet temperatures for both the FP and the Coo mass flow rates. The obtained dimensionless temperature and the resulting ΔT, between the *exp. reference* temperatures and the ones numerically obtained, are shown in Figure 4.26 and Figure 4.27, and are reported in Table 4.10 and Table 4.11.

As it is possible to observe, the minimum and the maximum practicable reductions of Coo air are registered, for all the performed simulations, by the sensor M6 and M4, respectively. This confirms that the effect due to the application of the blankets is less appreciable in the M6 zone, while the portion of the Casing plate located over the first Vane, where M4 is placed, benefits from the coupled action of the blanket and of its position near the Coo inlet.
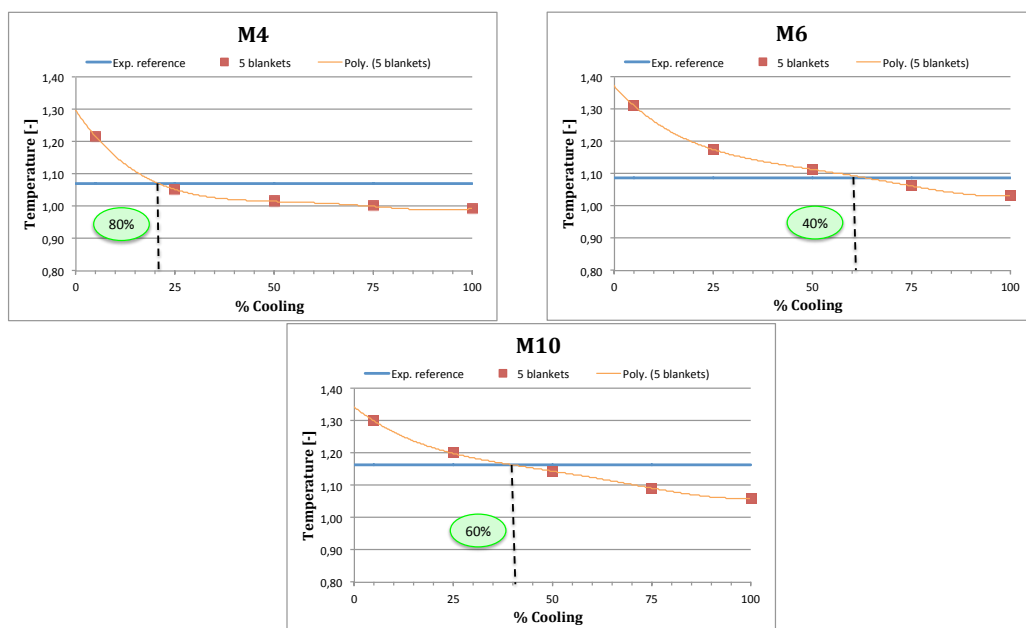
Figure 4.26: Numerical results for the Casing thermocouples – Set 2

Table 4.10: Casing thermocouples ΔT – Set 2

	Casing thermocouples ΔT		
% Coo	**M4**	**M6**	**M10**
100%	35,4	25,1	47,9
75%	32,5	11,7	33,3
50%	25,4	-12,2	8,9
25%	8,1	-40,6	-16,5
5%	-67,9	-103,5	-62,8
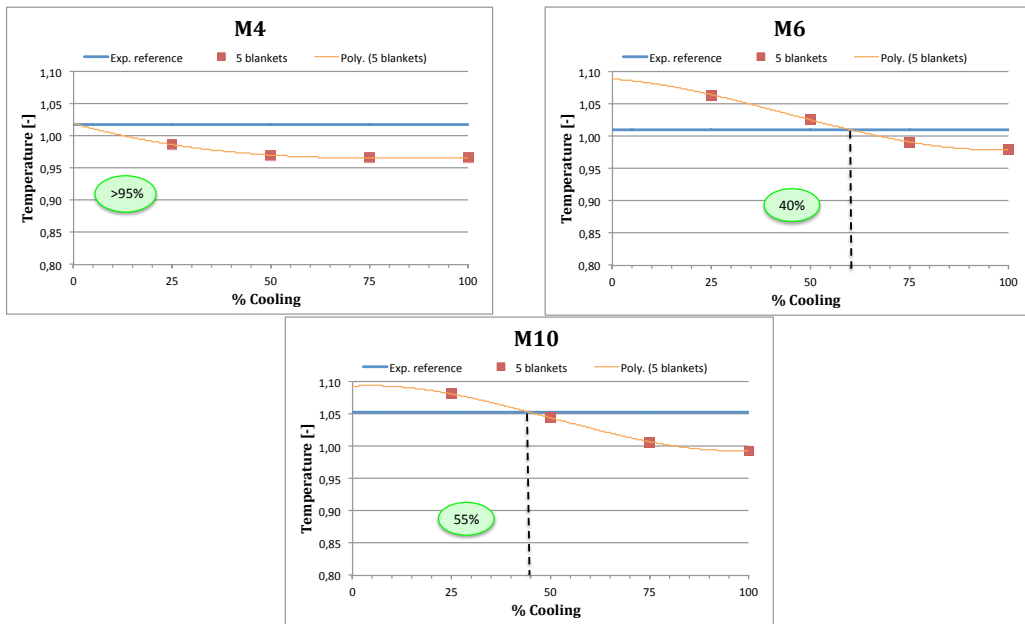
Figure 4.27: Numerical results for the Casing thermocouples –
Set 3

Table 4.11: Casing thermocouples ΔT – Set 3

	Casing thermocouples ΔT		
% Coo	M4	M6	M10
100%	23,7	13,7	27,5
75%	24,0	8,5	21,2
50%	21,7	-7,5	3,9
25%	14,1	-25,5	-13,2

In Table 4.12 the allowed reductions of the Coo mass flow rate, evaluated for all the test cases, are summarized.

Table 4.12: Allowed Coo mass flow rate reductions for the 3
Sets

	Allowed Coo mass flow rate reductions [%] - Casing		
	M4	M6	M10
Set 1	90	55	80
Set 2	80	40	60
Set 3	>95	40	55

The numerical simulations have shown that the maximum reduction of Coo mass flow rate, achievable without any sensor overcoming its reference temperature, ranges from 40% to 55%.

The numerical results, here presented, are obtained by running a well-tuned numerical model, which, as described in paragraph 3.2.7, satisfies the tolerance criteria, but despite this, still exhibits discrepancies between the experimental and the numerical data. These discrepancies can be evaluated as percentage errors (Eq. 7), as shown in Table 4.13, for the Set 1 (100% Coo).

$$e = \frac{T_{num} - T_{exp}}{T_{exp}} \cdot 100 \qquad (7)$$

Table 4.13: Percentage errors on temperatures - Set 1

Sensor	ΔT	Error [%]
M4	0,4	0,08
M6	-9,5	-1,68
M10	-19,4	-3,26

In order to evaluate how much these discrepancies can affect the final allowed Coo reductions, the temperatures, obtained running the model with the blankets, have been recalculated taking into account these percentage errors.

Then, the recalculated temperatures have been compared with the corresponding *exp. reference* temperatures, evaluating the new allowed reductions of Coo air.

The obtained results have shown these errors are responsible, for the sensors M6 and M10, for an underestimation of the reduction of the Cooling mass flow rate of about 10%, and consequently for an increased allowed reduction of the Cooling air up to 65% and 90%, respectively. Whilst for the sensor M4 the impact of the percentage error could be considered negligible.

Therefore, for this set of inlet conditions, the final allowed reduction of the Cooling mass flow rate, along the whole Casing length, is of about 65%.

The same analysis has been performed for the other 2 Sets of experiments reported in Table 4.8.

By comparing the recalculated temperatures with the corresponding *exp. reference* ones, the allowed reductions of the Coo air, reported in Table 4.12, exhibit a general increase for both the sensor M6 and M10.

The new allowed Coo air reductions, as shown in Table 4.14, are about 10% higher for the sensor M6, and about 20% and 25% higher for the sensor M10 for Set 2 and Set 3, respectively. Therefore, the new allowed reductions of the Coo mass flow rate range from 50% to 65%.

Table 4.14: New allowed Coo mass flow rate reductions for the 3 Sets

Allowed Coo mass flow rate reductions [%] - Casing

	M4	M6	M10
Set 1	90	65	90
Set 2	80	50	80
Set 3	>95	50	80

As previously said, the Coo air, injected into the Casing cavities to control the clearance height, has the main aim of cooling down actively the Casing plate. Therefore, the allowed reduction of the Coo mass flow rate has been evaluated only according to the achieved temperatures along the Casing plate.

Nevertheless, it is also important to verify if, in the zone near the Rails, the application of the blankets produces visible benefits or if, on the contrary, it introduces additional thermal gradients. With this aim, the same analyses and considerations that have been made for the Casing region have been extended to the selected sensors, placed near the Rail zones (Figure 4.28).

In what follows, for ease of reference, the sensors located near the Rails will be named Rails thermocouples.
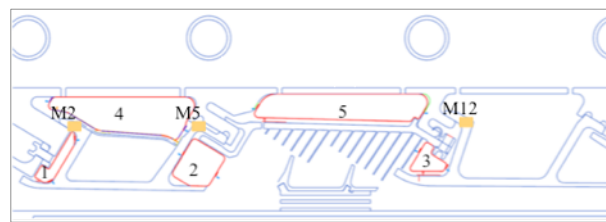
Figure 4.28: Rails thermocouples position

The simulations have been performed with the inlet boundary conditions for the 3 Sets shown in Table 4.8.

In Figure 4.29, Figure 4.30 and Figure 4.31 the numerical dimensionless temperatures, obtained with the blankets and different Coo mass flow rates, for the selected Rails sensors (M2, M5 and M12), are compared with the corresponding *exp. reference* temperatures.

In Table 4.15, Table 4.16 and Table 4.17 the ΔT between the *exp. reference* temperatures and the ones obtained by using the blankets and by varying the Coo mass flow rate, are reported. In addition, in Table 4.18 the evaluated allowed Coo air reductions are summarized.
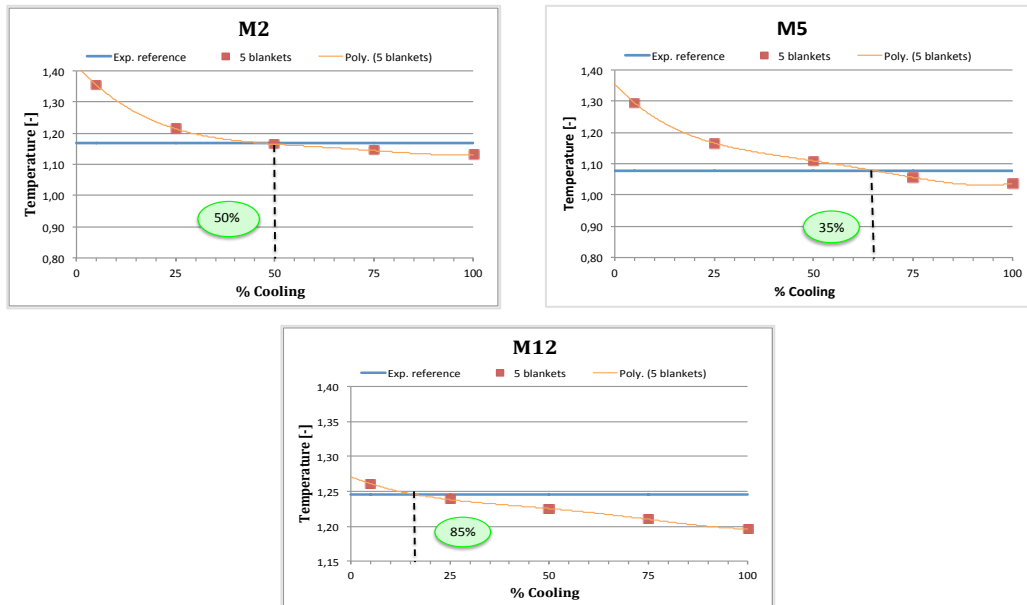
Figure 4.29: Numerical results for the Rails thermocouples –
Set 1

Table 4.15: Rails thermocouples ΔT – Set 1

	Casing thermocouples ΔT		
% Coo	M2	M5	M12
100%	21,2	22,1	28,2
75%	13,2	11,2	20,2
50%	1,4	-19,0	11,5
25%	-26,6	-51,5	4,2
5%	-107,2	-124,5	-8,8
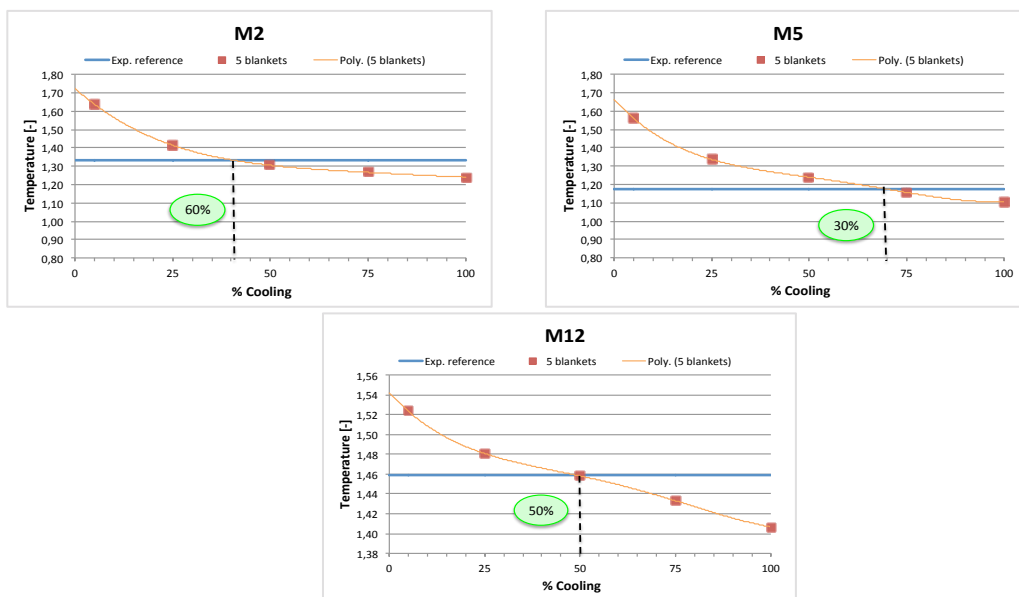
Figure 4.30: Numerical results for the Rails thermocouples – Set 2

Table 4.16: Rails thermocouples ΔT – Set 2

	Casing thermocouples ΔT		
% Coo	**M2**	**M5**	**M12**
100%	41,5	30,4	24,1
75%	29,1	7,7	11,9
50%	11,3	-30,4	0,4
25%	-39,2	-75,1	-10,0
5%	-142,2	-178,5	-29,7
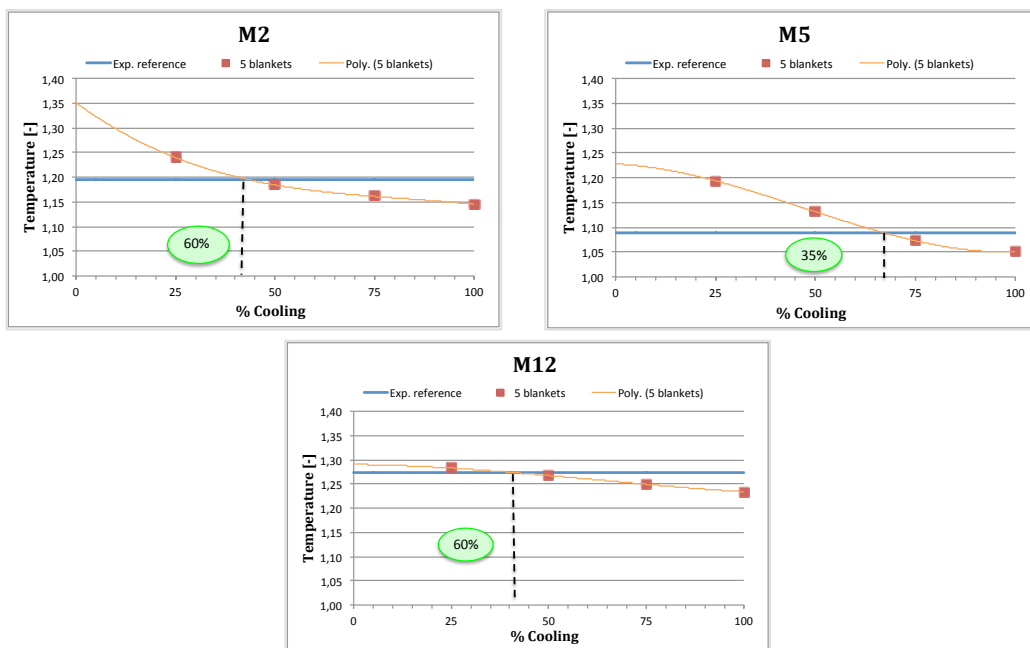
Figure 4.31: Numerical results for the Rails thermocouples – Set 3

Table 4.17: Rails thermocouples ΔT – Set 3

	Casing thermocouples ΔT		
% Coo	**M2**	**M5**	**M12**
100%	23,1	17,2	18,1
75%	15,6	6,7	10,7
50%	4,7	-20,3	2,4
25%	-20,8	-49,2	-4,7

Table 4.18: Allowed Coo mass flow rate reductions for the 3 Sets

Allowed Coo mass flow rate reductions [%] - Rails

	M2	M5	M12
Set 1	50	35	85
Set 2	60	30	50
Set 3	60	35	60

The resulting allowed reductions of the Coo mass flow rate, in the Rails zones, underline the benefits produced by the application of the blankets. In fact, an appreciable Coo air reduction can be performed without overcoming the reference values, also in these areas. The sensor, which controls the minimum allowed reduction of Coo air, in this case, is the M5 thermocouple. Indeed, looking at the results shown in Table 4.18, for this specific sensor, the evaluated Coo reduction ranges between 30% and 35%. The sensor M5, located on the right side of the first Vane is less affected by the introduction of the blanket 4 because, due to its position, it is directly invested by the air stream, canalized in the gap between the lower surfaces of the blanket 4 and the metal sheet. This air is hotter than the one flowing in the gap between the upper surface of the blanket 4 and the Casing surface, because it is exposed to components at higher temperatures.

The errors due to the starting numerical model, calculated as in Eq. 7, have to be taken into account, also for the results of the Rails. The percentage errors, due to the discrepancies resulting from the Thermal Match, are reported in Table 4.19.

Table 4.19: Temperatures percentage errors: Set 1

Sensor	ΔT	Error [%]
M2	-6,5	-0,98
M5	9,0	1,48
M12	0,1	0,02

These errors, as just done for the Casing thermocouples, are applied to the temperatures obtained by running the numerical model implemented with the 5 blankets. Comparing each recalculated temperature with the corresponding *exp. reference,* the allowed Coo reduction for the sensor M2 results to be underestimated, while for the sensor M5 it is overestimated. The impact of the percentage error on the sensor M12, for this Set of experiments, can be considered negligible. Therefore, given this set of inlet conditions, the final allowed reduction of the Cooling mass flow rate, in the Rails areas, is of about 30%.

The same corrections, applied to the numerical results obtained under the operating conditions of Set 2 and Set 3, lead to the allowed reductions of the Coo mass flow rate reported in Table 4.20.

Table 4.20: New allowed Coo mass flow rate reductions for the
3 Set

Allowed Coo mass flow rate reductions [%] - Rails

	M2	M5	M12
Set 1	60	30	85
Set 2	60	20	75
Set 3	65	25	80

4.4 Experimental validation

Starting from the results obtained during the first numerical activity, the thermal blankets have been fabricated and placed in the Thermalcase test rig facility. The second activity step (Figure 4.32), therefore, has been devoted to carrying out an experimental campaign during which the thermal blankets have been tested under different thermal conditions.

The obtained results have been subsequently analyzed, in order to evaluate the goodness, in terms of Coo air reduction, of the tested insulating solution.
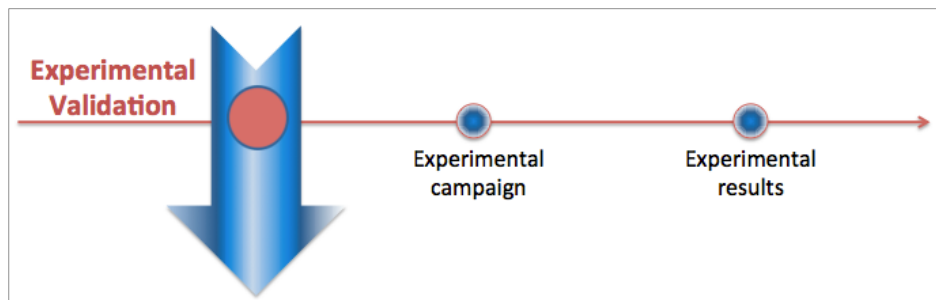
Figure 4.32: Experimental validation activities flow chart

4.4.1 Test campaign

Starting from the results of the numerical sensitivity, the design solution, shown in Figure 4.24, has been tested on the ThermalCase rig (Figure 4.33).

The 5 blankets have been manufactured (Figure 4.34) with the dimensions identified thanks to the previous numerical analyses, i.e. dimensions allowing not performing changes in the TA instrumentation.

Moreover, in order to guarantee: the desired gaps (blanket surface – surrounding cavity surfaces) and a good contact between the upper surfaces of the blankets 4 and 5 and the lower surface of the Casing, the blankets 4 and 5 have been provided with little metal legs with a support function.

Figure 4.33: Blankets application inside the Test Article
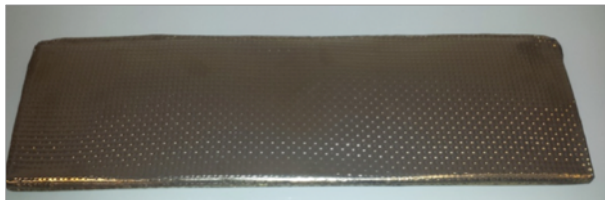
Figure 4.34: Example of manufactured blanket

During the experimental campaign, different sets of experimental tests have been performed under different inlet conditions, varying the Coo mass flow rate while maintaining at a fixed value the other inlet conditions (test matrix shown in Figure 4.35).

In general, all the experiments have been performed with:

- Cooling pressure ≈ 110% Flow Path pressure;
- Cooling base mass flow rate ≈ 10% Flow Path mass flow rate;
- Cooling mass flow rate variable: 100%, 75%, 50%, 25%;
- ACC mass flow rate ≈ constant values (0.013 kg/s);
- β ACC ≈ 1.05 ÷ 1.1
- ACC temperature ≈ room temperature.

	pin FP-PT1 (barA)		pin Cooling-PT2 (barA)		T_FP (°C)								FP mass flow rate	T_Coo (°C)		Coo mass flow rate					ACC mass flow rate
																					Re= ~5000
																					1.05÷1.1
Test	1,4	1,8	PT1+10%	PT1+10%	250	300	350	400	450	500	600	670		200	300	10% FP	7,5% FP	5% FP	2.5% FP	0%	portata base = ~0.013 kg/s
1	x		x						x				x		x	x					x
2		x		x					x				x	x		x					x
3		x		x					x				x	x				x			x
4		x		x					x				x	x				x			x
5		x		x					x				x	x	x	x					x
6		x		x					x				x		x		x				x
7		x		x					x				x		x			x			x
8		x		x					x				x		x				x		x
9		x		x						x			x	x		x					x
10		x		x						x			x	x			x				x
11		x		x						x			x	x				x			x
12		x		x						x			x		x	x					x
13		x		x						x			x		x		x				x
14		x		x						x			x		x			x			x
15		x		x						x	x		x		x				x		x

Figure 4.35: Test matrix experimental campaign with blankets

4.4.2 Experimental results

The experimental results, reported in what follows, refer to the three Sets of experiments, listed in Table 4.8, performed by changing the Coo inlet mass flow rate while maintaining at fixed values the other inlet conditions. .

The experimental temperatures recorded by each sensor, using the blankets and reducing the Cooling mass flow rate, have been compared one by one with the *exp. reference* temperature, exactly as already done for the numerical results. The evaluation of the reduction of the Cooling mass flow rate, which induces the overcoming of the *exp. reference* temperature, allows quantifying the advantages due to the application of the blankets.

In what follows, for each test case, the obtained results are reported for both the sensors placed over the Casing (M4, M6, M10) and near the Rails (M2, M5, M12), shown in Figure 4.36.

Moreover, for each recorded temperature, an error bar is provided. In fact, to correctly evaluate the advantages due to the application of the blankets, in each experimental test exactly the same inlet boundary conditions, as the ones set for the corresponding *exp. reference* test, should be reproduced. As a perfect adjustment, capable of exactly reproducing the *exp. reference* boundary conditions, is not possible, the uncertainties induced by the mismatch of the inlet boundary conditions, must be evaluated. The percentage errors on the inlet conditions (in comparison with the *reference*) and the resulting percentage errors on the measured temperatures are reported in the following bulleted list.
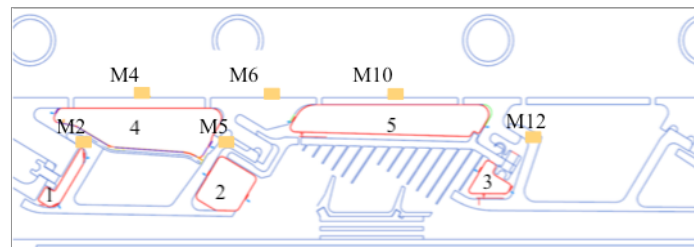
Figure 4.36: Casing and Rails Thermocouples

- **Experiments - Set 1**

In what follows, the results of the tests carried out by setting the FP temperature at 873 K and the Coo temperature at 573 K, are shown. In particular, in Figure 4.37 and Figure 4.38, for the sensors placed over the Casing and the ones near the Rails respectively, the dimensionless temperatures, obtained with the blankets, and the corresponding *exp. reference* tests, are sketched, together with the error bars.

In Table 4.21 and Table 4.22, the ΔT ($T_{reference}$ - $T_{blankets}$) between the *exp. reference* temperatures and the corresponding ones recorded during the experimental tests performed with the blankets, are reported.

In addition, in Table 4.23, the percentage discrepancies, due to the non-perfect reproduction of the incoming conditions of the *exp. reference*, are reported. In the following graphs the error bars are not noticeable when the corresponding calculated errors are negligible. The percentage discrepancies have been taken into account to calculate the percentage errors on temperatures, listed in Table 4.24.

Figure 4.37: Experimental results for the Casing thermocouples

Table 4.21: Casing thermocouples ΔT – Set 1

	Casing thermocouples ΔT		
% Coo	M4	M6	M10
100%	9,5	17,1	38,8
75%	10,4	13,9	35,2
50%	11,2	7,1	29,1
25%	-7,3	-26,6	0,7
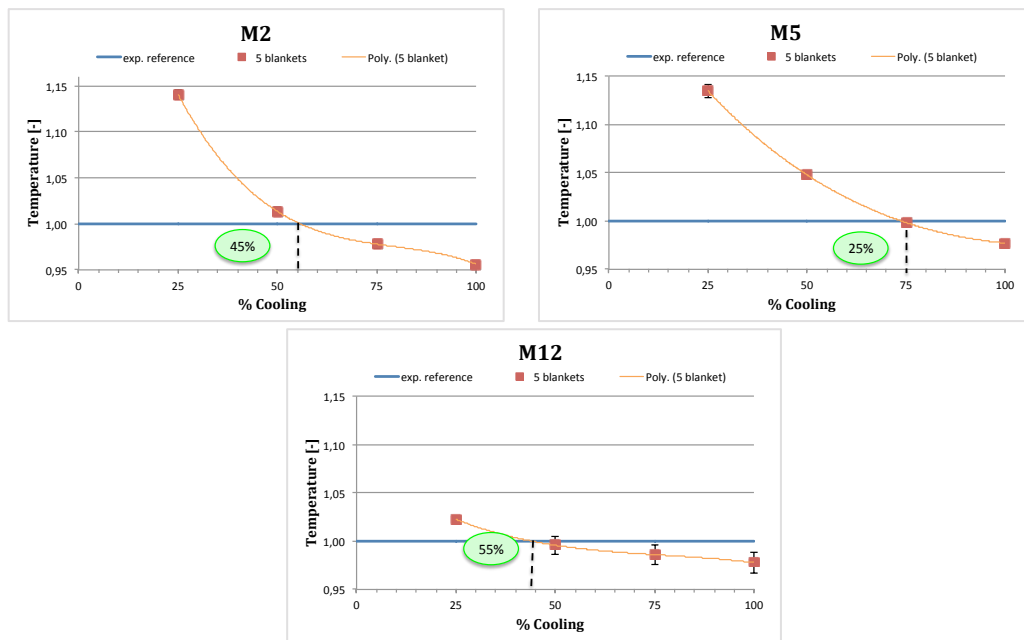
Figure 4.38: Experimental results for the Rails thermocouples

Table 4.22: Rails thermocouples ΔT – Set 1

	Rails thermocouples ΔT		
% Coo	M2	M5	M12
100%	29,0	14,0	15,7
75%	14,6	1,0	9,9
50%	-9,0	-29,3	3,0
25%	-93,4	-82,4	-16,0

Table 4.23: Inlet conditions discrepancies

Test	Flow Path			Cooling			ACC		
	Δm [%]	Δp [%]	ΔT [%]	Δm [%]	Δp [%]	ΔT [%]	Δm [%]	Δp [%]	ΔT [%]
100% Coo	1,51	0,99	5,05	2,08	0,92	0,29	0,35	0,34	8,70
75% Coo	2,01	0,17	3,37	2,52	0,02	0,20	0,47	0,41	8,81
50% Coo	1,73	0,33	3,16	2,17	0,06	0,13	0,79	0,38	10,83
25% Coo	2,75	0,25	2,62	7,43	0,63	0,73	0,84	0,57	5,67

Table 4.24: Percentage errors on temperatures

Test	Error [%]					
	M4	M6	M10	M2	M5	M12
100% Coo	0,016	0,418	0,710	0,410	0,207	1,114
75% Coo	0,010	0,379	0,645	0,448	0,291	1,037
50% Coo	0,002	0,297	0,461	0,465	0,319	0,952
25% Coo	1,564	0,975	0,702	0,207	0,589	0,267

As can be seen in the graphs, the application of the blankets influences positively not only the Casing regions but also the zones near the Rails. This is especially interesting because it means the blankets are not responsible for additional thermal gradients in the Rail regions.

By examining the metal thermocouples one by one, it is possible to note that the sensors, which benefit more from the presence of the blankets, are in general the ones placed in the Casing regions and in particular the M4 and the M10 sensors. These sensors allow a reduction of the Coo equal to 70% and 75%, respectively.

Examining the sensor M4, some small temperature oscillations can be noted, while reducing the Cooling mass flow rate from 100% to 50%. These temperature oscillations can be ascribed to the precision of the thermocouple and not to the reduction of the Cooling mass flow rate. In fact, by analyzing the percentage errors for this sensor, it is possible to note how these values are lower than 0,1%, while reducing the Cooling mass flow rate from 100% to 50%, and, therefore, the values remain inside the range of the thermocouple precision.

The sensor M6, instead, still placed over the Casing but farther away from the application regions of the blankets, since located in an intermediate position with respect to the previous two sensors, exhibits a reduction of the Coo air, slightly lower than the other sensors, of around 60%.

Therefore, considering the whole Casing length, the application of the 5 blankets, under the given boundary conditions, allows a decrease in the Coo mass flow rate of about 60%.

Regarding the thermocouples placed in the zones near the Rails, the temperatures recorded by the sensors M2 and M5, located in correspondence of the first Vane, overcome the respective *exp. reference* when the Coo air reductions are around 45% and 25%, respectively. Instead, the sensor M12, placed in correspondence of the second Vane, being more affected by the insulating effect, exhibits a 55% of Coo reduction.

- **Experiments - Set 2**

In what follows the results obtained for the test carried out by setting the FP temperature at 873 K and the Coo temperature at 473 K, are shown. The Figures and Tables, here reported, have been obtained as previously described for the experimental Set1.
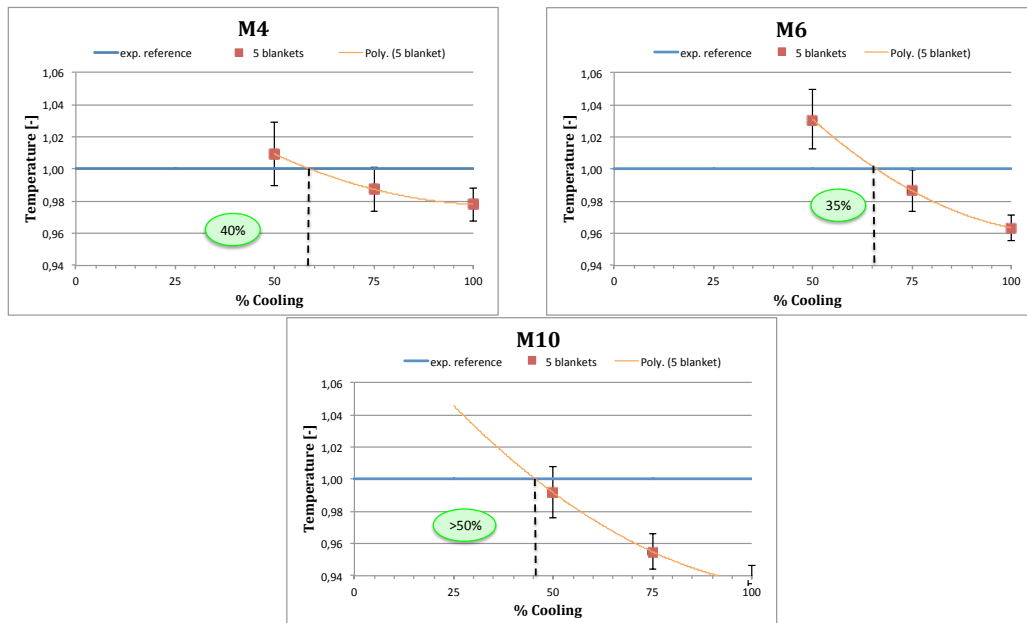
Figure 4.39: Experimental results for the Casing thermocouples

Table 4.25: Casing thermocouples ΔT – Set 2

| % Coo | Casing thermocouples ΔT | | |
	M4	M6	M10
100%	10,9	18,4	34,8
75%	6,2	6,7	24,2
50%	-4,5	-15,5	4,4
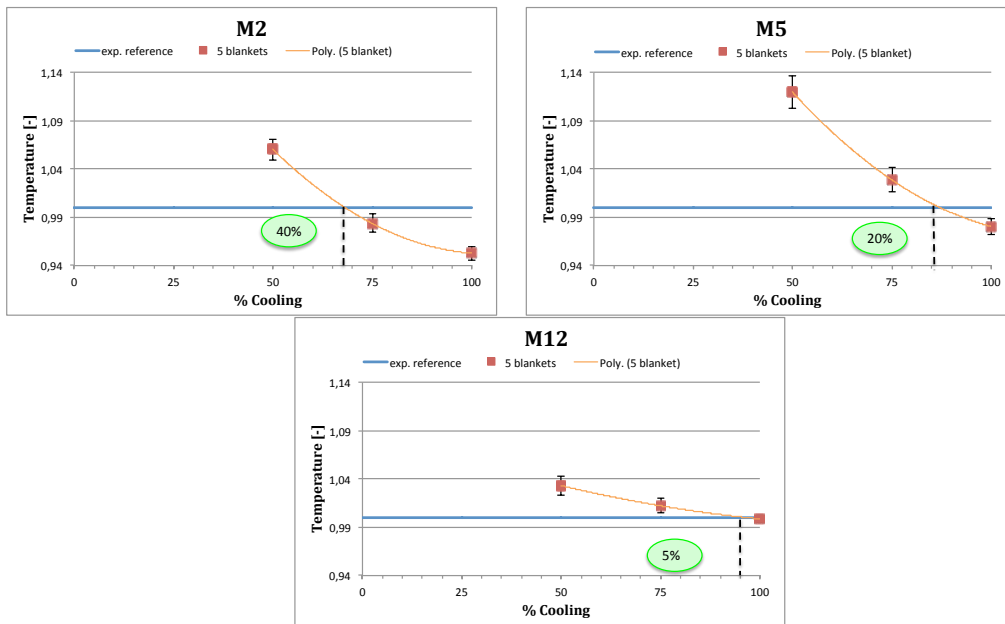
Figure 4.40: Experimental results for the Rails thermocouples

Table 4.26: Rails thermocouples ΔT – Set 2

	Rails thermocouples ΔT		
% Coo	**M2**	**M5**	**M12**
100%	29,0	10,6	0,9
75%	10,0	-15,6	-8,3
50%	-36,9	-64,7	-22,3

Table 4.27: Inlet conditions discrepancies

	Flow Path			**Cooling**			**ACC**		
Test	Δm [%]	Δp [%]	ΔT [%]	Δm [%]	Δp [%]	ΔT [%]	Δm [%]	Δp [%]	ΔT [%]
100% Coo	2,42	0,76	1,60	1,86	1,14	2,10	6,96	0,66	8,64
75% Coo	1,40	0,21	1,31	1,16	1,08	2,20	7,07	0,57	5,76
50% Coo	1,83	0,46	1,17	1,42	1,08	2,04	7,15	0,47	1,97

Table 4.28: Percentage errors on temperatures

	Error [%]					
Test	**M4**	**M6**	**M10**	**M2**	**M5**	**M12**
100% Coo	1,06	0,82	0,59	0,75	0,88	0,43
75% Coo	1,39	1,33	1,16	0,96	1,23	0,75
50% Coo	1,94	1,78	1,59	1,02	1,48	0,95

In this case also, examining each thermocouple it is possible to note that the sensors M4 and M10 show a higher benefit due to the blankets, allowing a Coo reduction of about 40% and higher than 50%, respectively.

The sensor M6, instead, exhibits a 30% of Coo air reduction. Therefore, considering the whole Casing length, the application of the 5 blankets, under the given boundary conditions, allows a decrease in Coo mass flow rate of around 30%.

Regarding to the thermocouples placed in the zones near the Rails, the temperatures recorded by the sensors M2 and M5 overcome their *exp. reference* when the Coo air reductions are 40% and 20%, respectively. Instead, the sensor M12 is less influenced by the insulating effect and allows only a 5% of Coo reduction.

- **Experiments - Set 3**

The results obtained for the test carried out by setting the FP temperature at 723 K and the Coo temperature at 473 K, are shown below. The Figures and the Tables, in what follows, have been obtained as previously described for the experimental Set 1.
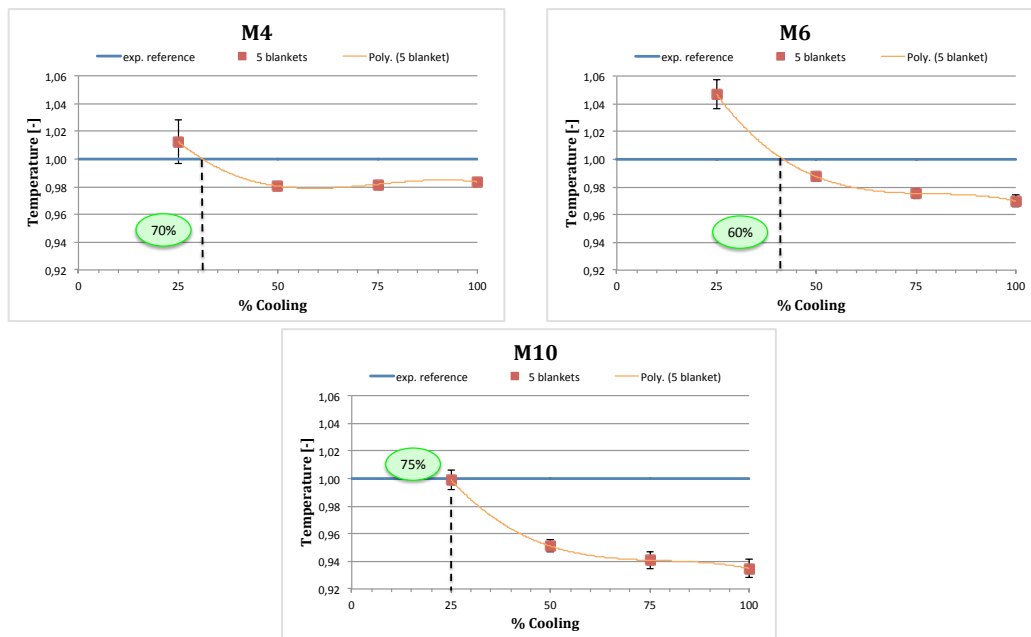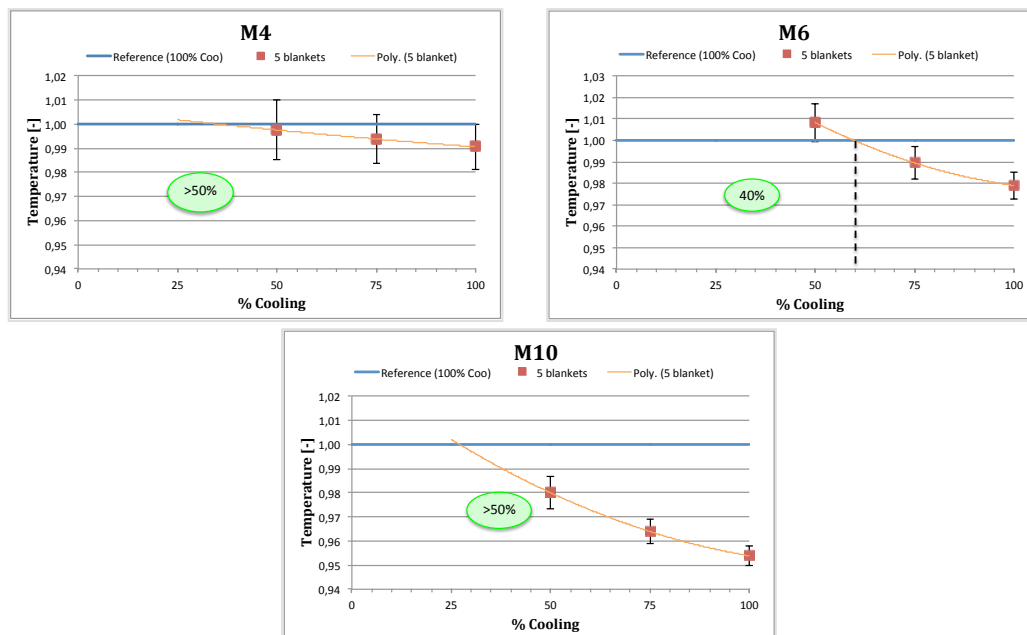

Figure 4.41: Experimental results for the Casing thermocouples

Table 4.29: Casing thermocouples ΔT – Set 3

	Casing thermocouples ΔT		
% Coo	**M4**	**M6**	**M10**
100%	4,4	9,8	22,5
75%	2,9	4,9	17,6
50%	1,2	-3,9	9,8
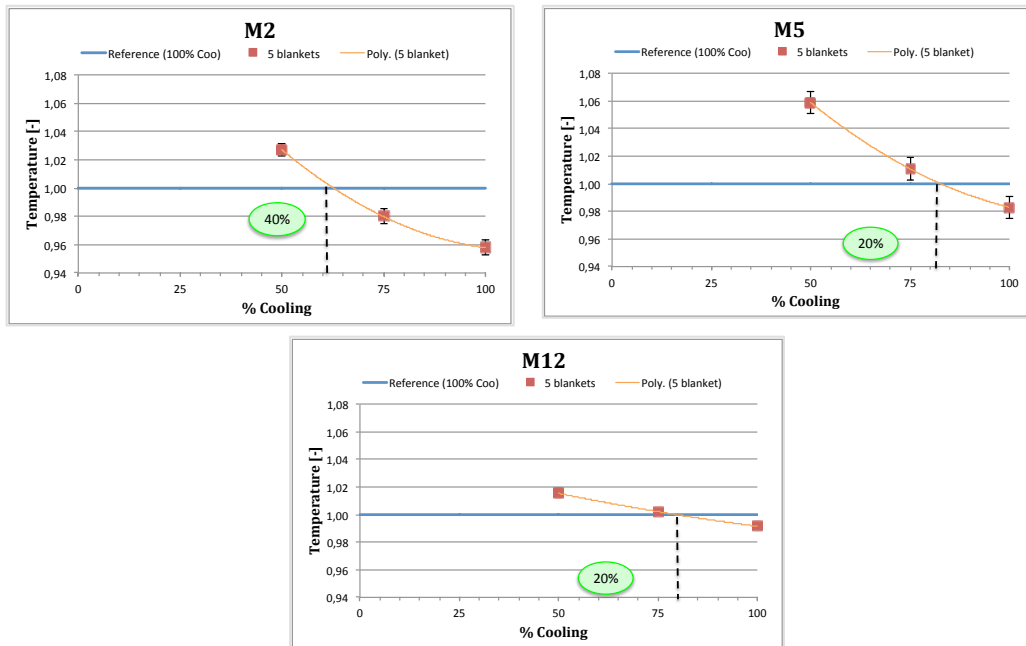
Figure 4.42: Experimental results for the Rails thermocouples

Table 4.30: Rails thermocouples ΔT – Set 3

	Rails thermocouples ΔT		
% Coo	**M2**	**M5**	**M12**
100%	23,4	8,6	5,0
75%	11,1	-5,5	-1,3
50%	-15,1	-29,6	-9,1

Table 4.31: Inlet conditions discrepancies

Test	Flow Path			Cooling			ACC		
	Δm [%]	**Δp [%]**	**ΔT [%]**	**Δm [%]**	**Δp [%]**	**ΔT [%]**	**Δm [%]**	**Δp [%]**	**ΔT [%]**
100% Coo	1,12	0,08	0,34	0,25	0,55	2,57	1,59	1,23	7,24
75% Coo	1,36	0,13	0,14	0,48	0,43	2,57	1,99	1,29	9,50
50% Coo	1,41	0,52	0,07	0,36	0,12	2,41	2,26	1,30	14,83

Table 4.32: Percentage errors on temperatures

	Error [%]					
Test	M4	M6	M10	M2	M5	M12
100% Coo	0,95	0,66	0,44	0,56	0,83	0,10
75% Coo	1,04	0,76	0,54	0,53	0,80	0,09
50% Coo	1,23	0,89	0,68	0,43	0,75	0,05

Examining each metal thermocouple it is possible to remark how, also in this case, the M4 and the M10 sensors are the ones that get a higher benefit from the presence of the blankets, allowing a Coo reduction higher than 50%. The sensor M6, instead, exhibits a Coo air reduction of around 40%. Therefore, considering the whole Casing length, the application of the 5 blankets, under these specific boundary conditions, allows a Coo reduction of about 40%.

Regarding the thermocouples placed in the zones near the Rails, the temperatures recorded by the sensor M2, overcomes the *exp. reference* when the Coo air reduction is around 40%. Instead, the sensors M5 and M12 are less influenced by the blankets and exhibit only a 20% of Coo reduction.

In Table 4.33, the allowed Coo air reductions, evaluated for each set of experiments, are summarized. The resulting allowed Coo mass flow rate, considering the whole Casing length, therefore, ranges between 35% and 60%.

Table 4.33: Allowed Coo air reductions for the 3 Sets of experiments

Allowed Coo mass flow rate reductions [%] - Casing		
M4	M6	M10
70	60	75
45	35	>50
>50	40	>50

The obtained experimental results confirm the trend observed during the numerical analyses. In fact, the minimum practicable reduction of Coo is evaluated, during each test, in correspondence of the thermocouples M6.

4.5 Data Post Processing

The last activity step (Figure 4.43), the data post processing, has been devoted to comparing the results, obtained during the experimental campaign, with the ones numerically forecasted, in order to evaluate the accuracy of the numerical model.
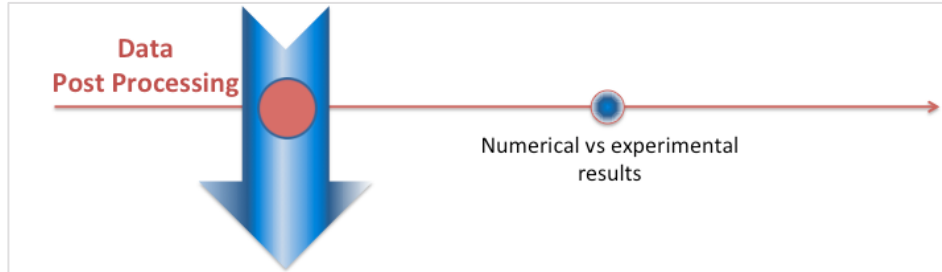
Figure 4.43: Data post processing activities – flow chart

4.5.1 Numerical vs experimental results

After the experimental campaign, the obtained temperatures and the allowed reductions of the Coo mass flow rate have been compared with the ones resulting from the numerical simulations. This comparison has been particular useful in evaluating the accuracy of the numerical models following the changes (e.g., introduction of the blankets in the 1D flow network, proper changes in the application of the heat transfer coefficients, etc.) implemented in order to insert the blankets in the TA models.

By comparing the data reported in Table 4.14 and Table 4.33, it is possible to notice how the Coo air reductions, experimentally obtained, are lower than the ones numerically forecasted.

There are three reasons for this mismatch:

1) A not perfect compliance between the fabricated blankets and the ones numerically tested, resulting in gaps among the blankets and the surroundings surfaces different from the ones set to run the numerical models.

2) The models, used to simulate the TA thermal behavior after the introduction of the blankets, are models for which the tuning has been performed referring to a case without blankets, therefore, even if these models are capable of reproducing, with a good accuracy, what happens inside the TA before the implementation of the blankets, they are not perfectly capable of simulating the new configuration.

3) The mismatch can also be ascribed to the small discrepancies between the experimental and the numerical data that the starting numerical models (i.e. the model without blankets) still presented after the tuning.

These three sources of errors, therefore, have been considered comparing the numerical and experimental data obtained with the application of the blankets.

1) Non-perfect compliance between blankets experimentally and numerically tested

Since the blankets, used for the experiments, are products that are not directly available on the market, it was necessary to create a mold, specific to each blanket, in order to manufacture them.

Due to some production problems, the molds for the blankets 1, 2 and 3 have been built about 4 cm shorter than the TA depth, producing unavoidable hot air leakages from the FP toward the Coo area.

In addition, a non-perfect compliance with the construction tolerances has led to gaps, for the blankets 4 and 5, which are greater than the ones set in the numerical simulations but still less appreciable compared to the gaps occurred during the realization of the blankets 1, 2 and 3.

To take into account numerically the differences in the geometrical dimensions between the designed blankets and the built ones, a new numerical model tuning has been performed, by changing, in the fluid network, only the Cd of the elements corresponding to the wrong gaps (blanket surface – surroundings cavity surfaces).

As previously done, for the starting model without blankets, also for this model, the calibration process has been performed on one test case and, then verified, by using the other available experimental tests.

Here, for briefness, only the temperature results obtained with the set of experimental data, used to carry out the tuning procedure, are shown. The test referred to is the one with temperatures for the FP and the Coo of 873 K and of 473 K, respectively. The criteria applied in evaluating the goodness of the match are the same reported above in chapter 3.2.5.

In Table 4.34, the differences pre and post tuning, between the experimental and numerical temperature values (ΔT), are reported.

As it is possible to observe, before the tuning procedure about 35% of the total number of sensors were outside the tolerance ranges, while after the match, only 5% of the sensors still remain outside the tolerance range.

In general, after the new tuning, the numerical temperatures have shown a good agreement with the experimental ones, satisfying the required tolerance criteria. In fact, by considering the three sets of experiments (Table 4.8) and the related reductions of Coo mass flow rate, the percentage of the temperature sensors outside the tolerance range is 9% of the total number of the thermocouples. Therefore, in what follows, the experimental data will be compared with the data obtained with the numerical model, which is matched on the basis of the real sizes of the manufactured blankets.

Pre Thermal Match						Post Thermal Match					
	ΔT			**ΔT**			**ΔT**			**ΔT**	
T1	0	✓	M1	-		T1	0	✓	M1	-	
T2	52,3	✗	M2	-11,1	✓	T2	13,1	✓	M2	-2,3	✓
T4	2,3	✓	M3	-13,1	✓	T4	-16,2	✓	M3	-14,1	✓
T5	-15,2	✓	M4	44,3	✗	T5	-25,2	✓	M4	5,1	✓
T6	-12,2	✓	M5	8,7	✓	T6	-6,8	✓	M5	0,7	✓
T7	-1,5	✓	M6	19,1	✓	T7	-0,1	✓	M6	-18,9	✓
T8	10,4	✓	M7	4,9	✓	T8	5,6	✓	M7	-14,0	✓
T9	66,1	✗	M8	11,3	✓	T9	16,3	✓	M8	-1,5	✓
T10	8,3	✓	M9	4,0	✓	T10	-18,0	✓	M9	-17,6	✓
T11	18,8	✓	M10	30,9	✗	T11	10,9	✓	M10	-24,9	✓
T12	64,4	✗	M11	30,8	✗	T12	-24,6	✓	M11	3,6	✓
T13	185,9	✗	M12	36,1	✗	T13	-4,0	✓	M12	-24,6	✓
T14	134,1	✗	M13	23,3	✓	T14	42,2	✗	M13	3,9	✓
T15	50,4	✗	M14	16,4	✓	T15	-13,2	✓	M14	-14,8	✓
T16	28,1	✗	M15	24,1	✓	T16	-18,3	✓	M15	-6,9	✓
T17	20,4	✓	M16	21,1	✓	T17	9,9	✓	M16	5,5	✓
T18	-15,8	✓	M17	70,5	✗	T18	-50,2	✗	M17	-2,4	✓

✓ Tolerance respected
✗ Outside tolerance

The model, after the new tuning, forecasts maximum allowed reductions of Coo air closer to the ones experimentally observed and summarized, for the 3 sets of experiments, in Table 4.38.

The details, concerning the comparisons between the *exp. reference* temperatures and the new ones numerically obtained are, instead, sketched in Figure 4.44, Figure 4.45 and Figure 4.46 and listed in Table 4.35, Table 4.36 and Table 4.37.
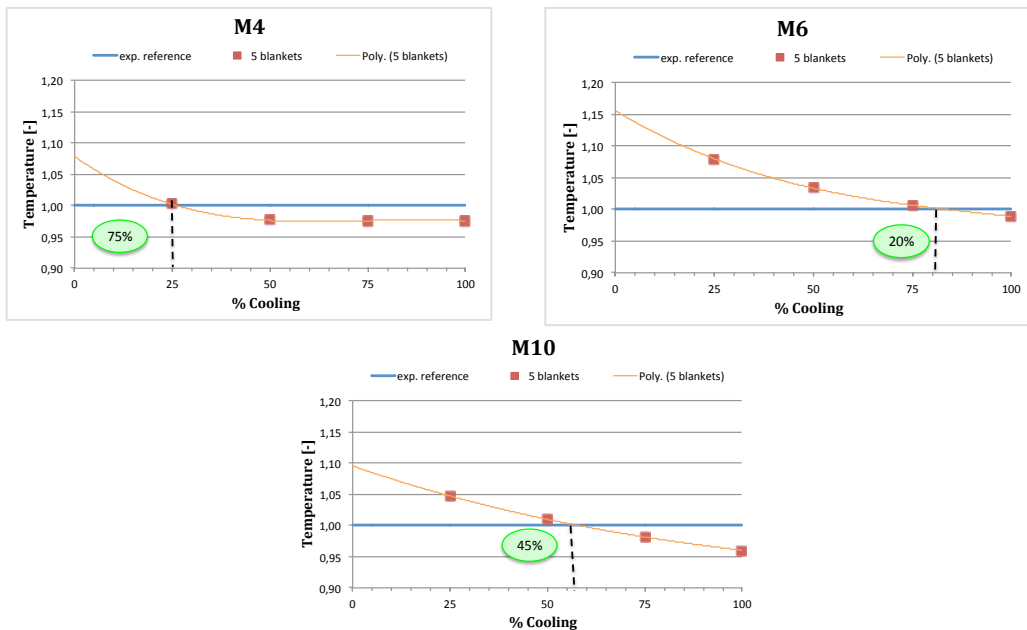
Figure 4.44: Numerical results post-tuning −Set 1

Table 4.35: Casing thermocouples ΔT – Set 1

	Casing thermocouples ΔT		
% Coo	M4	M6	M10
100%	13,9	6,2	10,9
75%	13,8	-3,8	10,9
50%	13,6	-19,1	-6,0
25%	-1,3	-45,4	-28,2
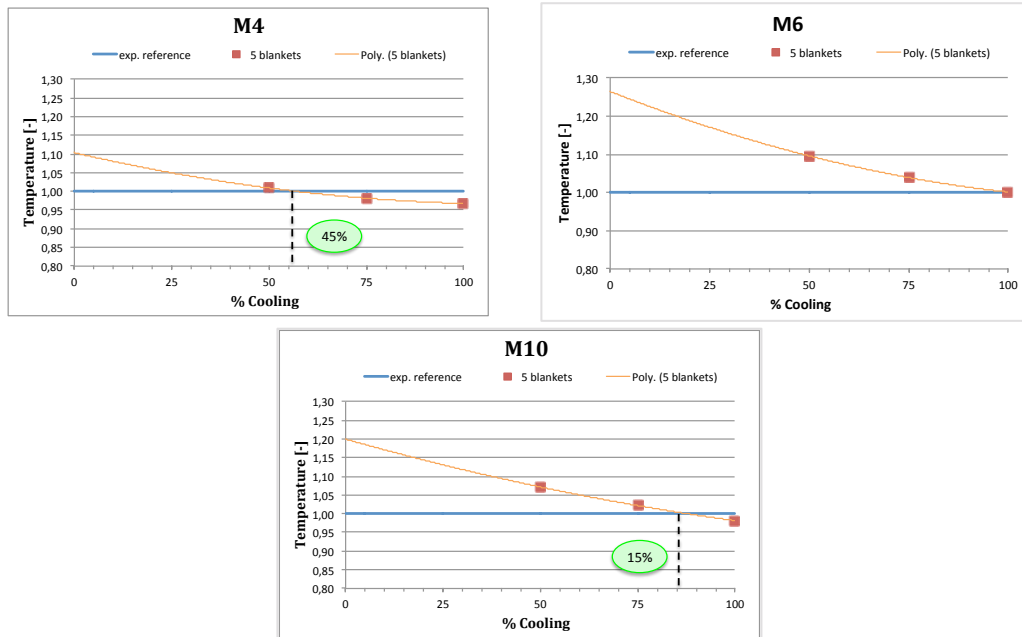
Figure 4.45: Numerical results post-tuning – Set 2

Table 4.36: Casing thermocouples ΔT – Set 2

	Casing thermocouples ΔT		
% Coo	M4	M6	M10
100%	16,0	-0,5	9,9
75%	9,0	-19,7	-11,7
50%	-4,5	-48,1	-38,5
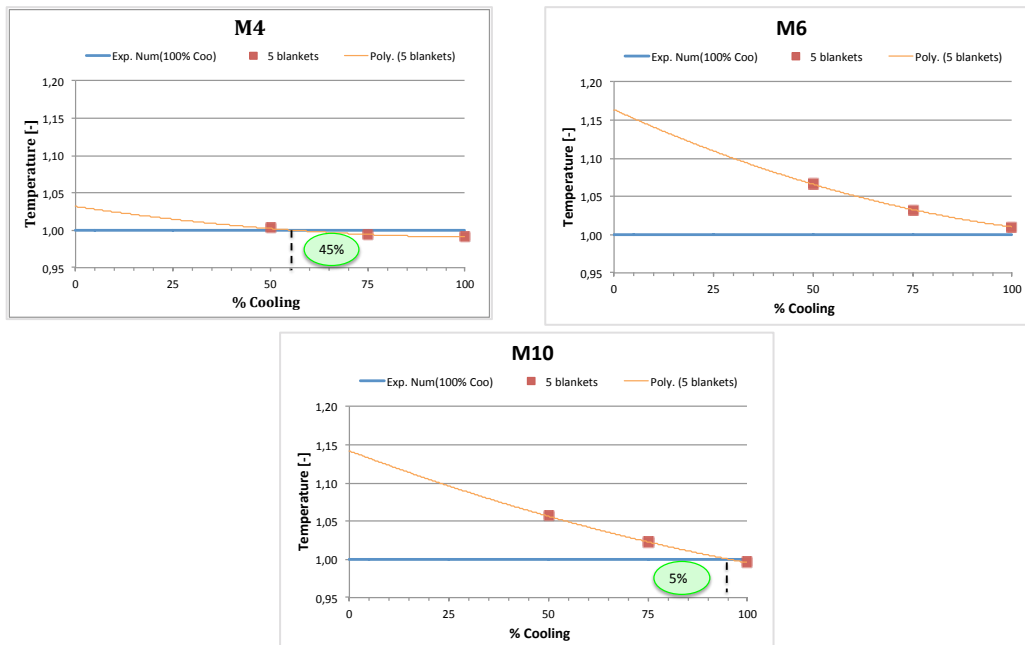
Figure 4.46: Numerical results post-tuning –Set 3

Table 4.37: Casing thermocouples ΔT – Set 3

	Casing thermocouples ΔT		
% Coo	**M4**	**M6**	**M10**
100%	4,3	-4,8	2,1
75%	2,7	-15,4	-11,2
50%	-1,1	-30,9	-27,6

Table 4.38: Allowed Coo air reductions for the 3 Sets

	Allowed Coo mass flow rate reduction [%]		
	M4	**M6**	**M10**
Set 1	75	20	45
Set 2	45	0	15
Set 3	45	0	5

Generally, for the thermocouples M6 and M10, in the numerical forecast, the temperatures obtained with the blankets exceed the corresponding *exp. reference* temperatures at lower Coo mass flow rates than in the experimental tests. On the contrary, the thermocouple M4 does not show a univocal behavior.

In Table 4.39 the percentage differences, reported in percentage point (pp), in terms of Coo air reduction between the numerical and experimental data, are reported. The negative sign before the values indicates that the numerical Coo

reduction underestimates the experimental one; conversely, the positive sign underlines a numerical overestimation.

If the whole Casing length is considered, the allowed reduction of the Coo air ranges between 0% and 20%, depending on the operating conditions.

Table 4.39: Coo air reduction overestimation/underestimation – numerical vs experimental

	Overestimation / Underestimation [pp]		
	M4	**M6**	**M10**
Set 1	+5	-40	-30
Set 2	0	-35	-35
Set 3	-5	-40	-45

2) Errors due to the starting tuned model (without blankets)

As previously done, in Chapter 4.3.3 the numerical results, here reported, have been corrected in order to account for the errors deriving from the residual discrepancies between the values of the experimental and numerical temperatures. In fact, as already explained, the tuned numerical model, even if it satisfies the required tolerance criteria, still shows discrepancies with the experimental data. These discrepancies, for the Set 1, evaluated as percentage errors, have been shown in Table 4.24.

Applying these same discrepancies to the obtained numerical temperatures, an increased reduction of the Coo mass flow rate, in particular for the sensors M6 and M10, is obtained. This way the allowed reductions of the Coo air, practicable without overcoming the *exp. reference,* are around 40% and 65% for the sensors M6 and M10, respectively. These values, for both the sensors, are 20% higher than the ones evaluated before (Table 4.38). The application of the discrepancy previously evaluated to the temperature of the M4 thermocouple, instead, doesn't entail any variation of the Cooling mass flow rate.

Therefore, for this set of inlet conditions, the final allowed reduction of the Cooling mass flow rate, along the whole Casing length, results of about 40%.

The same corrections, applied to the numerical results, obtained under the other operating conditions of the Set 2 and the Set 3 (Table 4.8), show a general increase in the Cooling mass flow rate reduction, ranging from 15% to 35%. The obtained new allowed reductions of the Cooling mass flow rate are shown in Table 4.40.

Therefore, taking into account the minimum applicable reductions of the Coo air for the 3 sets of experiments, it is possible to state that the final allowed reduction of the Cooling mass flow rate, along the whole Casing length, ranges from 15% to 40%.

Table 4.40: New allowed Coo mass flow rate reductions for the
3 Sets

Allowed Coo mass flow rate reductions [%] - Casing

	M4	M6	M10
Set 1	75	40	65
Set 2	45	15	40
Set 3	45	20	40

In Table 4.41 the differences, in terms of percentage reduction of Coo air, between the new numerical data (Table 4.40) and the experimental ones (Table 4.33), are reported. The negative sign before the values indicates that the numerical Coo reduction underestimates the experimental one, while the positive sign underlines a numerical overestimation.

Table 4.41: Coo air reduction overestimation/underestimation –
numerical vs experimental

Overestimation / Underestimation [pp]

	M4	M6	M10
Set 1	+5	-20	-10
Set 2	0	-20	-10
Set 3	-5	-20	-10

3) Errors due to the model of the blankets

From the comparison between the numerical and experimental reductions of the Coo (Table 4.41), it is still possible to observe a general underestimation of the experimental evidence. This underestimation is more evident for the sensors M6 and M10, while a lower error is associated with the thermocouple M4. This means that the changes in the model, implemented to introduce the blankets, have led to a lower accuracy in the model, which exhibits more remarkable discrepancies between the experimental and the numerical temperatures. These increased discrepancies result in additional percentage errors, listed for the Set 1, in Table 4.42.

Table 4.42: Percentage errors on temperature for the final
model – Set 1

Sensor	error [%]
M4	0,79
M6	-1,98
M10	-2,73

These different uncertainties result in a numerical underestimation of the allowed reductions of the Coo mass flow rate of about 20% compared to the experimental evidence.

Chapter 5

Thermal insulation selection

5.1 Selected solutions

The application of the Thermal Blankets (denominated in what follows *conventional* blankets) has exhibited some limits mainly related with the roughness of the metal layer of the blankets, which does not allow the blankets to perfectly adhere to the cavities surfaces and so does not allow a perfect sealing in the desired directions.

The last activity carried out, therefore, has been devoted to the selection of the thermal insulation in order to overcome the limits presented by the application of the *conventional* blankets.

Among the different analyzed solutions, some of which previously described in Chapter 4.2, the one considered most promising refers to the use of a different kind of blanket. The suggested new blankets still contain an insulating material, but the external metal layer is replaced with an adhesive layer. This new kind of coating has the double function of containing the inner material and, at the same time, of guaranteeing the sealing of the blanket surface with the desired cavity surface.

The chosen insulating material (Figure 5.1a) is the *3000°F Ceramic Paper*, produced by the Altatemperatura company, while the adhesive-paint, also produced by the same company, is denominated *2300°F Resbond 907* (Figure 5.1b).

The *Ceramic paper* is made of refractory ceramic fibers of high purity alumina. It offers an excellent resistance to high temperatures, up to 3000°F (1922 K). Among the other features of the *Ceramic paper*, the main ones are: resistance to thermal shocks and to corrosion, flexibility and machinability. In Figure 5.2 its main proprieties have been reported.
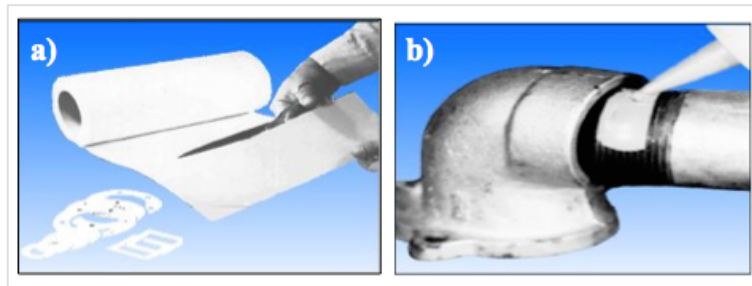
Figure 5.1: Materials of the new blankets -
a) insulating materials, b) adhesive paint

3000°F Ceramic Paper proprieties

Service temperature [K]	1922
Melting point [K]	2033
Density [kg/m^3]	192
Specific heat [J/kgK]	1046

Thermal conductivity [W/mK]	
288	0,041
533	0,055
810	0,087
1088	0,130
1366	0,192
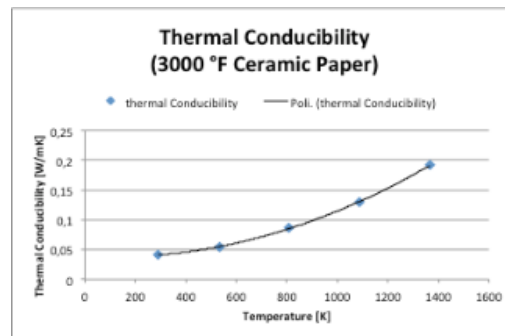
Figure 5.2: Main proprieties of the insulating material

Regarding the adhesive-paint (Table 5.1), it has been appositely chosen to adhere to the inner surface of the Casing, which is realized in AISI316. The adhesive-paint is a composite mica-based material with specific characteristics: fire-proof resistance, high gripping tenacity, high electrical resistance and high solvent resistance. It can be applied directly on steel, metal, etc., without any need for specific surface treatments. Its service temperature is up to 1533 K.

Table 5.1: Adhesive main proprieties

Resbond 907 proprieties	
Thermal conductivity [W/mK]	0,86
Thermal expansion [x10^4/ K]	1,7
Flexural Strength [bar]	86,2
Compressive Strength [bar]	241,3

5.2 Numerical analyses: sensitivity

The new insulating solution has been tested on the ThermalCase models in order to identify the suitable position, number and dimension of the blankets.The starting model, used to study the thermal behavior resulting from the application of the new blankets, is the model previously adopted for the conventional blankets (Figure 4.11b). In the model, 5 blankets, made with the new material, have been implemented again. In particular, three blankets have been located in the cavities below the Rails while the other two have been placed in the cavities immediately under the Casing plate. The gaps (Figure 5.3), set between the blankets and the surfaces facing them, are the ones used for the Sizing 2 (Table 5.2).
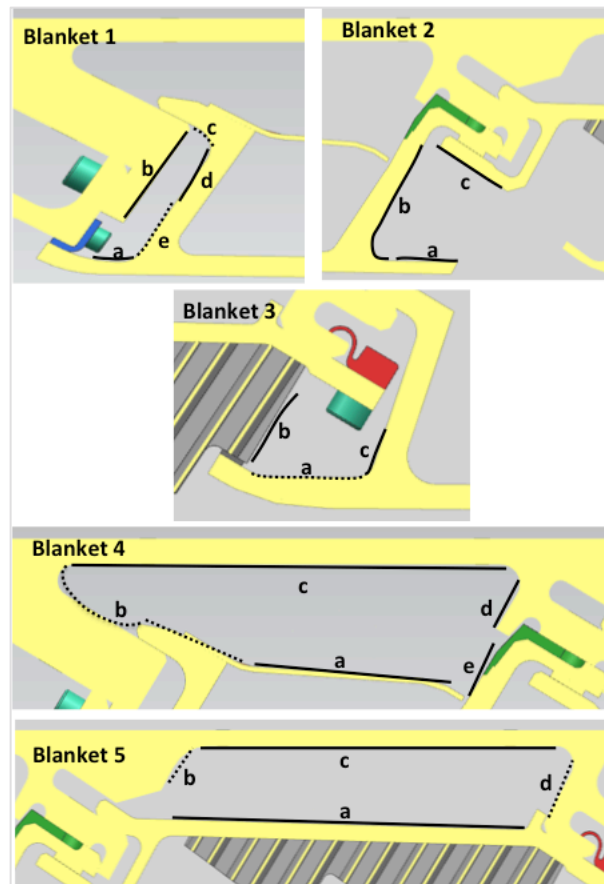
Figure 5.3: Blankets gaps position

Table 5.2: Sizing 2 gaps

Gap [%] - Sizing 2

Blanket n#	a	b	c	d	e
1	46	38	38	46	46
2	13	13	13	-	-
3	46	100	46	-	-
4	13	46	46	13	46
5	46	30	30	30	-

The model that has been chosen in order to implement the new blankets is the initial numerical one, described in Chapters 4.5.1. The reason why it has been chosen instead of the one matched with the blankets is that the match performed on this last model cannot be considered as a real Thermal Match, but only as a way to reproduce numerically the experimental evidence resulting from the non-conformity of the produced blankets with the ones numerically tested.

As previously done, the goodness of the proposed technology has been evaluated in terms of Cooling air reduction practicable without any Casing temperature overcoming the *reference* one. In what follows, only the results, obtained running the model with the FP and the Coo temperatures set at 873 K and 473 K, respectively, are discussed.

5.2.1 Position of blankets

Thanks to the new coating of the blankets, the only gaps required between the blankets and the surrounding surfaces are the ones required for the instrumentation, while no gaps are dictated by the surface roughness of the blankets.

Therefore, the sensitivity about the position of the blankets has been performed, starting from the 5 new blankets located as in the Sizing2, in order to identify the surfaces where the blankets have to be stuck, allowing the desired grip and, at the same time, blocking the air passage in those directions.

At the modeling level, in order to carry out the analyses about the position of the blankets, the main performed changes are: in the fluid network, where the blankets have been considered stuck against a cavity surface without any gap, the branches, which simulate the air passages between the blankets and the cavity surfaces, have been deleted; in the FEM model, the blankets completely adhering to the cavity surfaces have been modeled by creating a mesh equivalence in the contact zones between the two components (blanket surface – cavity surface).

In Figure 5.4 the configuration, considered more performing in terms of reductions of the Casing temperature, is shown. This configuration, which is considered to be the best, denominated Case A, is obtained by moving the blankets 1 and 2 in the upward direction, the blanket 3 in the right and downward direction, and, finally, the blankets 4 and 5 in the upward direction. In the mentioned directions, the blankets 4 and 5 completely adhere to the cavity surfaces, blocking the Coo passages between the blankets and the inner Casing surface. Using the *conventional* blankets, these air passages were unavoidable due to the roughness of the metal layer of the blankets.

In Figure 5.5 the thermal map, obtained by running the numerical model, implemented for the Case A, with the inlet boundary conditions of the Set 2 and with 100% of Coo mass flow rate, is shown.

In Figure 5.6, the comparisons between the temperature distributions of the *reference* case (i.e. the temperature obtained by running the *reference* model, without blankets and with the full amount of Coo air) and the ones obtained for

both the new blankets (Case A) and the 5 *conventional* blankets, with the full amount of Coo air (100%), are reported.

In Table 5.3, the numerical ΔT ($T_{reference}$ - $T_{blanket}$) evaluated for the Casing thermocouples are listed.
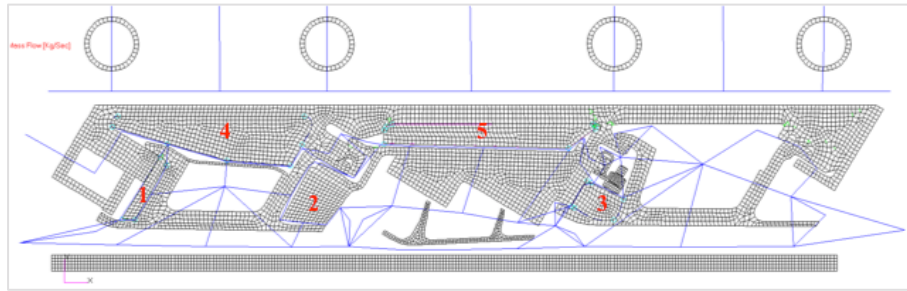
Figure 5.4: Case A – Best position configuration
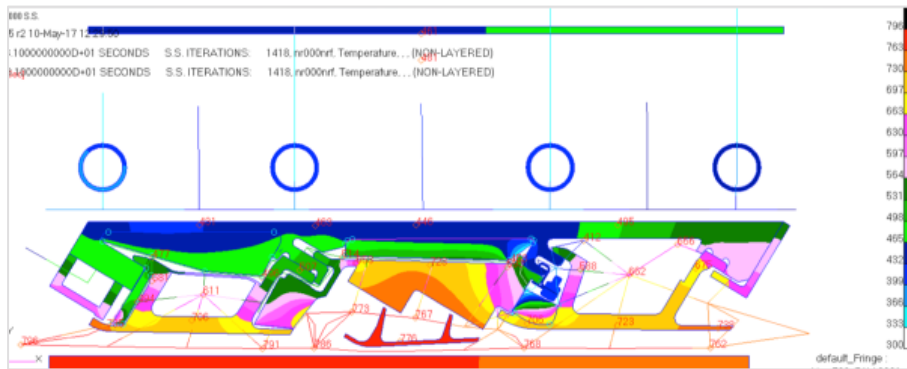
Figure 5.5: Case A thermal map – Set 2
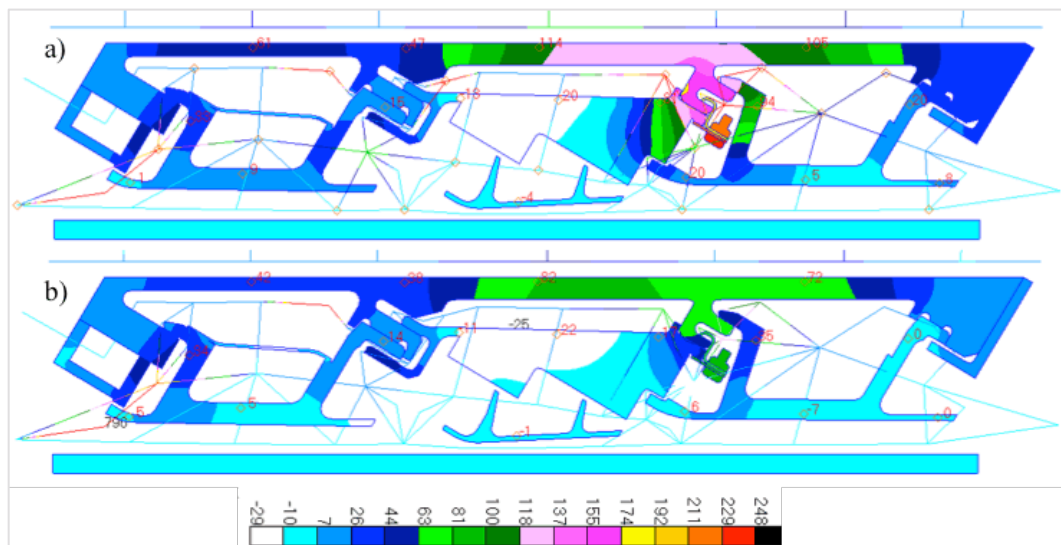
Figure 5.6: Thermal distribution differences ΔT, Set 2
a) *reference*–new blankets Case A, b) *reference–conventional* blankets

Table 5.3: ΔT Casing thermocouples, Set 2
a) *reference*–new blankets Case A, b) *reference*–*conventional* blankets

ΔT Casing thermocouples – Case A

	M4	M6	M10
a)	62	47	114
b)	42,0	38,7	82,1

In Table 5.4, for the examined cases, the percentage reductions of the Casing temperature, in comparison with the *reference* case, are reported. It is possible to note how, being the number of blankets equal, the configuration Case A allows a temperature reduction on the Casing plate higher than the one obtained with the 5 *conventional* blankets.

Table 5.4: Percentage of temperature reductions, Set 2

Temperature reduction [%]

	M4	M6	M10
Case A	12,5	9,3	20,4
Conventional	8,5	7,6	14,6

A supplementary comparison, between the experimental results, obtained during the testing phase without the blankets (*exp. reference*), for different reductions of the Coo mass flow rate, and the numerical results (CaseA), is provided in Table 5.5.

Table 5.5: Casing thermocouples ΔT – Set 2

Casing thermocouples ΔT

% Coo		M4	M6	M10
100%	*Case A*	61,9	38,4	89,9
75%	*Case A*	56,3	26,7	82,7
50%	*Case A*	46,7	6,7	70,8
25%	*Case A*	31,1	-18,5	56,6
5%	*Case A*	-18,3	-80,3	20,8

In Figure 5.7 the numeric dimensionless temperatures, recorded in correspondence of the selected Casing sensors (M4, M6 and M10) and obtained with the blankets for different Coo mass flow rates, are reported. In each graph, the temperature, measured by the same sensors but without the blankets and with the full Coo mass flow rate (*exp. reference*), is also displayed. The allowed reductions of the Coo mass flow rate are evaluated by means of the interpolating lines (Poly new blankets), which permits to identify at which percentage of Coo

reduction the calculated temperature overcomes the *exp. reference.* In addition, in Table 5.6, the allowed reductions of Coo air are listed.

Figure 5.7: Numerical results with the new blankets – Set 2

Table 5.6: Allowed Coo air reductions – Set 2

	Allowed Coo mass flow rate reduction [%]		
	M4	**M6**	**M10**
Case A	85	45	80

By considering the whole Casing length, the Coo mass flow rate can be reduced of about 45%. Moreover, using the Eq. 7, it is possible to take into account the errors due to the discrepancies between the temperatures recorded during the experiments and the ones numerically calculated by using the tuned starting model (Table 5.7). After this correction, the allowed reduction of the Coo mass flow rate increases up to 70% (Table 5.8).

Table 5.7: Percentage errors on temperatures test for the Set 2

Sensor	ΔT	Error [%]
M4	0,1	0,02
M6	-8,82	-1,76
M10	-24,48	-4,56

Table 5.8: New allowed Coo air reductions – Set 2

	Allowed Coo mass flow rate reduction [%]		
	M4	M6	M10
Case A	90	70	>95

In Table 5.9 the percentage difference, reported in percentage points, between the Coo air reductions obtainable with the new blankets and the one evaluated for the *conventional* blankets, is reported for each Casing sensor. The positive sign before the values indicates that the numerical Coo reduction obtained with the new blankets is higher than the one evaluated with the *conventional* ones.

Table 5.9: Coo air reduction differences, Set 2 new blankets (Case A) vs *conventional* blankets

	Cooling air reductions differences [pp]		
	M4	M6	M10
Set 2	+10	+20	+15

The study, previously performed for the Casing thermocouples, has been also carried out for the thermocouples located in the zones near the Rails. In Table 5.10, for the selected sensors M2, M5 and M12 the numerical differences ΔT ($T_{reference}$ - $T_{blanket}$) between the *reference* temperatures and the ones evaluated by running the numerical model with the blankets, both new and *conventional*, are listed.

Table 5.10: ΔT Rail thermocouples, Set 2 a) *reference*–new blankets Case A, b) *reference*–*conventional* blankets

	ΔT Rails thermocouples		
	M2	M5	M12
a)	33,7	15,8	94,5
b)	43,6	12,8	33,9

If the temperatures, evaluated in terms of percentage reduction with respect to the *reference* temperature (Table 5.12), are considered, for both the two analyzed cases, it is possible to note how, being the number of blankets equal, the configuration with the 5 *conventional* blankets results less performing only for the sensor M2, while for the other 2 sensors, especially for the M12, the Case A solution allows a higher temperature reduction.

Table 5.11: Percentage of temperature reductions

Temperature reduction [%]			
	M2	M5	M12
Case A	5,5	3,0	13,8
Conventional	7,1	2,4	5,0

In order to evaluate the advantages following the application of the new blankets, the obtained numerical temperatures have been compared with the *exp. reference* measured during the first test campaign without the blankets.

In Table 5.12 the ΔT between the *exp. reference* temperatures and the ones obtained with the new blankets (Case A) are reported.

Table 5.12: Rails thermocouples ΔT – Set 2

Rails thermocouples ΔT				
% Coo		M2	M5	M12
100%	*Case A*	31,6	33,5	84,7
75%	*Case A*	17,2	11,5	78,4
50%	*Case A*	-0,7	-24,0	73,4
25%	*Case A*	-51,3	-68,0	70,1
5%	*Case A*	-130,4	-188,7	57,8

In Figure 5.8 for the selected sensors, located in the zones near the Rails, the numerical dimensionless temperatures, obtained with the new blankets at different Coo mass flow rates, are reported. In each graph, the temperatures recorded by the same sensors, without the blankets and with the full Coo mass flow rate (*exp. reference*), are also displayed. The allowed reductions of the Coo mass flow rate are again evaluated by means of the interpolating lines (Poly new blankets), which allow identifying at which percentage of Coo reduction the calculated temperature overcomes the *exp. reference.* In addition, in Table 5.13, the obtained allowed reductions of Coo air are listed.
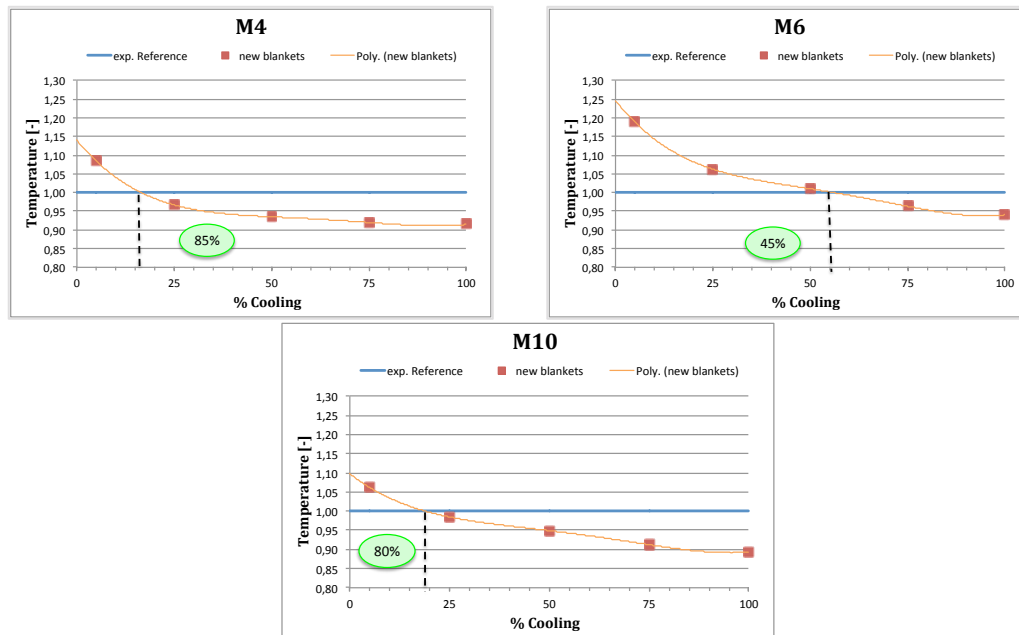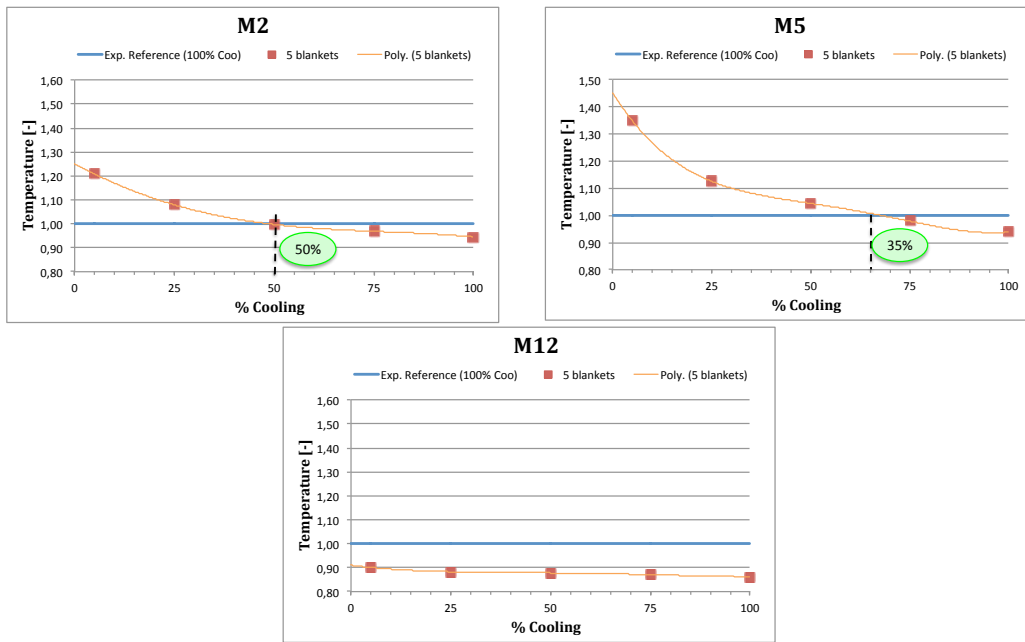
Figure 5.8: Numerical results with the new blankets – Set 2

Table 5.13: Allowed Coo air reductions – Set 2

	Allowed Coo mass flow rate reduction [%]		
	M2	M5	M112
Case A	50	35	>95

Moreover, taking into account the errors due to the discrepancies between the experimental and numerical temperatures for the tuned starting model (Table 5.14), it is possible to calculate the new allowed reductions of Coo mass flow rate, which are shown in Table 5.15.

Table 5.14: Percentage errors on temperatures for the Set 2

Sensor	ΔT	Error [%]
M2	-2,15	-0,35
M5	17,65	3,26
M12	-9,77	-1,45

Table 5.15: New allowed Coo air reductions – Set 2

	Allowed Coo mass flow rate reduction [%]		
	M2	M5	M12
Case A	50	25	>95

95

In Table 5.16 the percentage difference, reported in percentage points, between the Coo air reductions obtainable with the new blankets and the ones evaluated for the *conventional* blankets, is reported for each Rail sensor. The positive sign before the values indicates that the numerical Coo reduction obtained with the new blankets is higher than the one evaluated with the *conventional* ones.

Table 5.16: Coo air reduction differences, Set 2 new blankets (Case A) vs *conventional* blankets

Cooling air reductions differences [pp]

	M2	M5	M12
Set 2	-10	+5	+15

5.2.2 Number of the blankets

Being the new blankets more performing, it was possible to evaluate the impact, due to the reduction of the number of the blankets, on the cooling efficiency of the Casing plate. With this aim, starting from the configuration already introduced (Figure 5.4), the new blankets have been removed one by one from the numerical models, in order to identify the number of blankets that allows obtaining at least the same thermal insulation performance that the 5 *conventional* blankets exhibit.

In Figure 5.9 the configuration named Case B, obtained removing the blankets number 1, 2 and 3 and with the blankets 4 and 5 completely adhering to the inner surface of the Casing, is shown.

Moreover, in Figure 5.10, the thermal map obtained for the Case B, and, in Figure 5.11, the comparisons between the temperature distribution of the *reference* case and the ones obtained with the new blankets (Figure 5.12a) and with the *conventional* blankets (Figure 5.12b), are reported. All the obtained thermal maps have been calculated by running the numerical model with the inlet boundary conditions given for the Set 2 and with the total amount of Coo air. In addition, in Table 5.17, the numerical ΔT values ($T_{reference}$ - $T_{blanket}$), evaluated for the Casing thermocouples, are listed.
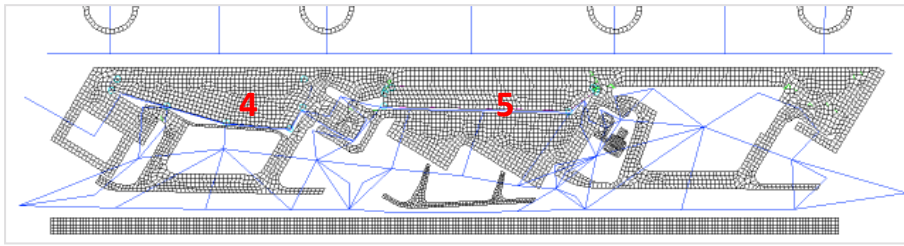
Figure 5.9: Case B – Best number configuration
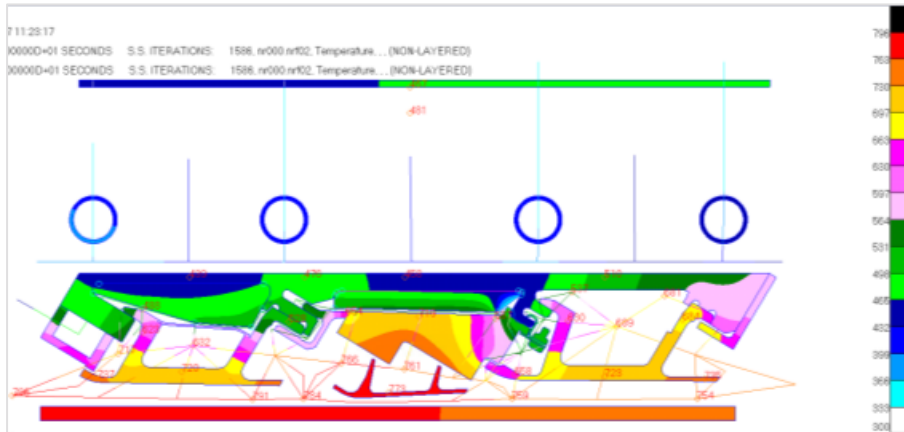
Figure 5.10: Case B thermal map – Set 2
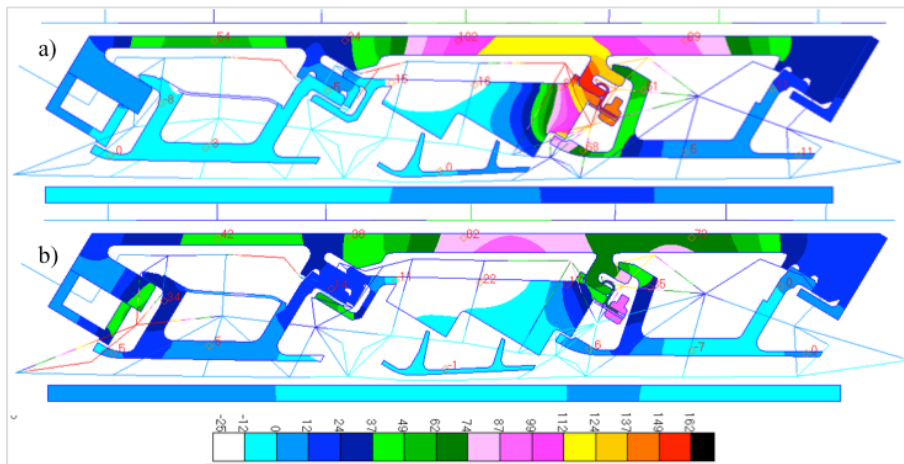
Figure 5.11: Thermal distribution differences ΔT, Set 2
a) *reference*–new blankets Case B, b) *reference*–*conventional*
blankets

ΔT Casing thermocouples

	M4	M6	M10
a)	54,3	34,2	102,8
b)	42,0	38,7	82,1

In Table 5.18 the percentages of temperature reduction, calculated with respect to the *reference* temperature, are considered for both the two analyzed cases. It is possible to note how, despite the reduction of the number of the blankets from 5 to 2, the configuration Case B still allows a temperature reduction, on the Casing plate, especially for the sensor M4 and M10, higher than the one obtained with the 5 *conventional* blankets. The sensor M6, instead, shows a slight decrease in the percentage of temperature reduction lower than one percentage point. Moreover, by comparing the obtained results (Table 5.17) with the ones of the Case A (Table 5.3), the cooling efficiency obtainable with only two blankets is lower than the one obtained with all the blankets. However, the differences in the temperature reductions are not so remarkable as to exclude the possibility of reducing the number of the blankets, especially considering the benefits that can be obtained in terms of weight.

Table 5.18: Percentage of temperature reductions

Temperature reduction [%]

	M4	M6	M10
Case B	11,0	6,7	18,3
Conventional	8,5	7,6	14,6

In order to evaluate the advantages following the application of the new blankets (Case B), the numerical temperatures, obtained giving the inlet boundary conditions of the Set 2 and reducing the Coo mass flow rate, have been compared with the *exp. reference* ones, measured during the first test campaign without the blankets.

In Table 5.19 the calculated ΔT ($T_{\text{exp}\cdot reference}$ - T_{CaseB}) are reported, while in Figure 5.13 the numerical dimensionless temperatures, obtained with the blankets at different Coo mass flow rates, are sketched and compared with the *exp. reference* temperatures.

In addition, in Table 5.20, the new allowed reductions of the Coo air are listed.

Table 5.19: Casing thermocouples ΔT – Set 2

% Coo		M4	M6	M10
		Casing thermocouples ΔT		
100%	*Case B*	54,4	25,4	78,4
75%	*Case B*	48,6	14,1	70,8
50%	*Case B*	38,6	-6,0	58,6
25%	*Case B*	26,2	-25,8	47,0
5%	*Case B*	-24,2	-87,8	11,8
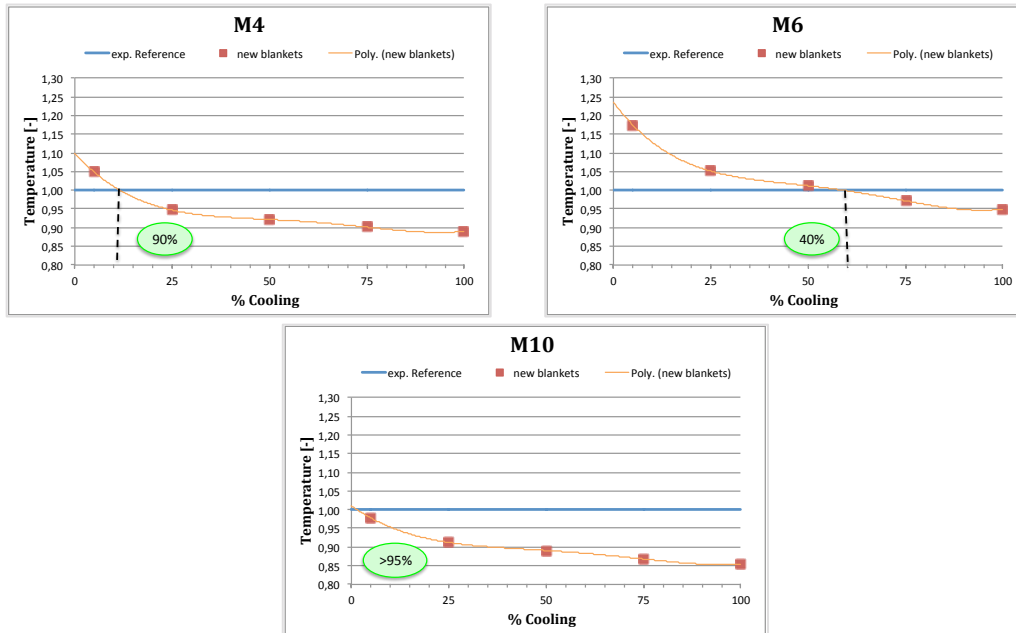
Figure 5.12: Numerical results with the new blankets – Case B

Table 5.20: Allowed Coo air reductions – Set 2

	M4	M6	M10
	Allowed Coo mass flow rate reduction [%]		
Case B	90	40	>95

As it possible to note, by considering the whole Casing length, the Coo mass flow rate can be reduced of about 40%. Moreover, taking into account the errors due to the starting tuned model (Table 5.7), the new allowed reductions of Coo air (Table 5.21) show a further possibility of reduction up to 55%.

In addition, in Table 5.22, the comparisons, in terms of percentage differences of Coo air reduction, between the numerical data obtained with the new and the *conventional* blankets, are reported.

Table 5.21: New allowed Coo air reductions – Set 2

Allowed Coo mass flow rate reduction [%]

	M4	M6	M10
Case B	90	55	>95

Table 5.22: Coo air reduction differences, Set 2 new blankets (Case B) vs *conventional* blankets

Cooling air reductions differences [pp]

	M4	M6	M10
Set 2	+10	+5	+15

The performed numerical simulations have shown that the number of the blankets can be reduced to two (Figure 5.9), maintaining anyway better thermal performances than the ones obtained using the 5 *conventional* blankets.

The study, previously performed for the Casing thermocouples, has been also carried out for the thermocouples located in the zones near the Rails.

For the selected sensors M2, M5 and M12, placed near the Rails, are reported: the numerical differences ΔT ($T_{reference}$ - $T_{blankets}$) obtained by comparing the *reference* temperatures with the ones obtained with the new (Case B) and the *conventional* blankets (Table 5.23); the percentage of temperature reductions, evaluated both for the new and the *conventional* blankets as a function of the *reference* temperatures (Table 5.24). By looking at these Tables, it is possible to note how, the reduction of the number of the blankets from 5 to 2 produces a temperature increase in correspondence with both the sensors M2 and M5, while in the zone where the sensor M12 is placed the effect of the application of the new blankets is still more appreciable than the one obtained with the 5 *conventional* blankets.

Table 5.23: ΔT Rail thermocouples, Set 2 a) *reference*–new blankets Case B, b) *reference*–*conventional* blankets

ΔT Rails thermocouples

	M2	M5	M12
a)	-8,8	-5,3	51,9
b)	43,6	12,8	33,9

Temperature reduction [%]			
	M2	**M5**	**M12**
Case B	-1,4	-1,0	7,6
Conventional	7,1	2,4	5,0

Moreover, with the aim of evaluating the effectiveness of the configuration of the new blankets (Case B) with different Coo mass flow rates, the obtained numerical temperatures have been compared with the *exp. reference* ones.

Table 5.25 reports the obtained ΔT ($T_{reference} - T_{CaseB}$), while in Figure 5.13 the obtained dimensionless temperatures, at different Coo mass flow rate, and the detected *exp. reference,* are displayed.

In addition, in Table 5.26 and Table 5.30 the allowed reductions of Coo air, evaluated before and after considering the errors due to the starting tuned numerical model, are listed, respectively.

Table 5.25: Rails thermocouples ΔT – Set 2

| Rails thermocouples ΔT				
% Coo		**M2**	**M5**	**M12**
100%	*Case B*	-10,9	12,4	42,1
75%	*Case B*	-18,0	-8,2	32,7
50%	*Case B*	-28,6	-41,8	28,1
25%	*Case B*	-44,5	-74,7	24,5
5%	*Case B*	-133,7	-198,6	13,2
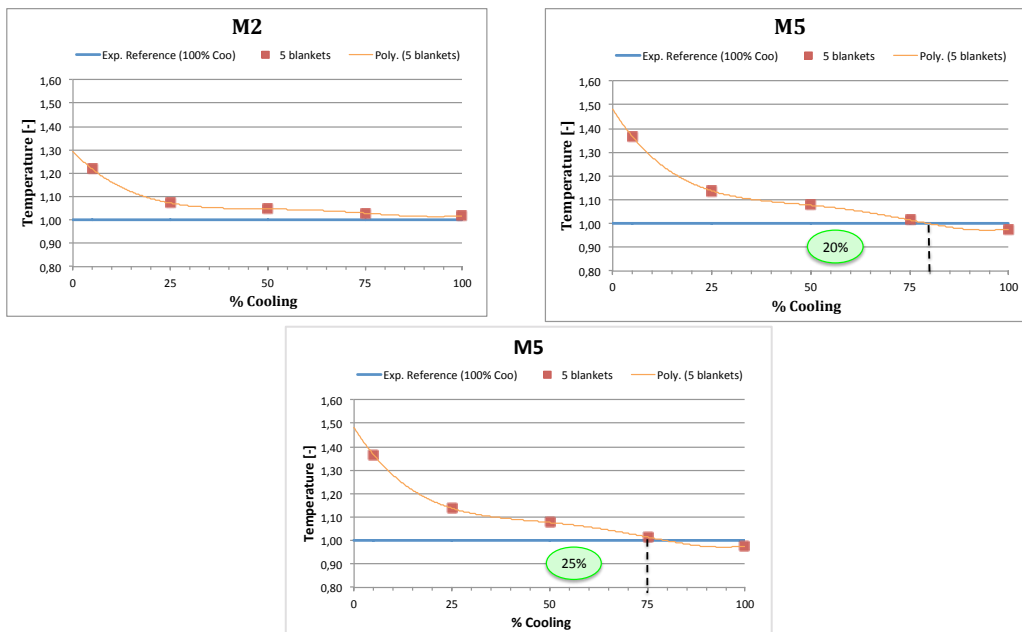
Figure 5.13: Numerical results with the new blankets – Set 2

Table 5.26: Allowed Coo air reductions – Set 2

	Allowed Coo mass flow rate reduction [%]		
	M2	M5	M12
Case B	0	20	>95

Table 5.27: New allowed Coo air reductions – Set 2

	Allowed Coo mass flow rate reduction [%]		
	M2	M5	M12
Case B	0	15	>95

In Table 5.28 the percentage differences, reported in percentage points, in terms of Coo air reduction, evaluated as already explained, are reported.

Table 5.28: Coo air reduction differences, Set 2 new blankets (Case B) vs *conventional* blankets

	Cooling air reductions differences [pp]		
	M2	M5	M12
Set 2	-60	-5	+15

5.2.3 Thickness of the blankets

On the basis of the results, presented in the previous paragraphs, it is possible to affirm that the configuration named Case B is more performing than the one experimentally tested on the Thermalcase rig. For this reason, a further study has been carried out, with the purpose of evaluating how much the thickness of the blankets can be reduced while preserving anyway at least the same performance obtained with the 5 *conventional* blankets.

The previously investigated configurations, carrying 5 or 2 blankets, made with the *Ceramic paper®,* require customized blankets, because this material is available on the market in rolls with thickness of 12 mm or 3 mm. For this reason, the following numerical analyses have been performed referring to insulating layers of 12 mm (Case C) or of 3 mm (Case D) in thickness. For both the examined cases only 2 blankets, placed in the upper cavities (Figure 5.14 and Figure 5.15), are considered.
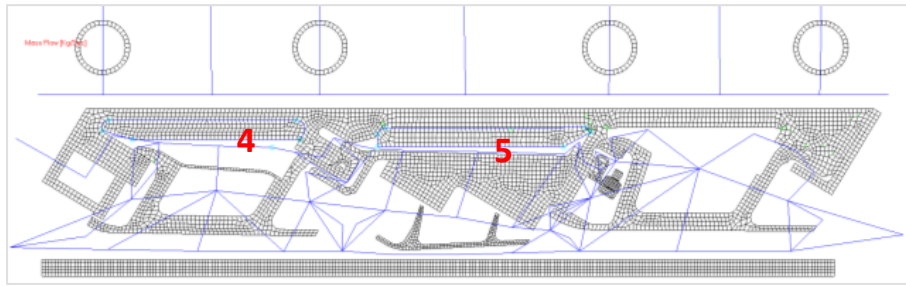
Figure 5.14: Case C – Configuration with 2 blankets (12 mm)
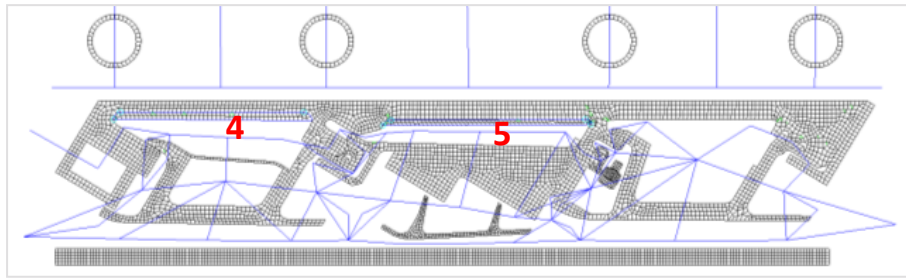
Figure 5.15: Case D – Configuration with 2 blankets (3mm)

In Figure 5.16 and in Figure 5.17 the thermal maps, obtained by running the numerical models, named Case C and Case D, with the inlet boundary conditions given for the Set 2 and with 100% of Coo mass flow rate, are shown. While in Figure 5.18 and in Figure 5.19 the comparisons with the *reference* case for the 5 *conventional* blankets case and for both the Case C and the Case D configurations, here examined, are reported. In addition, in Table 5.29 and in Table 5.30 the numerical ΔT values ($T_{reference}$ - $T_{blanket}$), evaluated only for the Casing thermocouples, are listed.
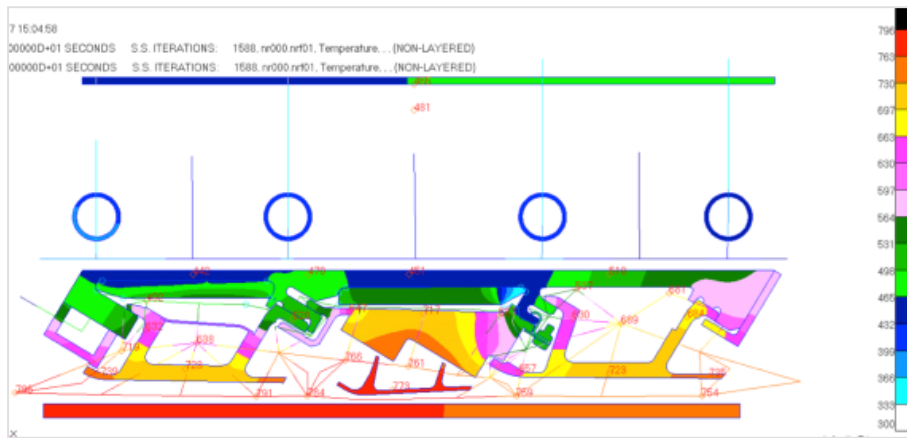
Figure 5.16: Case C thermal map – Set 2
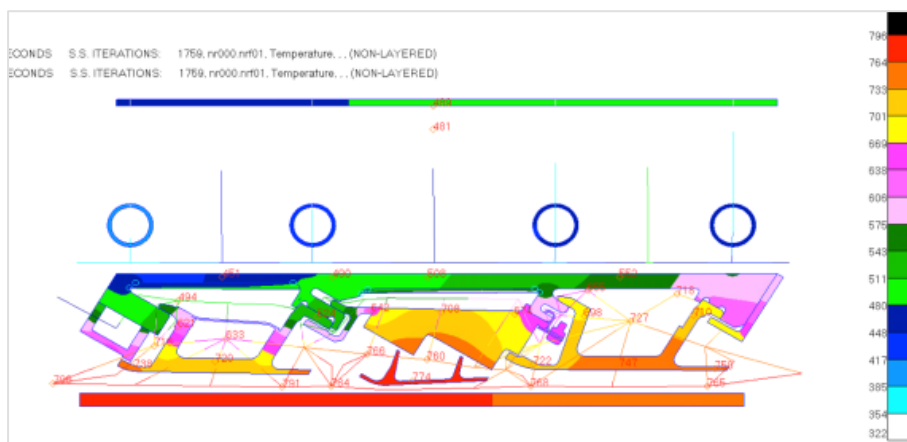
Figure 5.17: Case D thermal map – Set 2
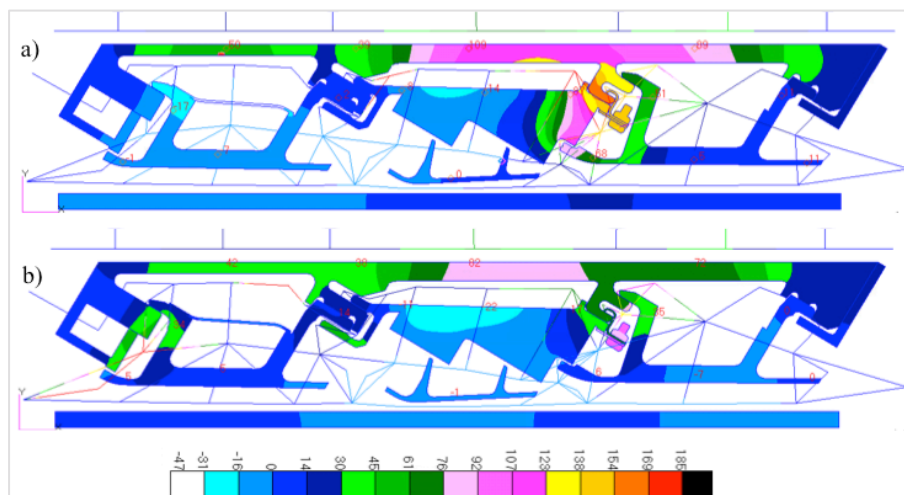
Figure 5.18: Thermal distribution differences ΔT, Set 2
a) *reference*–new blankets Case C, b) *reference*–*conventional*
blankets
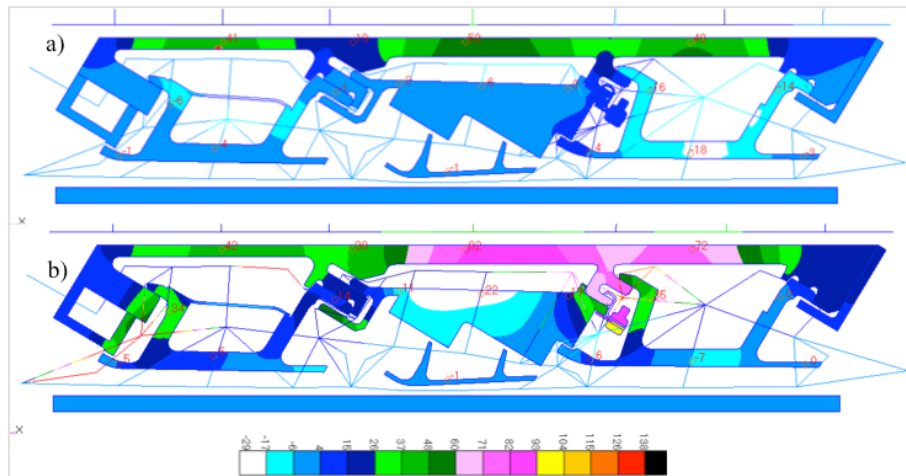
Figure 5.19: Thermal distribution differences ΔT, Set 2
a) *reference*–new blankets Case D, b) *reference*–*conventional* blankets

Table 5.29: ΔT Casing thermocouples, Set 2
a) *reference*–new blankets Case C, b) *reference*–*conventional* blankets

ΔT Casing thermocouples

	M4	M6	M10
a)	50,8	39,7	109,8
b)	42,0	38,7	82,1

Table 5.30: ΔT Casing thermocouples, Set 2
a) *reference*–new blankets Case D, b) *reference*–*conventional* blankets

ΔT Casing thermocouples

	M4	M6	M10
a)	41,7	19,9	53,1
b)	42,0	38,7	82,1

Evaluating the temperatures in terms of percentage reduction (Table 5.31, Table 5.32), as previously done, it is possible to note how two blankets of 12 mm in thickness, as in the Case C, exhibit better performances than the 5 *conventional* blankets.

The reduction of the thickness of the blankets to 3 mm, as in the Case D, results in a decreased effect of the thermal insulation compared to the one shown by the *conventional* solution.

Table 5.31: Percentage of temperature reductions – Case C

Temperature reduction [%]			
	M4	M6	M10
Case C	10,3	7,8	19,6
Conventional	8,5	7,6	14,6

Table 5.32: Percentage of temperature reductions – Case D

Temperature reduction [%]			
	M4	M6	M10
Case D	8,4	3,9	9,5
Conventional	8,5	7,6	14,6

In Table 5.33 and in Table 5.34 the ΔT between the *exp. reference* temperatures and the ones obtained with the new blankets (configurations named Case C and Case D, respectively) are reported.

Table 5.33: Casing thermocouples ΔT – Set 2 – Case C

% Coo	Casing thermocouples ΔT	M4	M6	M10
100%	*Case C*	50,9	30,9	85,3
75%	*Case C*	44,5	20,3	78,9
50%	*Case C*	33,5	0,9	68,6
25%	*Case C*	18,9	-19,0	58,3
5%	*Case C*	-32,1	-82,7	24,7

Table 5.34: Casing thermocouples ΔT – Set 2 – Case D

% Coo	Casing thermocouples ΔT	M4	M6	M10
100%	*Case D*	41,8	11,1	28,7
75%	*Case D*	35,6	-1,7	16,7
50%	*Case D*	25,2	-22,9	1,1
25%	*Case D*	11,6	-43,2	-12,5
5%	*Case D*	-43,0	-106,7	-49,4

In Figure 5.20 and in Figure 5.21, for the selected Casing sensors (M4, M6 and M10), the numerical dimensionless temperatures, obtained with the blankets

at different Coo mass flow rates, for the Case C and Case D respectively, are reported, while, in Table 5.35, the allowed reductions of Coo air are listed.
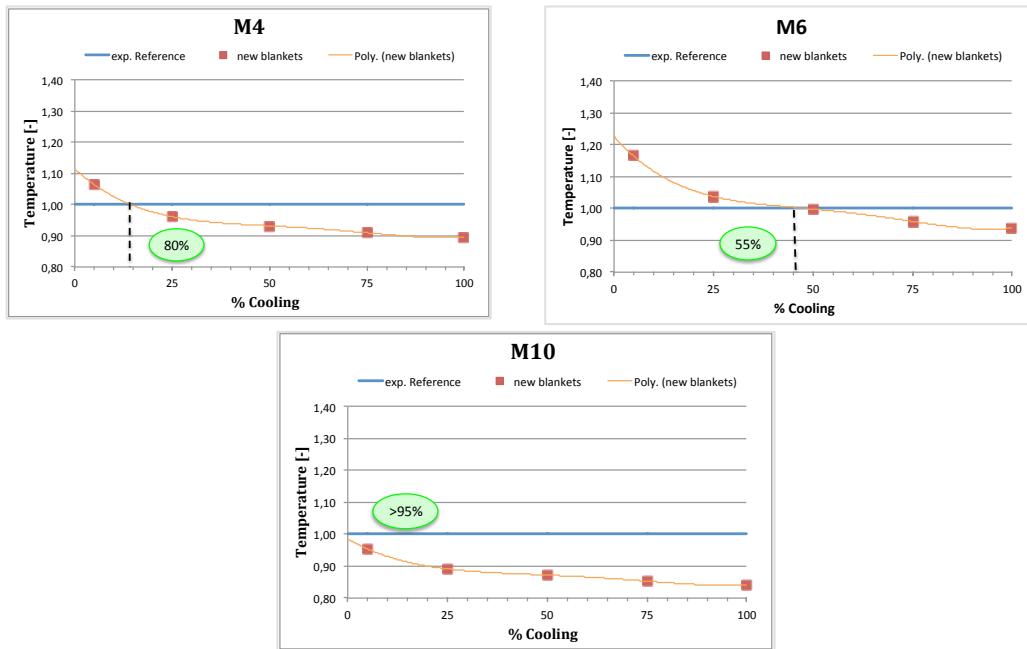
Figure 5.20: Numerical results with the new blankets –Case C
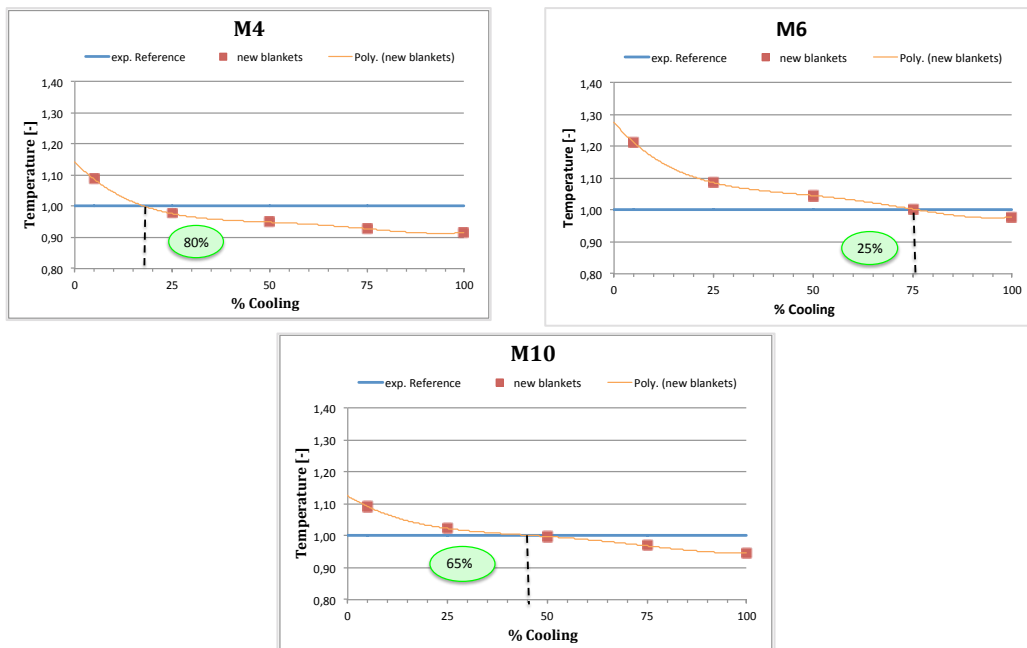
Figure 5.21: Numerical results with the new blankets –Case D

Table 5.35: Allowed Coo air reductions – Set 2

	Allowed Coo mass flow rate reduction [%]		
	M4	**M6**	**M10**
Case C	80	55	>95
Case D	80	25	65

By considering the whole Casing length, the Coo mass flow rate can be reduced of about 55% and of about 25% for the Case C and Case D, respectively.

Whilst, if the discrepancies between the experimental and the numerical temperatures of the tuned starting model are taken into account the (Table 5.7), it is possible to calculate the new allowed reductions of the Coo mass flow rate, shown in Table 5.36, which lead the practicable reduction of Coo air to 65% and to 30% for the Case C and the Case D, respectively. In Table 5.37, the percentage upgrade in terms of Coo air reduction is reported.

Table 5.36: New allowed Coo air reductions – Set 2

	Allowed Coo mass flow rate reduction [%]		
	M4	**M6**	**M10**
Case C	85	65	>95
Case D	80	30	85

Table 5.37: Coo air reduction differences, Set 2 new blankets (Case C, Case D) vs *conventional* blankets

	Cooling air reductions differences [pp]		
	M4	**M6**	**M10**
Case C	+5	+15	+15
Case D	0	-20	+5

As shown in Table 5.37, by using 2 blankets of 12 mm in thickness (Table 5.37), it is again possible to obtain thermal insulating performances better than the ones recorded for the 5 *conventional* blankets; while, the same performances cannot be achieved reducing the thickness of the blankets to 3 mm.

The study, previously performed for the Casing thermocouples, has been also carried out for the thermocouples located in the zones near the Rails.

In what follows, for the Rail sensors, M2, M5 and M12, the results obtained by running the numerical models with the inlet boundaries conditions of the Set 2 and using 2 blankets of 12 mm and of 3 mm in thickness, Case C and Case D respectively, are reported.

In Table 5.38 for the Case C the numerical differences ΔT ($T_{reference}$ - $T_{blanket}$) between the *reference* temperatures and the ones evaluated by running the

numerical model with the blankets, both new and *conventional*, are listed. While the ones obtained comparing the *reference* temperature with the Case D are reported in Table 5.39.

Table 5.38: ΔT Rail thermocouples, Set 2
a) *reference–*new blankets Case C, b) *reference–conventional* blankets

ΔT Rails thermocouples

	M2	M5	M12
a)	-17,4	2,9	51,9
b)	43,6	12,8	33,9

Table 5.39: ΔT Rail thermocouples, Set 2
a) *reference–*new blankets Case D, b) *reference–conventional* blankets

ΔT Rails thermocouples

	M2	M5	M12
a)	-6,6	-1,2	-16,3
b)	43,6	12,8	33,9

In Table 5.40 the temperatures, evaluated in terms of percentage reductions with respect to the *reference* temperature, are considered for all three the analyzed cases (Case C, Case D, *conventional*). It is possible to notice how the use of blankets of 12 mm in thickness decreases the temperature reduction, in comparison with the 5 *conventional* blankets configuration, for both the sensors M5 and M12, while a higher reduction is obtained for the sensor M12. On the contrary, the reduction of thickness to 3 mm produces worse performances.

Table 5.40: Percentage of temperature reductions

Temperature reduction [%]

	M2	M5	M12
Case C	-2,8	0,6	7,6
Case D	-1,1	-0,2	-2,4
Conventional	7,1	2,4	5,0

The numerical temperatures obtained with the new blankets (Case C and Case D) are compared with the *exp. reference* ones in order to evaluate the benefits in terms both of the reductions of the Rail temperatures (Table 5.41, Table 5.42) and of Coo mass flow rates (Figure 5.22, Figure 5.23).

Moreover, the obtained allowed reductions of the Coo air are summarized in Table 5.43.

Table 5.41: Rails thermocouples ΔT, Set 2, Case C

	Rails thermocouples ΔT			
% Coo		M2	M5	M12
100%	*Case C*	-19,6	20,6	42,1
75%	*Case C*	-27,4	1,3	32,4
50%	*Case C*	-39,7	-30,7	27,8
25%	*Case C*	-61,3	-63,6	24,3
5%	*Case C*	-135,6	-194,2	13,2

Table 5.42: Rails thermocouples ΔT, Set 2, Case D

	Rails thermocouples ΔT			
% Coo		M2	M5	M12
100%	*Case D*	-8,7	16,4	-26,1
75%	*Case D*	-18,4	-3,4	-39,2
50%	*Case D*	-33,6	-35,4	-48,8
25%	*Case D*	-60,8	-66,2	-56,7
5%	*Case D*	-142,2	-191,3	-74,5
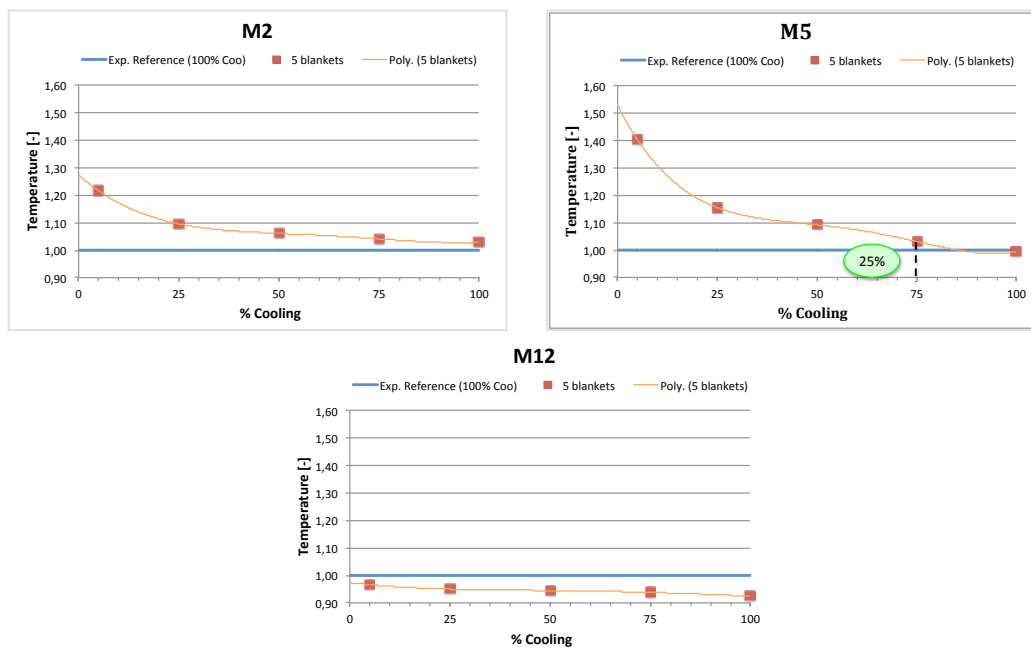
Figure 5.22: Numerical results with the new blankets, Case C
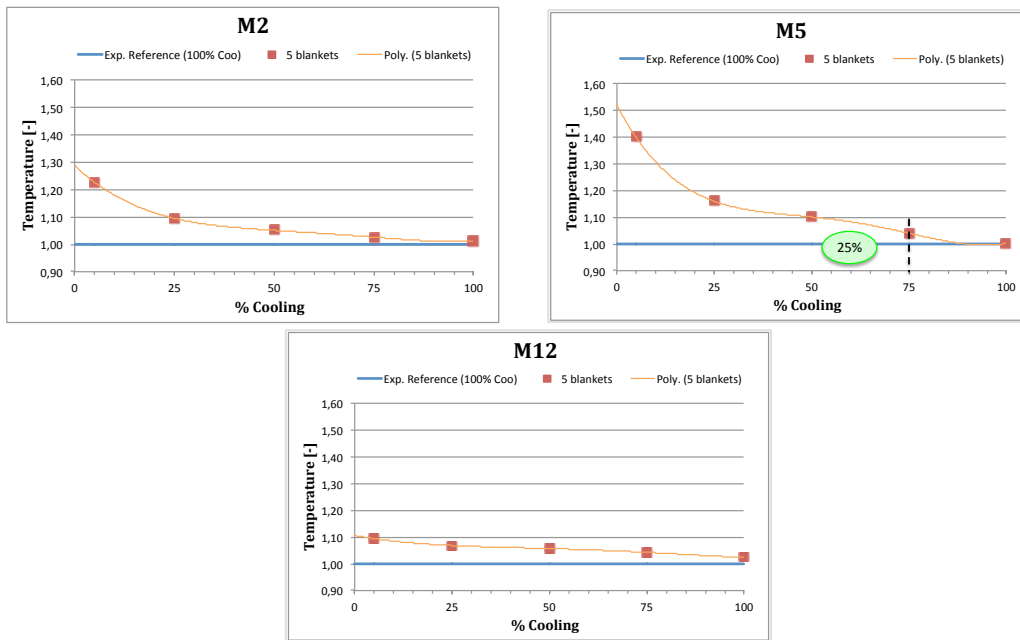
Figure 5.23: Numerical results with the new blankets, Case D

Table 5.43: Allowed Coo air reductions – Set 2

	Allowed Coo mass flow rate reduction [%]		
	M2	**M5**	**M12**
Case C	0	25	>95
Case D	0	25	0

The results, shown in Table 5.44, have been evaluated by considering the discrepancies between the experimental and numerical temperatures due to the tuned starting model (Table 5.14). These Coo air reductions are compared, in Table 5.45, with the ones obtained for the *conventional* blankets, showing a positive sign when the numerical Coo reductions obtained with the new blankets are higher.

Table 5.44: New allowed Coo air reductions – Set 2

	Allowed Coo mass flow rate reduction [%]		
	M2	**M5**	**M12**
Case C	0	15	>95
Case D	0	10	0

**Table 5.45: Coo air reduction differences, Set 2
new blankets (Case C, Case D) vs *conventional* blankets**

Cooling air reductions differences [pp]

	M2	M5	M12
Case C	-60	+5	+15
Case D	-60	+5	-75

The results obtained for the Rails thermocouples (Table 5.37), exhibit that for both the two configurations with only two blankets, the Cooling air cannot be reduced in correspondence of the sensor M2. Nevertheless, the configuration Case C, obtained by using 2 blankets of 12 mm in thickness, again allows obtaining insulating performances, in correspondence of the sensors M5 and M12, better than the ones recorded for the 5 *conventional* blankets.

On the contrary, the configuration Case D, implemented reducing the thickness of the blankets to 3 mm, does not allow achieving the same performances obtainable with the 5 *conventional* blankets, as just observed for the Casing thermocouples.

Nevertheless, following a deepened assessment of the cost– effectiveness, the configuration case C could be considered an alternative to the one with 5 blankets.

In fact, the advantages due to the Cooling air reduction could balance the disadvantages due to the higher thermal gradients resulting from the increase in temperature in the Rail#1 zone, where the sensor M2 is placed, against a decrease in temperatures on the casing.

5.3 Numerical data post-processing

In this paragraph an overview of the obtained results is provided.

5.3.1 Comparison of the proposed insulation solutions

The following tables summarize the results obtained during the sensitivity analyses and allow performing a comparison between the *conventional* blankets and the ones made with the *3000°F Ceramic Paper*.

In particular, referring to the set of experiments denominated Set 2 (Table 4.8), in Table 5.46 the percentage reductions of temperature, evaluated with respect to the *reference* temperature, are reported. Moreover, in Table 5.47 the allowed reductions of Cooling air are summarized.

Table 5.46: Percentage temperature reductions, Set 2, Casing

	Temperature reductions [%]		
	M4	**M6**	**M10**
Conventional	8,5	7,6	14,6
Case A	12,5	9,3	20,4
Case B	11,0	6,7	18,3
Case C	10,3	7,8	19,6
Case D	8,4	3,9	9,5

Table 5.47: Allowed Coo mass flow rate reductions, Set 2, Casing

	Allowed Coo mass flow rate reduction [%]		
	M4	**M6**	**M10**
Conventional	85	60	90
Case A	90	70	>95
Case B	90	55	>95
Case C	85	65	>95
Case D	80	30	85

On the basis of the comparisons reported above, it is possible to affirm that the use of the *3000°F Ceramic Paper* allows reducing both the number (Case B) and thickness (Case C) of the blankets and preserving the same performances obtainable with the 5 *conventional* blankets.

The same comparisons, carried out for the sensors placed near the Rails, are provided in Table 5.48 and Table 5.49.

Table 5.48: Percentage temperature reductions, Set 2, Rails

	Temperature reductions [%]		
	M2	M5	M12
Conventional	7,1	2,4	5,0
Case A	5,5	3,0	13,8
Case B	-1,4	-1,0	7,6
Case C	-2,8	0,6	7,6
Case D	-1,1	-0,2	-2,4

Table 5.49: Allowed Coo mass flow rate reductions, Set 2, Rails

	Allowed Coo mass flow rate reduction [%]		
	M2	M5	M12
Conventional	85	60	90
Case A	50	25	>95
Case B	0	15	>95
Case C	0	15	>95
Case D	0	25	0

Examining the different analyzed configurations, shown in the Tables reported above, the advantages due to the application of the new blankets, in the zones near the Rails, are more evident in the configuration referred to as Case A.

In fact, for this configuration, the advantages are appreciable in correspondence of all the sensors.

In the other configurations, referred to as Case B and as Case C, it is possible to achieve reductions of Coo air, without overcoming the *reference* temperature, only in correspondence of the sensors M5 and M12. Despite that, this two configurations could be considered alternative of the 5 *conventional* blankets, following a deepened assessment of the cost– effectiveness.

Finally, if the Case D is considered, the only sensor that records temperature values lower than the *reference* case is the sensor M5. For this reason, the configuration Case D cannot be taken in to consideration in order to optimize the blankets insulating performances.

5.3.2 Upgrades and benefits

The application of the new kind of blanket, made of a high performance insulating material (*3000°F Ceramic Paper*), enclosed in an adhesive layer (*2300 °F Resbond 907*), allows obtaining remarkable advantages in terms of weight and cost reduction with respect to the tested *conventional* blankets.

In fact, performing a preliminary estimation of the weight values (Table 5.50), the insulating solution that adopts the new blankets results lighter (more than 2 times in the Case C) than the one carrying the *conventional* ones. The main reasons of the reduced weight are: the new insulating material has a lower density than the *conventional* one (Case A, Case C), the number and the thickness of the new blankets are decreased (Case C); the new adhesive coating has a lower weight than the metal layer (Case A, Case C).

Table 5.50: Preliminary weight estimation

Blankets kind	Blankets n°	Insulating weight [kg]	External layer weight [kg]	Tot blankets weigh [kg]
Conventional	5	0,76	1,57	2,33
New (Case A)	5	0,58	0,79	1,37
New (Case C)	2	0,26	0,68	0,94

Considering the economic aspects and carrying out a preliminary estimation of the costs involved, it is possible to affirm that the cost of the new blankets, regardless of what configuration is taken into account, is about one order in magnitude lower than the one of the *conventional* blankets. The main reason is that the metal layer of the *conventional* blankets is manufactured through a molding process and it, therefore, requires specific molds for each blanket, which have to be fabricated ad hoc. The new blankets, instead, are easy to be produced because the insulating material can be modeled with simple shaping and the new coating does not require superficial treatment and, consequently, may be applied on the insulating material directly in the laboratory.

Chapter 6

Conclusions

The research activity, previously reported, has been carried out in order to point out innovative thermal insulating solutions, with the aim of minimizing the Cooling air, bled from a suitable compressor stage and injected into the LPT cavities, placed below the Casing surface. The Cooling air referred to is used to control the thermal expansions and contractions of the turbine components and represents a power loss for the engine, consequently penalizing its efficiency.

Identifying alternative solutions capable of decreasing the temperature of the Casing plate, therefore, would have the function of reducing the thermal load of the Casing plate, which requires specific materials to withstand high temperatures.

Thus, the Coo mass flow rate used to cool down the plate could be reduced, decreasing the input power for the compressor and improving the efficiency of the whole engine system.

The main object of the activity, that is the identification of an innovative insulating solution for a reduced temperature of the Casing plate, has been achieved through the use of an integrated fluid-thermal numerical analysis.

The accomplished studies have been started with the tuning and validation of the available numerical models (fluid and thermal), which reproduce the TA placed in the available rig Thermalcase. The numerical models, used to predict the thermal behavior of one stage of a LPT, have been tuned by using the data obtained during a first experimental campaign, carried out with the Thermalcase testing facility.

In general, the obtained numerical results have shown a good agreement with the experimental data, satisfying the tolerance criteria set for the pressure and temperature values. After the tuning only 15% of the total number of the pressure sensors is still outside the tolerance range, while, from the temperatures point of view, the total number of sensors is within the tolerance range.

The matched model has been used to study and compare different insulating configurations capable of reducing the temperature of the Casing surface and, consequently, of minimizing the Cooling air. The first analyzed solution proposes

the application, into the proper turbine cavities, of Thermal blankets, which are made of an external metallic layer, with high surface roughness, containing a conventional insulating material (glass wool). Different numerical analyses have been carried out with the aim of choosing the suitable number, position and sizing of the Thermal Blankets.

The results of the numerical analyses have shown that between the two examined configurations the one showing 5 blankets (3 blankets placed in the cavities below the Rails and 2 additional blankets located under the Casing plate, in correspondence of the first Vane and the Shroud) has better performances than the one with only 3 blankets. This configuration, in comparison with the *reference* model (i.e. the model without blankets and with 100% of Coo mass flow rate)*,* allows obtaining remarkable reductions of the numerical temperatures on the Casing plate, and particularly in the zones over the first Vane and the Shroud.

Furthermore, the sensitivity about the size of the blankets has shown negligible effects on the distributions of the temperature, at least in the range investigated. On this basis, during the experimental campaign, which is compulsory for the validation of the proposed technology, it has been possible to preserve the original TA instrumentation.

The design solution, resulting from the previous analyses, has been used to numerically forecast, under different thermal conditions, the effectiveness of the insulation methodology through the comparison of the obtained temperatures with the ones evaluated by using the numerical model without the blankets.

The distributions of the temperature within the Test Article have been examined with a special attention to the Casing temperatures, whose thermal expansion determines lower engine efficiency.

Furthermore, the temperatures recorded by the sensors placed on the Casing have been compared with their *exp. references*, i.e. the temperatures measured by the same sensors during the tests, previously performed, without the blankets and using the whole Cooling mass flow rate. This way, the advantages following the application of the blankets, are suggested, for each thermocouple, by the maximum reduction of Cooling air practicable without any sensor overcoming its *reference* temperature.

Overall, this numerical approach has allowed affirming that the proposed insulation technique could be one of the promising answers to the request of a more efficient LPT, with a lower demand of Cooling air.

In fact, the numerical simulations have forecasted, considering the whole Casing length, an allowed reduction of Cooling air that ranges between 50% and 65%, depending on the FP and Coo inlet conditions.

The experimental tests, carried out by inserting the Thermal Blankets in the Thermalcase rig facility, have confirmed a general decrease in the temperature of the Casing plate, even if lower than the one numerically forecasted.

In fact, in the experiments, the allowed reduction of Cooling air, considering the temperatures along the whole Casing length, varies between 30% and 60%, depending on the FP and Coo inlet conditions.

In particular, the Thermal Blankets result more performing when the temperatures of the FP and Coo inlet mass flow rates are 873 K and 573 K, respectively.

As the experimental results did not completely meet the ones obtained numerically, which had predicted a slightly higher reduction, further numerical analyses have been carried out in order to evaluate the impact of different factors (tolerances of fabrication non satisfied, model accuracy, etc.) on the temperatures recorded during the experiments. This last comparison has been particular useful in evaluating the accuracy of the numerical model after the changes implemented to insert the blankets in the TA models.

In general, it is possible to state that the numerical model, even if tuned on the basis of experimental data, obtained without blankets, is a useful tool in order to study the new configurations. Indeed, this notwithstanding, the model did not require further thermal calibration processes because it exhibited a good level of accuracy, with 91% of the total number of sensors inside the tolerance ranges.

Despite this, the errors due to the discrepancies between the experimental and numerical data have to be taken into account in order to not underestimate the final allowed reduction of the Cooling mass flow rate.

The good results obtained with the Thermal Blankets have encouraged to perform a selection of the thermal insulation, overcoming the limits due to the surface roughness of the blankets.

Further analyses have been carried out to optimize the thermal insulation of the blankets, also considering that the goodness of the proposed solution should be a tradeoff between the additional weight, due to the blankets, and the reduction in the compression power, which is obtainable by dropping the Cooling flow.

A deepened numerical study about the split of the mass flow rates in the turbine cavities, due to the presence of the blankets, has shown that the better insulating performances are obtained when the blankets, placed in the upper cavities, adhere perfectly to the Casing surface. In this configuration, the blanket behaves like a seal, inhibiting any flow between the insulating material and the Casing surface.

For this reason, among the solutions available on the market, a promising alternative has been identified in using a different kind of blanket, which is filled with a more performing and lighter insulating material, enclosed in an adhesive layer. The external adhesive layer, in this case, has the double function of containing the insulating material and of guaranteeing that the surface of the blankets completely adheres to the desired surfaces of the cavity.

The numerical analyses performed with the new kind of blanket have been subdivided in three macro sensitivities about: the position of the blankets, the number of the blankets and finally the sizing of the blankets. The results of the sensitivities have shown that the new material is more effective in reducing the thermal loads onto the Casing than the *conventional* one.

Furthermore, thanks to the better performances the new blankets exhibit, it is possible to reduce the insulation weight and costs by using only 2 blankets with reduced thickness, instead of 5, obtaining anyway the same insulation capability.

On the basis of the performed activities, it is possible to suggest two different insulating solutions. The first one, which allows achieving the best performances pointed out in this thesis, is the one obtained by using 5 blankets, made with the new materials and placed as indicated in the configuration named Case A. The second one, which allows maintaining the same performances obtained with the Thermal Blankets experimentally tested, is the one implemented by using only two new blankets of 12 mm in thickness (Case C), with a very interesting gain in terms of weight and costs.

Nevertheless, with a view to future application of the blankets in an actual turbine, the choice between the better thermal performances, shown in the Case A, and the lower additional weight, required by the Case C, has to be considered.

In both the cases examined, the advantages, consequent to the implementation of the new blankets, from the thermal point of view, in comparison with the ones obtained with the *conventional* blankets, are evident.

References

[1] Web site. https://www.reteclima.it/protocollo-di-kyoto

[2] Mercer, C.R. Haller W.J. Tong, M.T. (2006). Adaptive engine technologies for aviation C02 emission reduction. 42nd AIAA/ASME/SAE/ASEE Joint Propulsion Conference *& Exhibit*. Sacramento, California.

[3] Ruijgrok, G.J.J. Van Paassen, D.M. (2007). *Elements of aircraft pollution*. Delft Academic Press.

[4] Chin Han, J. Dutta, S. Ekkad, S. V. (2010). *Gas turbine heat transfer and cooling technology*. Taylor & Francis.

[5] Guha, A. (2001). Performance and optimization of gas turbines. *Proc. Instn Mech. Engrs, Part A. In Journal of Power and Energy*, Vol 215, pages 507-512

[6] Auxier, T. A. (2001). The importance of cooling technology in propulsion & power system. *Proc. RTO AVT Symposium on Advance Flow Management, Part B - Heat Transfer and Cooling in Propulsion and Power System*. Leon, Norway.

[7] Glezer, B. (2001). Selection of turbine cooling system applying multi-disciplinary design considerations. *In Journal of Heat Transfer in Gas Turbine System*. Vol 934 pages 222-232

[8] General Electric Aircraft Engines. (2005). NASA/CR--2005-213970. HPT Clearance Control Intelligent Engine Systems-Phase 1. Cincinnati, Ohio.

[9] DeCastro, J. Melcher, K. Noebe, R. (2005). System-level design of a shape memory alloy actuator for active clearance control in the high-pressure turbine. *In 41st AIAA/ASME/SAE/ASEE Joint Propulsion Conference & Exhibit*.

[10]. Lattime, S. B, Steinetz , B. M. (2004). High-pressure-turbine clearance control systems: Current practices and future direction. *In Journal of Propulsion and Power*, Vol 20, pages 302-311.

[11] Braun, E., Dullenkopf, K., Bauer, H. J. (2012). Optimization of Labyrinth Seal Performance Combining Experimental, Numerical and Data Mining Methods. *Proc. ASME Turbo Expo*, 4b, pages 1847 − 1854.

[12] Xu, W. Yang, J. (2016). Spiral-grooved gas face seal for steam turbine shroud tip leakage reduction: Performance and feasibility. *In Journal of Tribology International*. Vol 98 pages 242-252

[13] Yan, X., Li, J., Feng, Z. (2011). Effects of Sealing Clearance and Stepped Geometries on Discharge and Heat Transfer Characteristics of Stepped Labyrinths Seals. *In Proc. IMechE Part A: J. Power and Energy*, 225, pages 521 − 538.

[14] Desando, A., Rapisarda, A., Campagnoli, E., Taurino, R. (2015). Numerical Analysis of Honeycomb Labyrinth Seals: Cell Geometry and Fin Tip Thickness Impact on the Discharge Coefficient. In Proc. ASME Turbo Expo, Montreal, Canada.

[15] Denecke, J., Dullenkopf, K., Wittig, S., Bauer, H. J. (2005) Experimental Investigation of the Total Temperature Increase and Swirl Development in Rotating Labyrinth Seals. *In Proc. ASME Turbo Expo*, 3, pp. 1161 – 1171.

[16] Kyprianidis, K. G., Intech. (2011). *Future aero engine designs: an evolving vision.* Ch. 1, pages 1-23.

[17] De Servi, G. M., Azzini, L., Pini, M., Gangoli Rao, A., Colonna, P., (2017) Exploratory assessment of a combined-cycle engine concept for aircraft propulsion. *In Proc. Global Propulsion and Power Forum.* Vol. 1Zurich, Switzerland

[18] Kyprianidis, K. G., Rolt, A. M. (2015). On the optimization of a geared fan intercooled core engine design. I*n Journal of Engineering for Gas Turbine and Power.* Vol. 137 (4).

[19] Kumar, R. (2017) A critical review on energy, exergy, exergoeconomic and economic (4-E) analysis of thermal power plants, *In Engineering Science and Technology*, pages. 283–292

[20] Monterossi, M. P., Campagnoli, E. (2016). A new test rig facility to study aeronautic low pressure turbine thermal behavior. *Poster Proc. of Asme Turbo Expo Conference.* Seoul, South Korea

[21] Barbera, A. M. A., (2011), Thermal Control and Optimization of the Turbine Clearance. *PhD Thesis*, Energy Dept., Politecnico di Torino.

[22] Montrossi, M. P., Campagnoli, E., (2015). Numerical modelling for the prediction of aircraft cooled components thermal behavior. *Proc. of CAE International Conference.* Pacengo del Garda, Italy.

[23] Peschiulli, A., Coutandin, D., Del Cioppo, M., Damasio, M. (2009). Development of a numerical procedure for integrated multidisciplinary thermal-fluid-structural analysis of an aeroengine turbine. *In Proc. of ASME Turbo Expo – Power for Land*, Sea and Air. Orlando, Florida

[24] Mainini, L. (2012). Multidisciplinary and multi-fidelity optimization environment for wing integrated design. *PhD thesis.* Mechanical and Aerospace Department, Politecnico di Torino.

[25] Chen, X., Yan, L., Luo, W., Xu, L., Zhao, Y., Wang, Z. (2006). Research on theory and application of multidisciplinary design optimization of flight vehicles. *47th AIAA/ASME/ASCE/AHS/ASC Structures, Structural Dynamics, and Materials Conference.* Newport, Rhode Island.

[26] Sobieszczanski-Sobieski, J. Haftka, R. T. (1997). Multidisciplinary aerospace design optimization: survey of recent developments. *In Structural Optimization.* Vol. 14, pages 1-23.

[28] Morris, M. D. (1991). Factorial Sampling Plans for Preliminary Computational Experiments. *In Technometrics*, Vol. 33, No. 2, pages 161-174.

[29] De Weck, O.L. (2004). Multiobjective optimization: history and promise. *In CJK-OSM3*. Kanazawa.

[30] Deb, K. (1999). Multi-Objective Genetic Algorithms: Problem Difficulties and Construction of Test Problems. In *Evolutionary Computation.* Vol 7(3) pages 205-230.

[31]Deb, K., Agrawal, S., Pratap, A., Meyarivan, T. (2000). A fast Elitist. Non-Dominated Sorting Genetic Algorithm for Multi-Objective Optimization: NSGA-II. *In IEEE Transactions on Evolutionary Computation.*

[32] *Fundamental of gas turbine engine.*

[33] Poursaeidi, E. Taheri, M. Farhangi A. (2014). Non- uniform temperature distribution of turbine casing and its effect on turbine casing distortion. *In Journal of Applied Thermal Engineering* Vol.71 pages 443-444

[34] Morris et al. (2002). Gas turbine disk cavity ingestion inhibitor. *United State Patent Application Publication* No US 2002/0159880°1

[35] Elovic. (1981). Cooling air Cooler for a gas turbofan engine. *United State Patent* No 4,254,618

[36] Lee at al. (2014). Flow Control Insert In cooling Passage For Turbine Vane. *United State Patent* No US 8,864,438 B1

[37] Lim. (1992). Thermal insulation blanket. *United State Patent* No 5,139,839

[38]Barney et al. (2003). Thermal Insulating Conformal Blanket. *United State Patent* US 6,652,950 B2

[39]Smith. (2002). Fire-Blocking insulating blanket. *United States Patent* US 6,358,591 B1

[40]Web site. http://aeromodelbasic.blogspot.it/2012/01/exhaust-system-construction-and.html

[41] Maheshwari et al. (2012). Laminar Thermal Insulation blanket for aircraft applications and process therefor. *United State Patent Application* Publication US 2012/0308369 A1

[42]Web site. https://atfinet.com/index.php/applications/thermal-management/high-emissivity-coatings